Università degli Studi di Cagliari

PHD DEGREE

SCIENZE E TECNOLOGIE DELLA TERRA E DELL'AMBIENTE

Cycle XXXII

TITLE OF THE PHD THESIS

Groundwater resource management: methodological approaches and analysis of space-time data useful for assessing environmental impacts in drought contexts

Scientific Disciplinary Sector(s)

Area 04 – Applied Geology GEO/05

PhD Student: Andrea Zirulia

Coordinator of the PhD Programme Prof. Giorgio Ghiglieri

Supervisor	Prof. Antonio Funedda
Co-advisor	Prof. Luigi Carmignani
Co-advisor	Prof. Paolo Conti
Co-advisor	Prof. Giorgio Ghiglieri
Co-advisor	Dott. Enrico Guastaldi

Final exam. Academic Year 2018 – 2019

Thesis defence: January-February 2020 Session

Università degli Studi di Cagliari
dipartimento di scienze chimiche e geologiche
dottorato di ricerca in scienze e teconologie della terra
e dell'ambiente
Ciclo XXXII

Groundwater resource management: methodological approaches and analysis of space-time data useful for assessing environmental impacts in drought contexts

PhD Thesis

ANDREA ZIRULIA

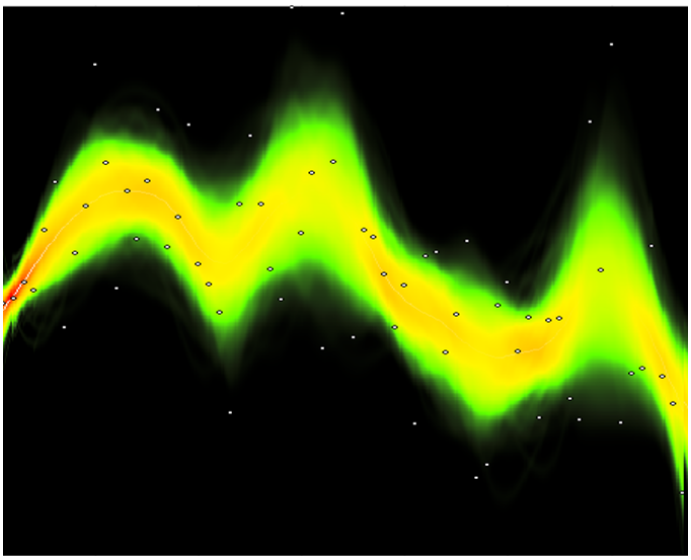

Cagliari, PhD defense, 26 February 2020

Università degli Studi di Cagliari

Abstract

European Water Framework Directive (2000/60/EC) regards underground water resource protection and one of its main challenges is to provide a quantitative and qualitative monitoring activities in order to achieve a "good" status of groundwater resources. A good environmental status of the groundwater resource is linked to its chemical conditions and to its quantitative state, which depends on the equilibrium between withdrawals in the medium-long term and natural recharge. The main objective of this research was to use alternative and non-conventional methods of analysis useful for groundwater resources management and sustainable procurement in environments characterized by dry events and water deficit, paying particular attention to the evaluation of the natural groundwater recharge sources. The specific objective of this thesis was defining the episodes of natural recharge in a porous aquifer located in an area of Tuscany considered semi-arid and characterized by dry events. In order to do this, hydrological and hydrogeological assessments based on automated methods, such as the recession curves MRC (*Master Recession Curve*) were used. These methods represent the relationship between the value of a hydrograph response and its rate of change over time (dR/dt) at a time when there is no infiltration or other entry of water. The MRC calculated for the time series of the response variable (i.e. the groundwater level) also allowed to determine the recharge *episodes* through the EMR *Episodic Master Recession* method. The EMR method is based on the level fluctuation algorithm (Water Table Fluctuation-WTF) and is suitable for identifying discrete recharging episodes from the hydrograph, the recharge amounts attributable to each episode and the amount of precipitation that caused this answer. This method considers a recharge flow in a saturated zone, that causes an increase of groundwater level before that dissipation processes that take place in the saturated zone bring it back to its steady state. This phenomenon is the product of the *Specific yield* (Sy) of the aquifer and the groundwater table level change ($H = \Delta H/dt$) attributable to recharge. The main challenge of the WTF method is to estimate Sy in groundwater zone fluctuation. Thanks to field measurements obtained with geophysical methods, the actual Sy parameter value was obtained. The integration of utilizes procedures and techniques was useful not only for evaluating recharge episodes, but also for assessing the relationship between recharge events and possible climate changes taking place in the study area. Thus, this research was able to link climatic changes with the modifications in the water level of the studied aquifer.

Keywords

Groundwater Recharge, Climate change, Statistics, Electrical Resistivity Tomography

To little Maria,
in whom all my hope lies.

Contents

List of Figures

List of Tables

Preface

"You're only given a little spark of madness
and if you lose that, you're nothing"
Robin Williams

Having undertaken a PhD co-funded by the University of Cagliari and GEOexplorer Impresa Sociale S.r.l. (an innovative start-up company of the CGT (Centre for GeoTechnologies of University of Siena, Italy), I have got the great opportunity to carry out this task in contact with the "real world" work in the hydrogeological and environmental fields. This allowed me to deeply know the real problems related to groundwater management.

During my first PhD year, I carried out a bibliographic study to investigate the environmental impacts (e.g. climate change, human pressure) on the groundwater resource, and to identify where new researches should head to fill the gaps between the current knowledge and the applied water management. From this analysis it emerged that a sustainable groundwater management is highly sensitive to the quality of input (e.g. natural recharging) and output (e.g. withdrawals and natural discharge) data, especially in order to determine its behavior and its sustainable long-term performance.

In the groundwater management framework, recharge is one of the most important inputs, having deep implications in terms of quality and quantity. As an example, groundwater numerical modeling is often used to predict the long-term balance of an aquifer. However, without a good space-time distribution of the recharge value, the modeling process becomes unreliable and management decisions based on it, faulty. Thus, Determining the natural recharge rate is a fundamental prerequisite for a sustainable groundwater management, chiefly in areas such as the Mediterranean Region where water is often a limiting factor to the economic development. Accordingly, this study aims to propose an approach that allows a cost-effective evaluation of the natural groundwater recharge and its behaviour in a climate change scenario, by integrating multiple disciplines (i.e. hydrogeology, geognostics, geophysics applied to hydrogeology, hydrology, hydrogeochemistry, hydroinformatics, statistics and geoinformatics).

On a practical level, as part of the research project funded by ASA Azienda Servizi Ambientali S.p.A. Water Utility to GEOexplorer Impresa Sociale S.r.l. titled (*"Overcoming of the critical quality and sustainable exploitation of the underground water resource - Coast of Tuscany"*), I have got to study and work in different areas of Tuscany (Central West Italy) that were all characterized by severe drought periods during the recent past and a general water deficit (province of Livorno).

Data gathering fieldworks have been carried out in the Livorno province in cities and villages (such as Castagneto Carducci, Rosignano Marittimo, Bibbona), alluvial plains (the main of which were Cecina River and Cornia River valleys), and a small island (Elba Island). Throughout these fieldworks I was able to deepen and become more familiar with the methods of field data ac-

quisition and instruments management necessary for carrying out hydrogeological, topographic and geophysical surveys in porous aquifers. In the initial stage, I was involved in water points census (wells, piezometers and springs). Each point was located via GPS survey, using the Real Time Kinematic survey methodology. In addition, I prepared detailed tabs for each water point detected. Afterwards, I measured and monitored the groundwater heads, flow rates and the main physical-chemical groundwater parameters (electrical conductivity, temperature, oxidation/reduction potential or ORP, dissolved oxygen, etc.).

To carry out these operations, the following instruments were utilized: OTT flat tape Water Level Meter (200 m) and Hydrolab MS5 multi-parameter water quality probe (200 m) equipped with the following sensors: Temperature, Specific Conductance, pH, ORP, dissolved oxygen (with agitator) and turbidity sensor. Where necessary the determinations were carried out after a preventive bleeding performed manually with a "Eijkelkamp" double valve bailer. To better understand the hydraulic characteristics of the soils located in the project areas, on-site tests were also carried determining its punctual hydraulic conductivity using a classic open double ring infiltrometer. The use of a double-ring, compared to a single-ring, guarantees a mostly vertical water flow of the liquid contained in the inner ring. The lateral losses linked to the suction of the surrounding dry soil are minimized thanks to the water level maintained also in the outer ring. Thanks to these instruments it was possible to develop the conference poster *"Integrated system for field acquisition, processing and management of environmental data in an open source environment"*, doi.org/10.1088/1475-7516/2016/03/048.

Furthermore, in order to deepen my knowledge on direct and indirect drilling exploration techniques, I participated to some exploratory boreholes drilling, carried out at Campo nell'Elba, Rio Elba and Porto Azzurro municipalities (Elba island). This allowed me to deepen my knowledge of drilling techniques, to carry out site geological assistance and stratigraphic logging, and to perform the hydrogeophysical logs in boreholes. This is the reason I acquired the required safety certifications needed to provide field assistance during exploratory drilling surveys. I was also involved in another project for the acquisition of hydrogeological and geophysical data in Laterina municipality, province of Arezzo (Tuscany, Italy). This allowed me to gain greater familiarity with the use of the Syscal Pro tool.

Integration of the hydrogeological study with the geophysical study matured in Laterina, replicated also in some areas of the Livorno coastal plain, culminated with the scientific publication: "Potential shallow aquifers characterization through an integrated geophysical method: multivariate approach by means of k-means algorithms", doi.org/10.7343/as-2017-278. By desk activities, I was able to excecute an in-depth analysis of geological, hydrological and hydrogeological data relating to these areas and to local databases from the regional authorities (including all the data relating to the Significant Underground Water Bodies of the Region Tuscany; DGRT n. 225/2003 Law of Tuscany Region). In particular, I had the opportunity to conduct a first study on the hydrogeological data relating to the Cornia River valley (Province of Livorno), which have been interpreted, homogenized, and categorized for the statistical reconstruction of the area's aquifer (conceptual hydrogeological model). From this study derived the article *"Stochastic 3D reconstruction of the Cornia River valley alluvial aquifer"*, doi.org/10.7343/as-2017-278, and the abstract *"Using flood water in Managed Aquifer Recharge schemes as a solution for groundwater management in the Cornia River valley (Italy)"*, doi.org/10.7343/as-2017-278. Consistent with

the objectives of the doctorate, four courses were chosen and attended at the CGT, which allowed me to acquire the necessary foundations for:

- *Direct sampling methodologies of the environmental matrices established by technical regulations;*
- *Use IT tools capable of simulating groundwater flow and contaminant transport;*
- *Management of environmental variables in the open source software QGIS;*
- *Understand the main chemical-physical mechanisms related to geochemistry of soils and waters;*
- *Statistical analysis, also through open source tools such as software R, oriented to the production of thematic maps of geostatistical prediction of the behavior of chemical-physical variables and to the hydro-climatic variables analysis over time.*

The second year of the doctorate was characterized by a research period of 6 months spent in Italy and 6 months spent abroad. Oman (6 months) was chosen as a study area in which to carry out research activities due to its arid climate and its complex water resource management system. In particular, the Al Batinah plain in the north of the Sultanate (where I conducted my studies) is characterized by a large aquifer, which currently appears to be overexploited due to a raise in domestic, agricultural and industrial consumption. This has also led to a growing in the water balance deficit over time as well as an increasing in salt water intrusion from the sea, similar to what happens in the Tuscan coast. The data provided by the Omani Ministry of the Environment consisted of a time series (in some cases of up to 40 years) as follows: phreatimetric (106 monitoring wells), salinity (59 monitoring wells), and rainfall (115 pluviometers) values. All sampling wells and pluviometers where located along the coast of southern plain of Al Batinah.

In March 2018 it was possible to carry out the following field activities to integrate existing data: survey of wells in the area of interest, phreatimetric measurements and electrical conductivity. Given the characteristics of the databases provided, the amount of data available and the knowledge of statistical analysis acquired during the first year, the open source programming language R was chosen as the analysis software, due to its powerful computing skill and the almost infinitive contributions by scientists from everywhere. In particular, this language appears to be suitable for applications in hydro-information technology due to the good quantity of components ("packages") related to hydrology (hydrological data for example are often time series), water resources, climatology, soil science and meteorology, giving access to both consolidated and experimental computational methods.

During my stay at the German University of Technology in Oman I studied the time series theory, which was later applied to understand the significant trends of the given hydroclimatic variables. In particular, two case studies were addressed. The first one has seen the evaluation of the phreatimetric levels trends of a particular area of the Al Batinah plain called Wadi M'awill. The paper: "Trends in Groundwater Observation Data and Implications" was subsequently presented at the Water Science and Technology Association (WSTA) 13^{th} Conference on Gulf water held in Kuwait in March 2019. The second case study, still under development, concerns the study of the effective artificial recharge capacity of groundwater by particular dams built downstream

of the Hajar mountain range, again using the time series provided. I also had the opportunity to apply to the data provided cluster analysis techniques and the ARIMA forecast models (Autoregressive Moving Average), useful for obtaining and completing further information on the possible effect of climate change on natural phenomena of groundwater recharge.

Finally, the educational activities I conducted at the German University of Technology were:

- *attending the courses of Hydrogeology I, Hydrogeology II and Hydraulic testing held by Prof. Holzbecker;*
- *support and assistance to Prof. Ivan Callegari regarding the use of GIS / R software for geology and hydrogeology;*
- *supervision and examination of the subjects in the various departments of the university, including geosciences.*

In the 6 months of the second year of doctorate spent in Italy, first I evaluated the best calculation method of the hydroclimatic time series and geoelectrical measurements, considering the quality and the type of these data. Consequently, I decided to use the MRC recession curves (Master Recession Curve) for the time series of the response variable (i.e. the water level and cumulative precipitation) that allowed the determination of the recharge episodes through the EMR (Episodic Master Recession method, which in turn is based on the algorithm of fluctuation of the levels of the Water Table Fluctuation), in which the Specific yield (Sy) is a fundamental parameter. This gave rise to the idea of measuring the Sy parameter (which is almost always taken from bibliographic sources) through geoelectrical measurements to make its value as accurate as possible and therefore be able to use it within the calculation estimate.

For the evaluation of the possible study areas of recharge I considered the field activities carried out the previous year, the available hydroclimatic data, the field activities and the problems encountered in the first months spent in Italy. Initially the island of Elba had been considered as a hypothetical study area, due to its well documented chronic problems of water deficit. In fact, on the island I was able to take part in the operations of boreholes drilling and hydrogeophysical logs performed at "Reale" area (Municipality of Porto Azzurro, Elba island) and at "San Giuseppe" area (Municipality of Rio Marina, Elba Island), useful for the understanding and interpreting the stratigraphic data and the direct hydrogeological characterization of coastal aquifers. I was also able to carry out a census of the wells located in the central eastern sector of the island, aimed at verifying the current fractional levels. However, I chosen to not consider the aforementioned area due to the impossibility of carrying out geoelectrical surveys, the absence of historical phreatimetric series and the high logistic costs.

Later I analyzed the location of the geoelectrical lines performed during the previous geophysical data acquisition fieldworks regarding to the hydrological service measurement stations, identifying two subareas suitable to study the process of groundwater recharge. This areas where included within the aquifer between Cecina and San Vincenzo villages (province of Livorno). Once the relative electrical tomographies of resistivity were interpreted, I identified a method in the literature that could be used to calculate the value of Sy.

Finally, in this year I also studied the characteristics of the datasets related to the hydroclimatic variables belonging to the hydrological service of the Tuscany region and I performed the

statistical treatment for the time series of pluviometric, hydrometric, thermometric and phreatometric data on the basis of temporal irregularities, validation years and their location relative to the study subareas and the power lines. Finally, the first simulations were performed to calculate the recharge episodes on the Castagneto Carducci municipality using an R script developed by USGS.

During the third year of the PhD program I had the opportunity to participate in the geophysical data survey carried out in Kenya as part of the "FLOWERED" project ("de - FLuoridation technologies for imprOving quality of WatEr and agRo - animal products along the East African Rift Valley in the context of aDaptation to climate change", a project aimed at developing a sustainable water management system in the areas affected by fluorine contamination in water, soil and food in the African Rift Valley countries, as part of the Horizon 2020 research and innovation program funded by the European Union). Thanks to this experience I was able to further improve my geological and hydrogeological knowledge in a semi-arid environment, and in the components that constitute the prerequisite (conceptual model) for the implementation of sustainable water management. This lead to the presentation of the abstract titled "Multidisciplinary geophysical surveys for 3D hydrogeological conceptual model reconstruction in areas contaminated by fluoride in the Nakuru area, East African Rift System (Kenya)" at the FLOWPATH 2019 congress held in Milan.

Thanks to the experience gained in statistical analysis of environmental data, during the first two years of this PhD, I was also able to hold a lecture called "Evolution and representation of hydroclimatic variables in different environmental contexts" (Second level Master's Degree in Environmental Geotechnologies organized by the University of Siena at CGT), with the aim of providing students with the logical tools useful for the correct manipulation and representation of the environmental data and its evolution through the use of the R software. I was also able to present an abstract at the 2nd World Congress on Climate Change: "Time Series Analysis of Hydro-Climatic Variables in an Arid Environment" held at Berlin.

Furthermore, I had the opportunity to act as tutor of two students who attended the final training internship of the aforementioned master's course, and to obtain certification of knowledge of the English language level B2 in accordance with the European Framework of Reference for Languages.

As part of the 18th International conference "Applied Stochastic Models and Data Analysis" held in Florence in June 2019, I presented the paper entitled "Groundwater level forecasting for water resource management". The forecast analysis was carried out in order to study the temporal trend of the phreatimetric levels recorded continuously in four wells located in the chosen study area, using the ARIMA model theory studied in Oman. During the two months spent abroad at the Energy and Water Agency of the state of Malta, I was able to study in depth the statistical analysis methods of the island's pluviometric data. This allowed me not only to understand and verify the possible connections between groundwater and climate change, but also to evaluate the possible relationships between recharging events and possible climatic changes taking place in the study area. Finally, the last months of the third year were devoted to the analysis of the remaining points located in the area of study and to the drafting of the thesis.

Chapter 1

Hydrogeological problems addressed in this thesis

"Some people thought we were at war with the Germans. Incorrect. We were at war with the clock"

Alan Turing, by Benedict Cumberbatch in Imitation Game

Currently, the role of groundwater for society is very important. In fact, groundwater not only plays a key role on natural ecosystems scale, but also in various human productive contexts. The progress of technologies, combined with the need for water in the production sectors, has given a strong impetus to the exploitation of this resource which, over the decades, has been seriously impoverished both from a qualitative and quantitative point of view. The deficit of groundwater resources has become a global issue, as demonstrated by recent studies conducted using satellite data that enable the detection of dynamic changes in large-scale underground water reservoirs and show a rapid depletion of groundwater reserves. These studies highlight how most of the population use and abuse these reserves unaware that they are rapidly depleting and might run out in the near future [5]. In particular, the current agricultural production demands high quantities of fresh water for irrigation and processing, which is also associated with decrease in soil water content, increased evapotranspiration from farming areas, raised temperature and reduced rainfall. All of this put on severe stress on groundwater reservoirs [6]. The groundwater resources represent 43% of the total water used for irrigation worldwide [7]. Irrigation with groundwater plays a key role in agri-food economies, food security and living conditions of people in many countries [8, 9]. Therefore, global changes can have a serious impact on rural economies and on the livelihoods of people living in regions where irrigation is dependent on groundwater [10, 11]. The growing in temperatures due to global change will increase the rate of evapotranspiration, which will in turn augment irrigation demand [12] and decrease the availability of irrigation water from both surfaces [13] and underground sources [14]. Today the effects of climate change are starting to have a greater impact on the water resource, since the potential decrease in precipitation could cause a crisis in linked biosystems.

To overcome this, a strategy is the exploitation of deeper aquifer levels. However this is proved to be more difficult, considering the energy costs associated. In fact, the decreasing in groundwater levels [15] will also contribute to higher carbon emissions from irrigated agriculture [16].

Hence, a lack of adequate understanding of the groundwater system can generate higher drilling costs and higher energy expenditure [17].

1.1 The key role of natural groundwater recharge

Understanding the mechanisms concerning the natural water supplies can improve the management of natural resources, saving time for planning and providing indications on the scope and potential costs of future work. The sustainable exploitation of groundwater should not exceed the recharge rate of the corresponding water basin, so it is important to understand the spatial variability of the recharge itself [18].

Producing a reliable estimate of the natural recharge rates of groundwater is useful for determining the quantities of water that can be renewed over time and for deriving a threshold for human consumption [19]. Groundwater recharge is an important component of the water balance that is difficult to quantify. It is often approximated with literature values [20–23] and recharge temporal changes are uncertain due to the complex nature of recharge processes and the lack of observational data [19, 24].

One of the major challenges in hydrogeology is the temporal estimation of recharge rates [25], which is often considered as a fixed percentage of precipitation and difficult to determine [26]. Generally an over-exploitation of the groundwater resource causes a decline in groundwater levels, so the spatiotemporal analysis of the levels could then reveal important information about the underground water system [27] and would be useful in order to estimate the recharge in different areas [28].

The study of recharge is fundamental to understand the underground water flows [29] in order to reduce the gap between water supply and demand with more efficient irrigation systems [30,31], to model underground aquifers [32–34], to define possible changes in quantity and quality [35–37], as a prerequisite for the sustainable management of groundwater, especially in regions where the demand for water is high and the economy of the area depends on it [38].

1.2 Links between climate change and groundwater recharge

In temperate regions, studies aimed to understand the response of recharge to heavy rainfall are very scarce [20].

In the Mediterranean basin, as well as in other parts of the world, cases of coastal aquifers that are not subject to over-exploitation are now rare and there are significant drops in water resources that will have an environmental, economic and social impact [39]. Moreover, the Mediterranean area has been recognized as a hot spot for climate change projections [40] which foresees a decrease in annual rainfall during the hot season and, for the northern regions, a significant increase in rainfall. However it is not clear how changes in precipitation affect recharge rates [19, 41]. The uncertainty of the recharge process will be compounded by the uncertainty associated with the forecast of future climate scenarios [42]. In particular, in the case of arid or semi-arid environments [39] there are still considerable doubts about the impact that climate change will have on groundwater recharge, since the aridity of the climate generates smaller and more variable recharge flows in space and time [38].

Most of the consequences of the groundwater recharge changes will be detrimental to the understanding of the dynamics and interactions of processes that affect recharge over time. Thus,

understanding this changes is crucial for the assessment of the quality and quantity of groundwater [13, 24, 43].

Policy makers are becoming more sensitive to the sustainable management of groundwater and the challenges posed for their better management are acknowledged, including groundwater and climate change issues among the priorities of the political agenda in many world regions [24, 44, 45].

1.3 Research Objectives

The general objective of this work is to estimate natural recharge quantities of a shallow aquifer through multitemporal time series evaluation of piezometric levels fluctuations and possible climatic variations connected to it. The reproducibility of proposed workflow is guaranteed by use and enhancement of public regional monitoring time series and open source software. This general objective was developed in order to provide an alternative and unconventional analysis work flow useful to improve understanding and guide integrated groundwater management in light of climate change. In particular to achieve this goal, the attention will be based on the following specific objectives:

- **Recharge computing in a shallow aquifer within an area shifting towards a semi-arid climate condition:**

  In literature, a few attention has been paid to the effect of climate change on the natural recharge of aquifers [46]. In arid and semi-arid regions, for example the western coast of Tuscany, low rainfall and continuous water consumption limit the quantities of groundwater [47]. Traditionally it has been assumed a yearly recharge value ranging between 20 and 30% of the annual cumulative rainfall. However, after an exhaustive literature review only a few references for this value have been found. In particular, an author reports a table with some recharge values in areas in which climate changes is underway [38]. Very often groundwater flow is modelled in study areas where it is very complex to obtain a direct recharge value by means common techniques (e.g. isotope tracing, lysimeter).

  In sections 4.1, 4.2 and 4.3 of this thesis an integration of methods to estimate natural recharge values is proposed, taking into account the error sources associated with recharge calculation method selected. Thus, the proposed workflow is able to provide site-specific recharge values useful for modeling and it consists in a sustainable groundwater managing by means of environmental data available in regional databases through the open source statistical software R [48].

- **Specific yield estimation:**

  The Specific yield (Sy) is the volume of water that drains from a saturated soil due to gravity relative to its total volume [49]. The main challenge of the Water Table Fluctuation (WTF) method involves the estimation of the Sy of the aquifer at the depth of the zone of water table fluctuation [50]. As will be demonstrated later, the main difficulty in applying this formula is having a reliable estimate of aquifer Sy [51]. Perhaps the main drawback is the uncertainty in obtaining a representative value of Sy [52]. This will be addressed in section 4.2. For this study, following common practice, Sy was set at a constant value. However, in reality

Sy varies as a function of the depth of the water table. It also varies over time in response to the wetting and draining history of the aquifer. If multiple rises occur closely spaced in time, the sediments may not fully drain between rises. In theory, it would be appropriate to assign different values of Sy to different rises. In practice, however, the information and resources required to make these accommodations are rarely available [25, 38].

- **Assessing the connection between groundwater recharge and climate change in a semi-arid environment:**

  In the "Intergovernmental Panel on Climate Change" fifth evaluation report [53] areas such as the Mediterranean basin are particularly vulnerable to future alterations of rainfall events and extreme droughts periods. As such, it is suggested to deeply analyze the variability and the distribution of precipitation also at the sub-regional level. In section 5.2 the links between aquifer recharge and climate change are studied on the basis of precipitation analysis over a 70 years period at local scale.

Chapter 2

Study Area

"The Nation that destroys its soil
destroys itself"
Franklin Delano Roosevelt

2.1 Location and extent of study area

The municipality of Castagneto Carducci, with a territorial extension of approximately 142 km^2, is the largest municipality in the Province of Livorno (Tuscany, Italy). The Geographic position is 43°10' latitude North and 10°36' longitude West; maximum elevation is 585 meters above mean sea level (amsl). From morphological point of view, the study area consists of two distinct zones (figure 2.1): a zone has a low-to-medium steep layout with altitude between a few tens of meters and 500/550 meters amsl; the second one is very broad, mostly flat, and has a weak and almost continuous slope towards the sea (figure 2.2). The steeper zone characterizes the eastern part of Castagneto Carducci municipality, where the hills crown a vast flat area that extends above all between the Castagneto-Bolgheri villages line and the sea. Furthermore, the hilly zone is affected by strong incisions of the water courses, whose main flowing directions are from East to West in the norther part, where the plain is more extended, or from south-east to north-west in the southern part.

2.2 Geological context

The study area is characterized by geological formations of the Neo-Autochthonous Complex, the Sub-Ligurian and Ligurian Domain, and the Tuscan Domain complex. The various complexes can be distinguished in geological formations with alluvial deposits from the bottom upwards as follows (figure 2.3):

- *Formations of the Tuscan Domain (MAC, STO)*:
  they constitute the pre-neogenic substrate and emerge in the south-eastern portion of the study area.
- *Formations of the Sub-Ligurian and Ligurian Domain (ACC, APA, ARB, DSA, ELM, OFI)*:
  they consist of the Ophiolic and Austroalpine Units. They rise to the north and east and surround the entire basin of the Bolgheri stream.

- *Formations of the Neo-Autochthonous (EMO, FAA, MES, VIL)*:
  consisting of Miocene deposits and Pliocene and Pleistocene deposits. The latter constitute the edges of the reliefs, up to the western coastal plain.

- *Recent and current deposits (OLO, PLE)*:
  they are found in the valley depressions of most watercourses and in the northern portion along the low plain of the Bolgheri stream.

More in detail, the alluvional plain forming the studied aquifer is characterized by the following Neo-Autochthonous deposits of Pleistocenic sands and limestone, and recent and current alluvional deposits:

- *Sands and limestone of Donoratico (Upper Pleistocene)*: the formation consists of orange-red fine sands with intercalated calcarenitic lenses formed in three transgressive cycles of the Terriniano. In the coastal plain calcarenitic and conglomeratic deposits constitute the hydrogeological units of the drinking water aquifers of Castagneto Carducci municipality.

- *Alluvial deposits (Holocene)*: they are identified by alternations of silts, sands and pebbles in particular along the course of the Bolgheri stream where they reach thicknesses of over 10 m.

- *Marsh stocked deposits (Holocene)*: they are made up of silts, black plastic gray clays with fossils, present from the dune cordons up to the alluvial plain of the stream of Bolgheri. They are identified by alternating silt sands and pebbles.

2.3 Hydrogeological context

The "Coastal Aquifer between Cecina River and San Vincenzo village" is located in the Livorno province (Tuscany, Italy) [54]. This aquifer is formed by a sequence of permeable gravel and sand layer separated by impermeable silty-clayey deposits. The bedrock of this sequence is represented by: sands and clays in the northern sector, low-permeability Ligurian units in the southern sector, and clayey deposits of uncertain stratigraphic position in the sector between Cecina river and Bolgheri.

The general hydrogeological scheme is characterized by a multi-layer system with levels overlapping aquifers, represented by the deposits of sand, sand and gravel, calcarenites and conglomerates separated by clayey and clayey-muddy layers that give it characteristics of artesianity. However, due to the discontinuous nature of the impermeable deposits and the presence of several boreholes that connect the permeable layers situated at different depths, this multi-layer system can be considered to behave as a single-layer aquifer [55]. From the observation of the geological map it appears that there is a prevalence in outcrop of hydrogeological units characterized by permeable deposits, while markedly impermeable deposits (poor / zero permeability) outcrop in a very small percentage and mainly in the mountain ranges that surround the coastal plain of Castagneto Carducci from North-East to South-West. Indeed, the whole flat part up to the first hilly slopes is constituted by alluvial, eolic and marine deposits with variable permeability, high in sandy and gravelly levels, which pinch-out towards west where they come in contact with the medium to low

permeability rock outcrops of the hilly areas. These deposits have thicknesses of between 40 and 60 - 65 meters and end at the base with a clay level below which it was sometimes encountered (from data relating to the drilling of water wells) a rocky substrate.

It is then possible to locally distinguish in the aforementioned deposits (consisting of sands, gravels, silts, clays, conglomerates, sandstone levels, calcarenites) two types of aquifer [55]:

- *Unconfined Shallow Aquifer.*
  It is made up of deposits of sand, sand and gravel, silt, with intercalations of lenticulars levels of clays and clayey silts. These deposits extend from the sea to the first hill slopes, with thicknesses varying from 10 to 25 meters; they host water of poor quality chemical qualities, regulated by the trend of rainfall. It is now exploited by few wells that manage to give the low quantities of water required by users, in the months from October to April/May, remaining almost dry in the summer period.

- *Deep confined Aquifer.*
  This rich aquifer is a source of large quantities of water, exploited for drinking water and agricultural purposes. It consists of sand, sand and gravel deposits, gravel, sandstone and conglomerate levels, "bench" limestone, silt, separated from the upper aquifer by clay and clay-silt levels that give it artesian characteristics. However, these levels do not have a homogeneity for the whole plain. The clay levels, placed above the deeper porous deposits, locally seal the groundwater from surface pollutants. The deep aquifer has an average thickness of 25/30 meters with maximums of 35/40 meters.

However, as discussed before, this two aquifers while are sometimes locally clearly separated, overall are generally interconnected.

The overall aquifer is mainly recharged by both meteoric waters that infiltrate through the vadoze zone, from the ground surface to the aquifer (zenithal recharge), and by the lateral flow contributions from the embedding rocks with medium-low permeability which are in contact with the coastal deposits at the height of the first hilly slopes. An extra minor inflow is due to the sub-riverbed contributions of the watercourses present in the coastal plain. The potentiometric surface (figure 2.4) of this coastal water body behaves quite similarly to the one from the nearby aquifers (e.g. "Cecina Valley" and "Between River Fine and Cecina River"), decreasing from the western hilly aquifer boundary towards the sea level in the eastern margin. During the year, the groundwater head is influenced by the precipitation seasonal distribution, but the main groundwater flow directions remain constant. The periods of maximum stress are detected in the summer months when drought is added up high levies for the needs of agriculture and the strong tourist presence.

In the southern area of the aquifer, where this study is focused, an exploratory drilling was carried out (and concluded on 5/12/2017) about 300 m east from a regional water level recording station (figure 2.3). The stratigraphic log (figure 2.5) shows the presence of sands and silts with a conglomerate level of 7 to 27 meters, the site of a probable phreatic surface aquifer, interspersed by a small clay layer; an alternation of gravel-sandy levels and subordinate clayey compact layers from 32 to 54 meters, the site of a probable deeper stratum isolated by an impermeable level of clays.

Unfortunately, for this focused study area, it was not possible to find direct estimation of the aquifer hydrodynamic parameters since past investigations have never been carried out by the water utility, let alone by private individuals.

2.4 Water resource assessment

2.4.1 Climate conditions and land use

Tuscany has a moderate climatic variability that has extreme per-humid and micro-thermal climates in the higher parts of the northern Apennines and the Apuan Alps, and semi-arid types in the southern coastal part [47] (figure 2.6). This climatic variety is due to its geographical position with respect to the prevailing direction of western perturbations, to the topographic and morphological profile and to the distance from the sea of continental areas. Due to a variety of factors including summer dryness, winter drought episodes, improper land use, over-exploitation of water resources and demographic and tourist pressure, Tuscany areas are sensitive to land degradation phenomena. For this reason soil has been included among the non-renewable resources and its monitoring is essential. With reference to planning document of the municipality of Castagneto Carducci [55], table 2.1 shows the percentages of land use at local level (municipal boundaries).

Table 2.1: *Land use in the study area.*

Land use	**Area** km^2
Residential	6.2
Industrial	0.8
Forest	64.6
Agricltural	64.8
Recreation areas	0.3
Infrastructure	2.3
Beach	0.8
Waters	1.0
Other	1.2
Total	142

2.4.2 Hydrogeochemical water characteristics

Studies conducted by Cerrina-Feroni et alii [54] have shown that the groundwater of the aquifer between Cecina and S. Vincenzo is characterized by high concentrations of HCO_3^- and Ca^{2+}, although in some areas Cl^- is also an important ion. According to these authors, SO_4^{2-} is of relevance only in wells abstracting water from gypsum or anhidritic lithologies, which crop out in the nearby hills. Based on the shape of the potentiometric surface together with available $\delta^{18}O$ values, these authors also confirm the above mentioned conceptual model in which the studied aquifer is mostly recharged by both local precipitations (mainly in the plains) and meteoric water infiltration in the nearby hills. Furthermore, ongoing studies currently being undertaken at the University of Siena (Center for GeoTechnologies), applying multivariate statistical techniques to the physico-chemical data collected by the local authorities for the period 2008-2018, are in line

with this (figures 2.7 and 2.8). The analysis of the data obtained also showed high concentrations of Ca^{2+}, HCO_3^- and Cl^- and very low contents of K^+. The use of different multivariate statistical analysis (i.e. Self-organizing maps and hierarchical clustering) showed the presence of three groups of waters (C1, C2 and C3), based on the predominance of Ca^{2+},HCO_3^-, SO_4^{2-} and Cl^- ions, indicating that there were wells where waters could be grouped together with waters associated to local rainfall. This result is being taken as a further prove of the influence exerted by local precipitations as a recharge source for this aquifer.

Figure 2.1: *Photograph representing the landscape of the study area.*

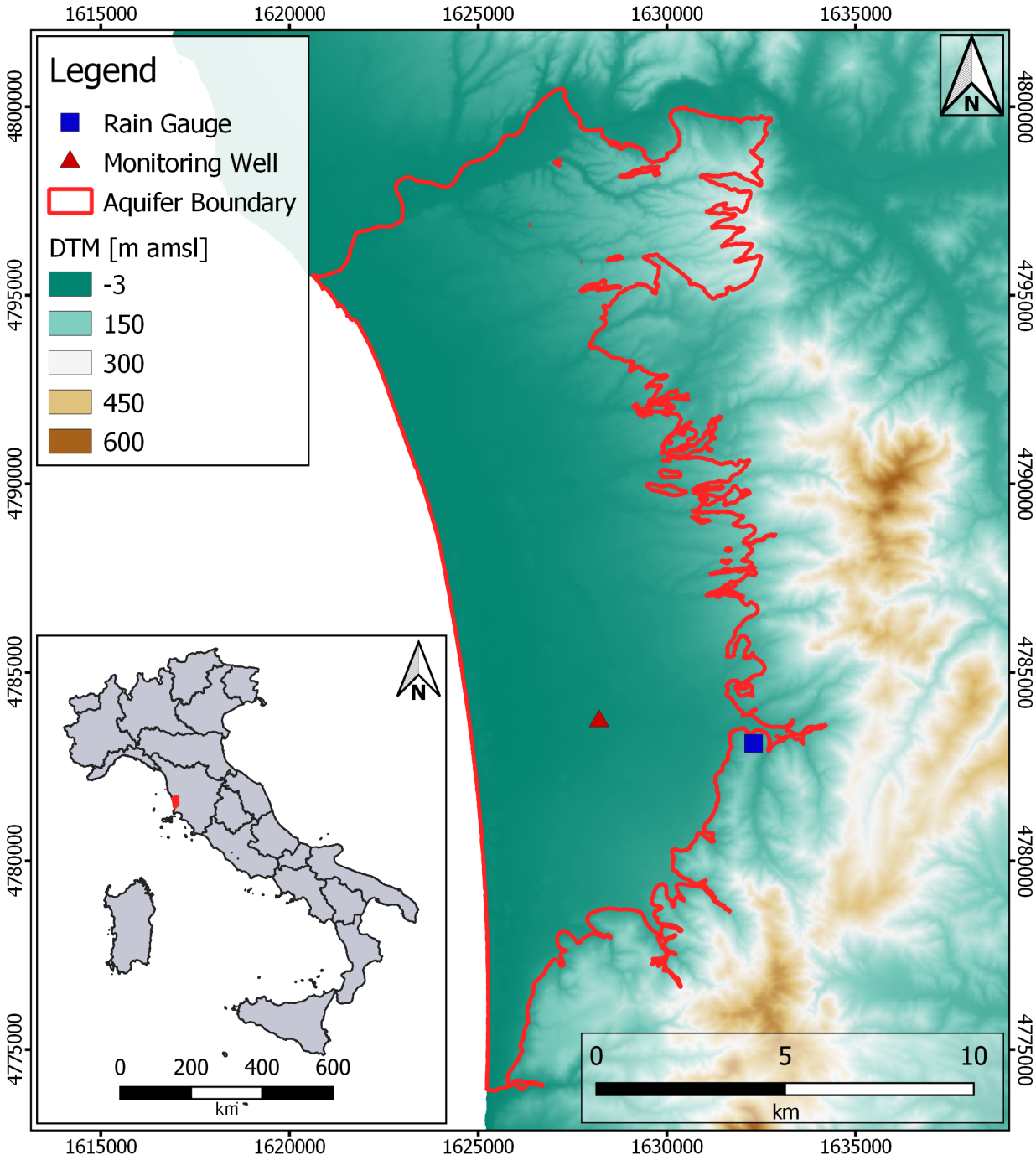

Figure 2.2: *Digital elevation model of the study area; the studied aquifer "Coastal Aquifer between Cecina River and San Vincenzo village" [54, 56] (red polygon) is located in the Livorno province (central Italy). The main rain gauge (blue square) and the monitoring well (red triangle) used for this work are also shown.*

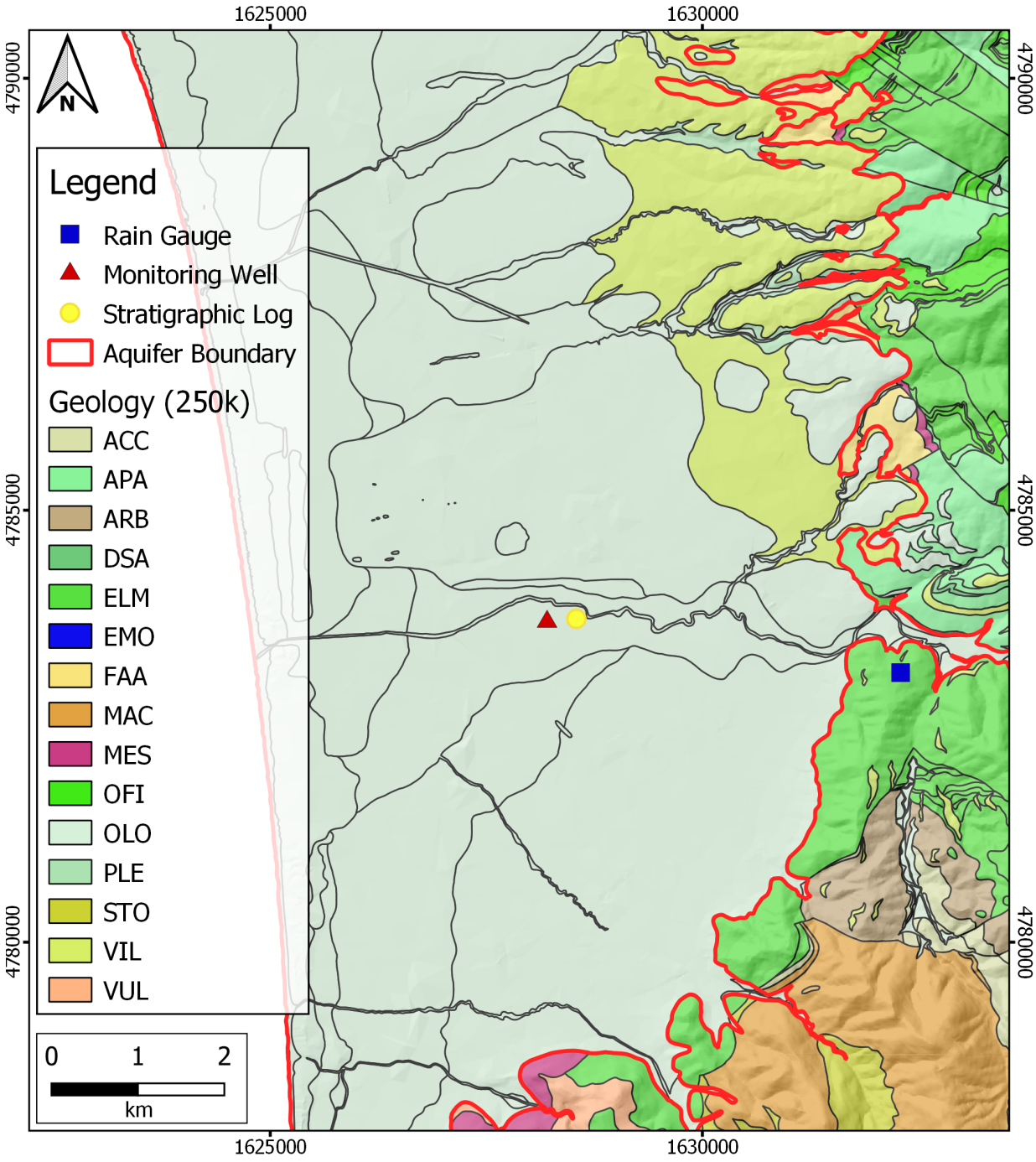

Figure 2.3: *Location of the monitoring well (red triangle) on the geological map of the north area of Castagneto Carducci municipality (1:250000 scale).*

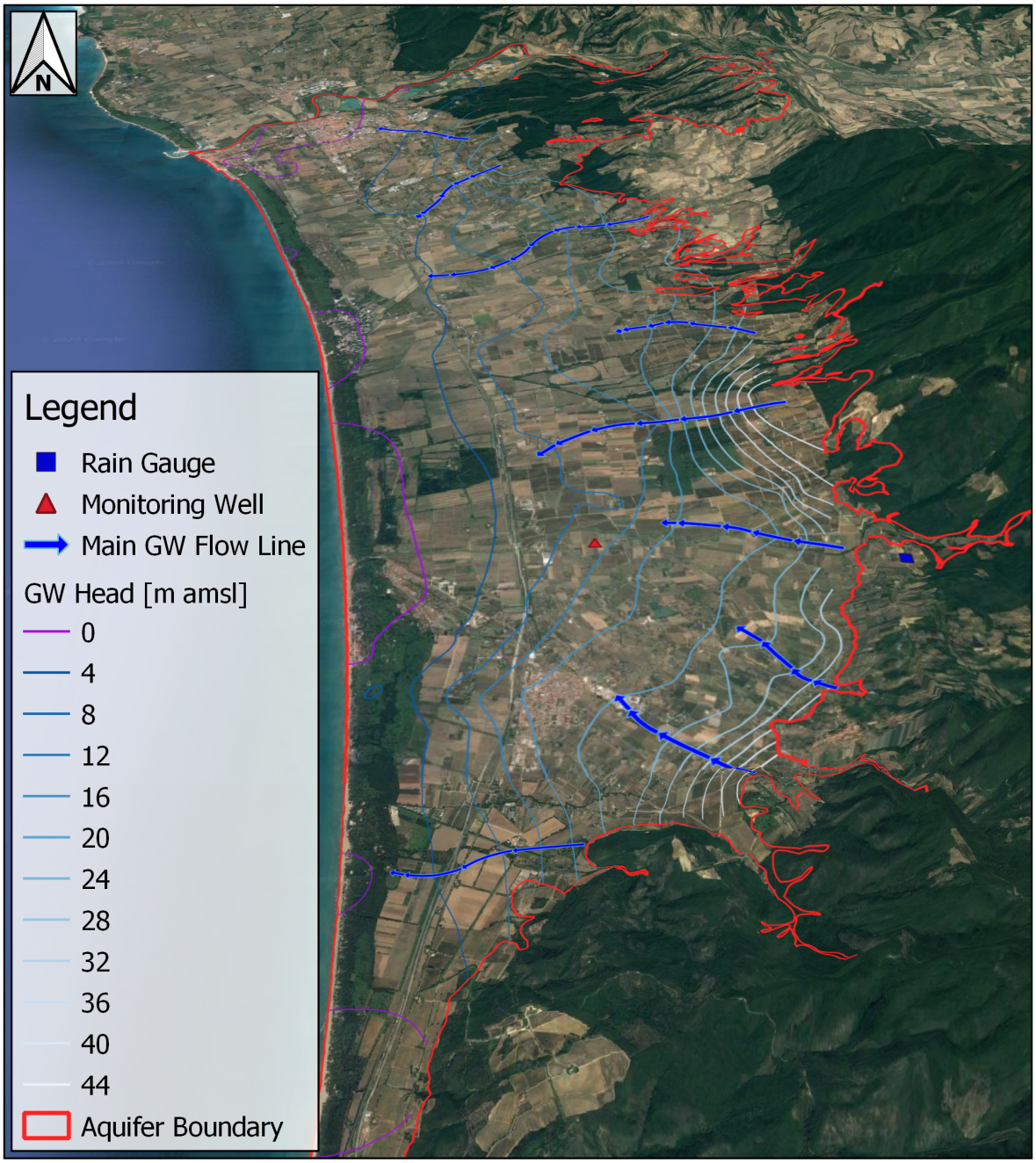

Figure 2.4: *Potentiometric surface of the Coastal Aquifer between Cecina River and San Vincenzo village.*

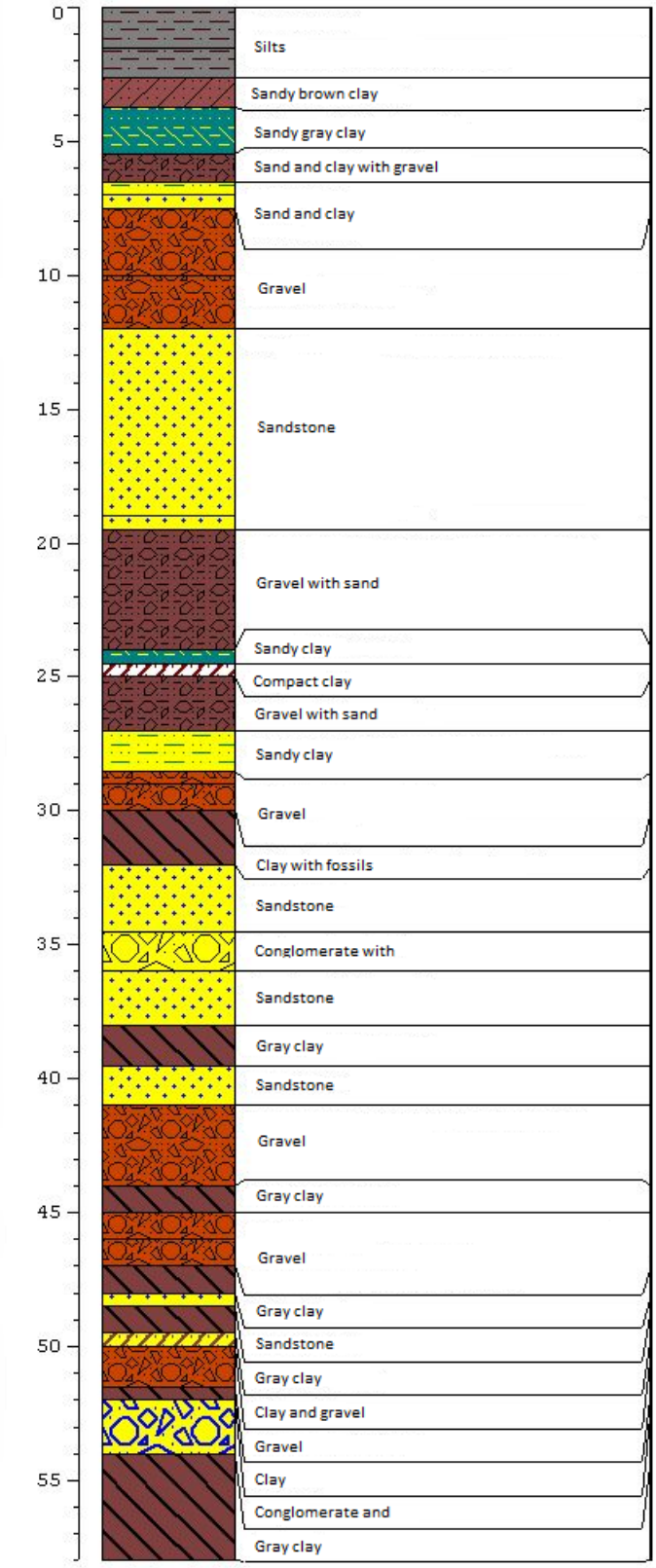

Figure 2.5: *Detailed stratigraphic log (meters above sea level) of the exploratory survey performed on December 2017. The coring location of the stratigraphic log is shown in Figure 4.46.*

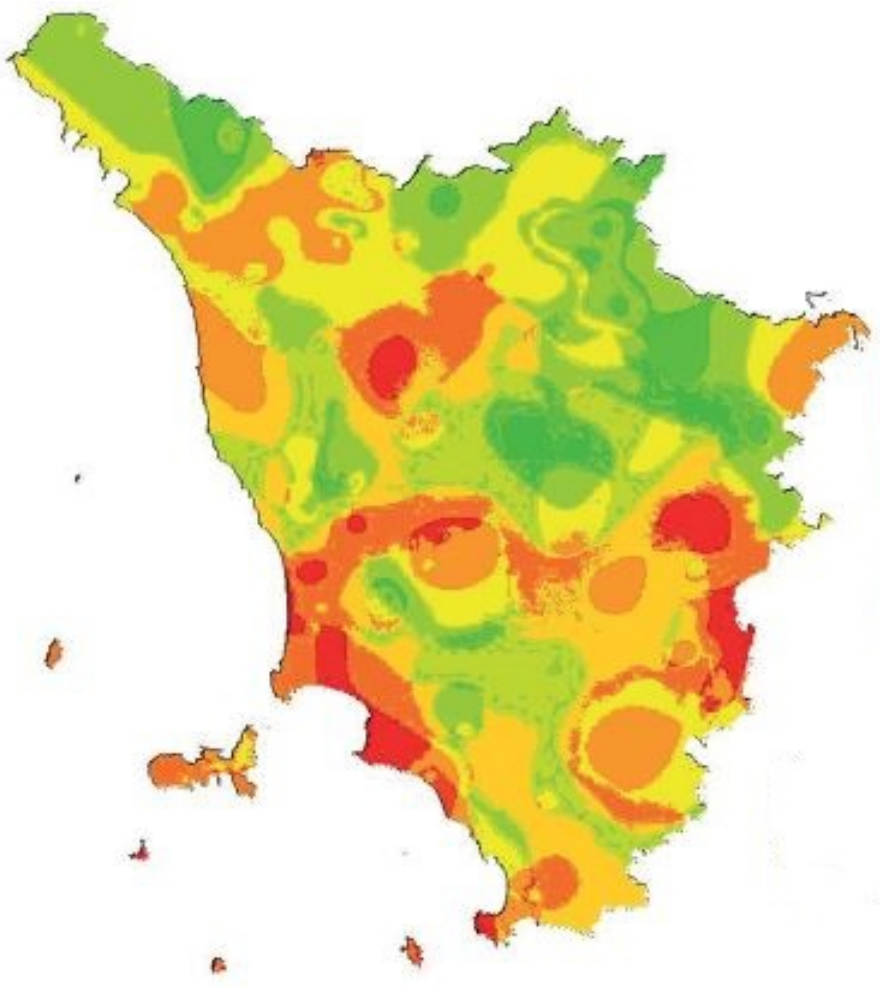

Figure 2.6: *Joint representation of the aridity and drought indices (climate quality) for the year 2008 for the Tuscany region [57]. From the point of view of climatic criticality the areas with a color from yellow-orange to red present a higher risk. In particular, the study area falls into the latter category and where the most important element of sensitivity is the climate, with dry summers and dry winters.*

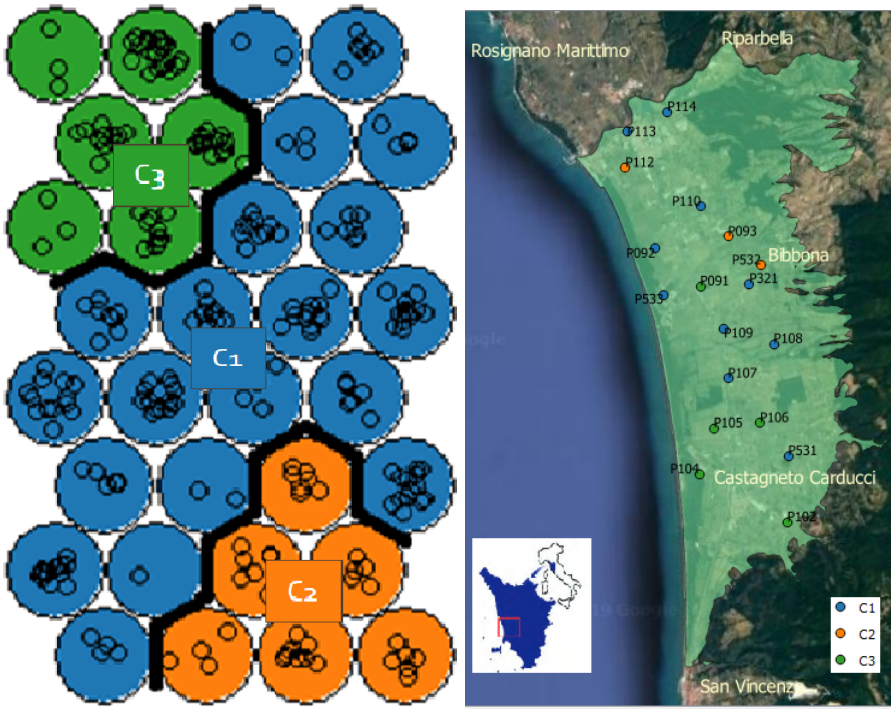

Figure 2.7: *The "Self-organizing map" presented on the left of double figure maps all data into a set of discrete locations, organized in a regular grid. Associated with every location is a prototypical object, called codebook vector. Thus, individual objects from the data set can be mapped to this set of positions, by assigning them to the unit with the most similar codebook vector. The density of these vectors is greatest in areas where the density of points is greatest. When the codebook vectors are shown at their SOM positions, the individual objects are shown at a random position close to "their" codebook vector. In SOMs objects that are mapped to the same or to neighbouring units are likely to be similar, an advantage when working with high dimensional data. The codebook vectors are acquired after an iterative process that involves three steps: (i) competition between nodes; (ii) selection of a winning node defined as the Best-Matching Unit (BMU); and (iii) update of the codebook vector of each node [58–61]. SOM's are also specially good for clustering the data applying hierarchical clustering methods to the codebook vectors obtained [59, 61]. This Figure shows the results of Ward's clustering to the hydrogeochemical dataset, where the rainwater sample was included on C3, together with sampling wells near the area of Castagneto Carducci (P102, P104, P105 e P106). In the right figure it is possible to observe the geographical location of the clustered points from the self organizing maps for the year 2018. In the southern part of the territory the waters are characterized by a hydro-chemical composition similar to rainwater (green dots). Only one point is blue, even if its location in the cluster over time has always been found to be on the border between the C1 cluster and the C3 clusters.*

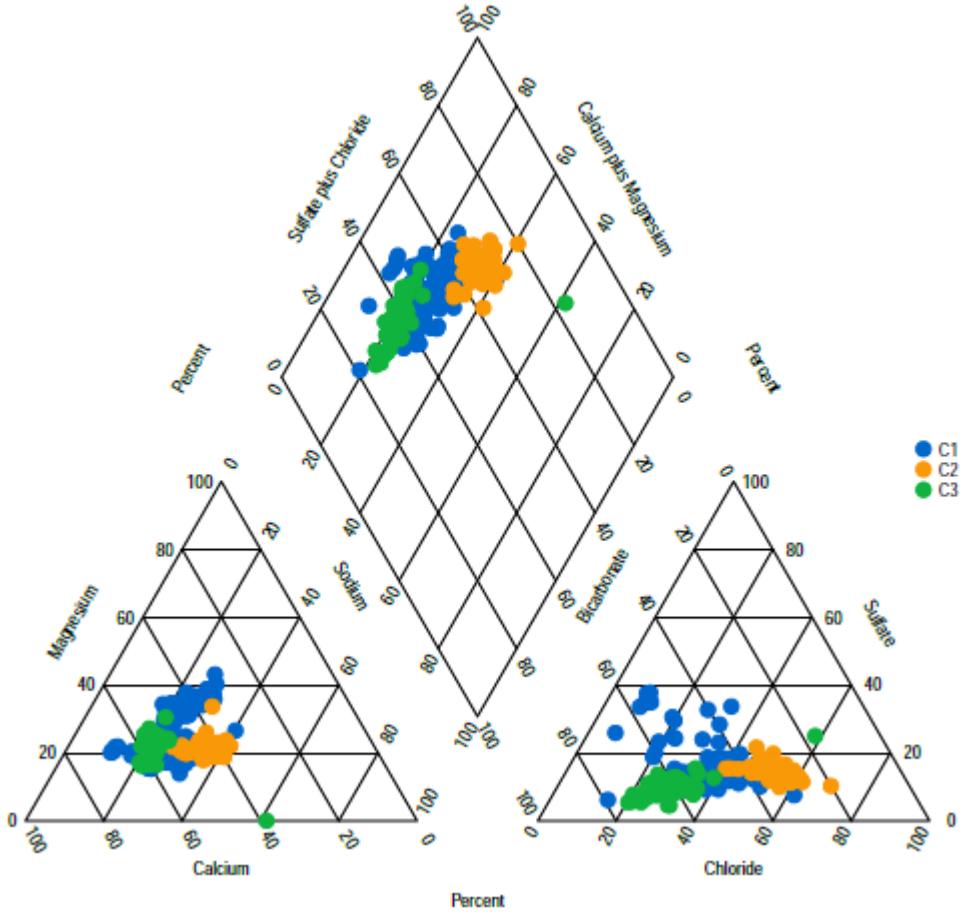

Figure 2.8: *A Piper diagram [62] is shown with all the data points used coloured according to the SOM clustering. All points associated to C3 fell within the magnesium-bicarbonate facies, except one. This point fell in the same location that other 2 points in the SOM map, as a consequence of the simultaneous consideration of all chemical parameters and of the standardization of the values. However, in the traditional Piper diagram, the more dominant ions exert a stronger influence over the location of the point in the central diamond. Thus, the similarities that may exist on the other ions is disregarded and underlying processes might be overlooked.*

Chapter 3

Material and Methods

"Believe you can
and you're halfway there"
Theodore Roosevelt

3.1 Recharge estimation

Several studies have been carried out focused on groundwater recharge estimation all in different geological, geomorphological, climatic and technological settings. Many factors must be considered to select an appropriate recharge calculation method, like: aquifer depth, degree of soil moisture, subsoil lithology, rainfall time series and temperatures. A correct interpretation of the geological structure an the evaluation of soil types and their use is also of particular importance for selecting the calculation method. Furthermore, the choice of space-time scale is also an important factor to be considered. In many cases, an integration of methods has been used to improve the recharge calculation which, even today, remains the most difficult parameter to measure [38] in groundwater resources evaluation.

3.1.1 Overview of the methods for groundwater recharge calculation

Groundwater recharge can be calculated using physical, chemical, empirical and indirect techniques. Lysimeters are widely used to measure water percolation under the vegetation zone and after evapotranspiration processes. It is the most important direct method to measure water drainage. Through its use, the recharge value can be indirectly estimated from a balance equation. Generally measurements must be taken at the beginning of the rainy season, at a certain time of the year, and they are calculated weekly. Although it is a direct method useful for the evaluation of low-flow infiltration recharge, lysimeters must have adequate dimensions to carry out measurements for long monitoring periods. Thus, the main limitations for this technique are its high costs and its scarce ability to represent the natural spatial variability of the subsoil [63,64]. Other direct methods that allow the determination of groundwater recharge involve using seepage meters and infiltration meters.The seepage meter consists of a watertight seepage cup connected by a tube to a flexible bag for holding water. The cup isolates a known surface area of canal bottom. Water seeping through this area comes from the flexible bag and may be measured. The flexible bag of water, being submerged, maintains the same head on the test meter as the surrounding area of

the canal bed. On the other hand, infiltration meters allow the determination of the amount of water infiltrating downwards. This method requires several measurements over long time periods. It has the advantages of being easy to use, fast and economic, it also provides precise estimates of the top level. However, to produce representative values it would be necessary to carry out several measurements in several points of the study area.

An empirical method to calculate groundwater recharge, is the water budget of a hydrological unit. This budget takes into account all incoming and outgoing water quantities over a specific period of time.The water budget method is based on a balance equation in which the recharge term is estimated as a "residual" of the equation [65, 66]. It is applicable to different time space scales and it is easily applicable if all the components are accurately measured. Thus, in order to be applied it requires a detailed knowledge of the regional or watershed hydrological processes. Unfortunately, it is difficult to estimate all the parameters with adequate accuracy. This method provides reasonable estimates when rainfall significantly exceeds evaporation. For example, if rainfall and evapotranspiration quantities are similar (semi-arid environments), this estimate is less accurate [67, 68].

Other empirical methods are: soil moisture balance and Darcy's law method. The soil moisture balance method is used when there is not significant outflow and from a simple balance equation it is possible to derive the recharge term [69]. This method is easy to apply, but requires complex evapotranspiration measurements and precise estimates of precipitation and losses for the considered system. In the humid and arid regions, this method turns out to be unsuitable [70], providing unreliable recharge measurements.

In the Darcy's law method for the unsaturated zone, only the gravity (constant) is taken into account, so that the quantities of water that tend to go downwards (recharge) will be equal to the hydraulic conductivity of the ground multiplied by the hydraulic gradient. Hence, the water that passes through the unsaturated zone contributes to the recharge in a one-dimensional flow [68]. The major difficulties that can be encountered applying this method are: the measurement of the soil-water potential gradient and the evaluation of the variability of soil hydraulic properties of the study area. The Darcy's law method provides a precise recharge estimation in a wide time interval and the method's goodness depends on the degree of accuracy of both the hydraulic conductivity measurement and the moisture content. Moreover, this approach does not indicate total recharge since it only takes into account the diffused flow or the matrix; while if the top-up is due to preferential flows it must be determined separately [38].

Darcy's law is also used to estimate the groundwater flow of a confined aquifer, considering a constant flow and no water extraction. The flow is calculated by multiplying the hydraulic conductivity by the hydraulic gradient. The hydraulic gradient must be estimated along the flow path and must be at a right angle to it. The volumetric flow in the cross section of an aquifer is equal to the recharging speed multiplied by the surface. This approach can be applied to large surfaces ($Area \approx 1 - 10.000 km^2$), although it is not suitable for areas where there is significant variability in hydraulic conductivity and hydraulic gradient [66]. Furthermore, the high variability present over large areas generates uncertainty both on the recharge estimates, on the accuracy of the estimation of saturated aquifer thicknesses.

The zero-flow plane method considers the plane in which the vertical hydraulic gradient is equal to zero, so if the water present in the soil moves upwards above this plane this happens thanks to

evapotranspiration, while below is the phenomenon of percolation [70]. The recharge estimation depends on the accuracy of the water content measurements. Furthermore, the method provides a precise estimate of the top-up, so multiple measurements are required in multiple positions for a representative estimate of the study site. Finally, this approach requires experience and is relatively expensive in terms of tools required and of amount of data collected.

Another possibility is to quantify groundwater recharge through the basic flow discharge using the water balance. In this approach, groundwater recharge is equal to the discharge. Then, assuming a balance between discharge and recharge, this will be equal to the basic flow [68]. The critical points of this method concern the parameters useful for recharging. These in fact must be reliable and independently calculated. Moreover the method is not very accurate if applied in basins with pumping, evapotranspiration and significant underflow towards deep aquifers. However, the method is simple, easy to apply, and appropriate for areas where the groundwater is shallow and flows are generally increasing [70].

Recharge rates on large areas are also calculated by modeling rainfall runoff, where it is a residue in the water balance equation. The estimate is regulated by the accuracy of the measurement of the balance's parameters at a given time scale [71]. For example, Lumped models, perform a unique recharge estimate for the entire basin. Other models can be spatially divided into units based on their hydrological or hydrogeomorphological response. These small scale models are more suitable to obtain the measurements of the balance parameters. The measurements performed at a daily pace are better because they allow a more precise measurement of the recharge, this being a larger component of the water balance at smaller time scales [38]. This indirect method allows to measure the recharged quantities as a residue through a good measurement accuracy of the water balance parameters.

The evolution of computers, together with the increased development of specific calculation codes has enabled the generation of long-term simulations of groundwater recharge. For the unsaturated zone, the recharge estimates are made on the vertical and horizontal drainage rates, even if these do not always reflect the actual recharge rates. These techniques are often applied to unsaturated zones located in areas considered arid or semi-arid [38]. The reliability and accuracy of the recharge estimation through these techniques should be compared with other methods such as lysimeter or tracers. Moreover, many approaches are used to simulate the flow in the unsaturated medium, such as the numerical solutions of the Richards equation [72]. The positive points of this method are its fast calculation time and ability to evaluate the sensitivity calculation output for various parameters, making it possible to predict future recharge scenarios according to the different environmental conditions. However this type of models are limited to the study of small areas ($Area \leq 100m^2$) or to the one-dimensional flow in the subsoil ($Depth \leq 15m$). So, considering non-linear relations between recharge, hydraulic conductivity and water content, these measurements when performed in the unsaturated medium can be highly uncertain.

Evaluation of recharge through groundwater models gives parameter values with a good degree of accuracy [73]. The data obtained can be verified afterwards by comparison with values obtained using the water table fluctuation method or the infiltration equation [74]. The limitations of this recharge calculation method are related to errors due to the characteristics of the model itself and associated to the validation process.

The central concept of the tracer technique is that it retains its mass by moving freely in the

water, not being absorbed by the soil or vegetation. These conditions are also the conditions of uncertainty of the method. The tracers are divided into two categories: chemical and isotopic. In the first case we speak of natural or artificial tracers. Once applied they provide accurate recharge estimates because they are independent of the outflow conditions of the investigated system. The application of the tracers allows to control the execution times, the positioning and the quantities used in the study area and finally the uncertainty relative to the first meter of soil can be avoided if injected below this meter [75].

To estimate the recharge, the tracers are applied to the soil surface, or at a specific depth, so that rainfall or irrigation water carries the tracer downwards. Once a certain period of time has been established, its distribution in the subsoil is studied by digging a trench or by drilling at the injection point. The spatial distribution of the tracer makes it possible to establish the recharge rate [65, 76]. The chemical tracers are applied in single points and on small areas. The hydrological interpretation of this application not only depends on the time between application and sampling, and the application depth. The validity of the physical model used to describe the flow of water in the system studied also affects its interpretation [77]. The application of this method does not present risks of environmental pollution, it is easy to perform, generally has low costs and can be seen through the use of appropriate associated dyes [64]. Despite this, the presence of preferential routes could give inaccurate estimates of the actual recharge. Furthermore, the process of absorption of some chemicals by the vegetation could be significant, while attention should be paid to the concentrations of tracer in input as these tend to become negligible with depth [64].

Isotopes are currently widely used for hydrogeological and hydrological environmental studies and assessments. These are divided into two categories: stable and radioactive. Stable isotopes ^{18}O, ^{1}H and ^{2}H are generally used to identify the recharge of river and lake aquifers. This is because the isotopic composition of O and H in groundwater does not change considering the water-rock interactions at low temperatures.However, its use to estimate the recharge is cumbersome because the time scales range from seasonal in high-flow areas to hundreds of years in low-flow areas [38].

Currently ^{3}H is the most conservative of all radioactive tracers, but its use is prohibited in many regions for environmental protection reasons. As with the chemical tracers, either stable or radioactive isotopes are injected through the surface of the ground or at a certain depth and its vertical distribution is used to estimate the recharging speed. These tracers can be applied to multiple sites, and coupled with methods such as kriging or Thissen polygons the evaluation of the reload in the study area can be improved [76]. X-ray tracers fall into the category of direct methods, allow accurate results to be obtained, have no absorption problems and do not require long sampling periods. On the contrary, in some countries they may be prohibited and have high analysis costs.

In many cases the groundwater recharge calculation has been performed using the chloride concentration (natural tracer) method [65, 78–81]. To implement this method it must be assumed that: chloride is the only source of Cl in groundwater, there is no loss of Cl during evapotranspiration, the geological formation of the unsaturated zone does not contain chloride, there is no significant run off, there is no drainage in the subsoil by minor rivers or streams, agricultural activities are not a source of chlorine, vegetation does not absorb chlorine, there are no inputs from industrial activities, and recharging occurs through the soil matrix [69, 82]. The degree of

uncertainty therefore depends on the compliance with all the above mentioned conditions. In arid or semi-arid regions where rainfall is considered scarce (500 - 700 mm per year) the outflow is negligible. In humid and sub-humid regions (1000 - 2500 mm per year) instead a good quantity of water is drained through surface runoff www.fao.org. Furthermore it is difficult to assess the degree of influence of cultivated fields, as well as the possible amounts of chlorine released by the surrounding industries [83, 84]. Consequently the calculation of the recharge through the use of the concentration of chlorine is difficult to measure exactly. This approach is simple to apply, low cost and suitable for dry areas.

The recharge can be calculated through historical tracers that derive from human activities occurred in the past (bromide, nitrate, atrazine or arsenic). Despite this, the geochemistry of these elements makes recharge estimation difficult. For example, a deep infiltration of thermonuclear tracers has been observed in sandy soils in dry environments [85]. The advantage of this method is that there are no costs for the use of the tracer, while the uncertainties generally derive from the difficulty of sampling and from the depth of infiltration of the tracer.

By estimating the age of the groundwater it is possible to determine the recharge rates. The age of the groundwater, or the time elapsed once the water enters the saturated zone, can be calculated from the ratio between tritium and tritiogenic helium, while the recharge rates are average rates calculated in the period represented by the age of the waters underground. The recharge can be estimated through calculation of the age along vertical profiles positioned in more points or using the speed reversing the age gradient and multiplying this speed by the porosity inside the depth interval [86]. This approach is easy to implement when the survey instrument is available, however it is very expensive.

Finally, in recent years, for estimating groundwater recharge at a regional scale, technical combinations of remote sensing, GIS and geostatistical approaches have also been used [87–90].

3.1.2 Water table fluctuation method

The Water Table Fluctuation (WTF) approach is useful to estimate recharge in shallow unconfined aquifers that show steep water level rises and declines [28]. This method considers a significant input flux (infiltration of precipitation) that causes a rise in the water table level, once entering the saturated zone. After this effect, the dissipative processes that take place in the saturated zone bring the water table into a steady-state level [91].

Then, the effective change in time attributable to recharge Δh multiplied to specific yield S_y gives the recharge estimation:

$$R_r = \frac{S_y \times (h_1 - h_2)}{(t_1 - t_2)} = \frac{S_y \times \Delta h}{\Delta t} \tag{3.1}$$

where water-table data are expressed as a height Δh (meters) above the steady state position.

Under these conditions, the amount of recharge water that compensates recessional processes (evaporation, discharge to springs or lateral saturated-zone transport) needs to be corrected for. In fact, possible error sources for this method are [92]:

- Diurnal fluctuations driven by high evapotranspiration

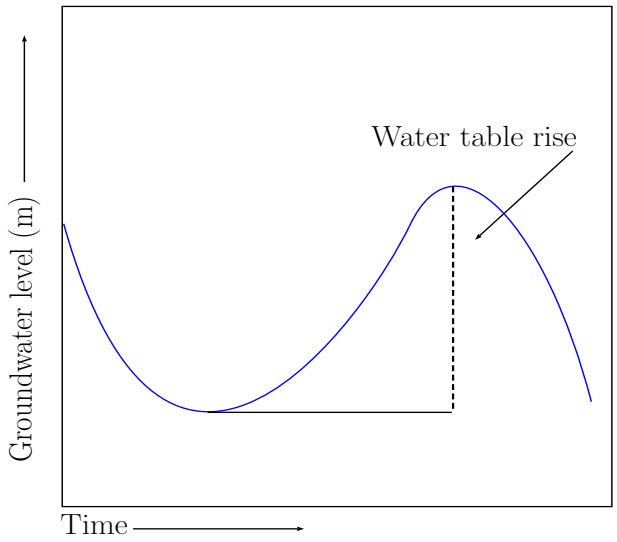

Figure 3.1: *A simple outline of underground water table level rise.*

- Heavy groundwater pumping
- S_y calculation
- Changes in atmospheric pressure
- Pressure changes due to entrapped air
- Rapid conversion of capillary water to phreatic water where the water table is near the ground surface

Despite the uncertainties associated to it, the WTF approach is widely used because it is simple and requires little data for analysis. Furthermore the mechanism of water displacement in the unsaturated area is independent, as well as the areal integration of the recharge [93]. To verify the presence of different processes, mechanisms or sources of error, the time series of precipitation should be compared with the recharge estimates obtained with this method [38].

Another advantage of the WTF method is that it takes into account the combination of all recharging sources and the existence of preferential flow paths does not imply a limitation [93]. It also provides information on transient recharge trends [80] and it is possible to verify long-term changes in recharge quantities calculated due to climate changes [2, 38].

3.1.3 Master recession curve (MRC)

A Master Recession Curve (MRC) can be defined as the relation between the value of a measured response R (in our case water table level) and its rate of change in time within a period, when there aren't any others external inputs to the system [2,70,91,94]. Thus, understanding water table level recession periods is fundamental not only for the groundwater component, but also to better understand unconfined aquifers properties [94]. For the recession analysis, hydrograph analysis is necessary to determine the baseflow component [95, 96]. This, usually can be achieved through three different approaches [97]:

i. Analytical expressions for recession analysis

ii. Graphical methods for master recession curve determination

iii. Parameterization based on the flow recession rates as a function of flow

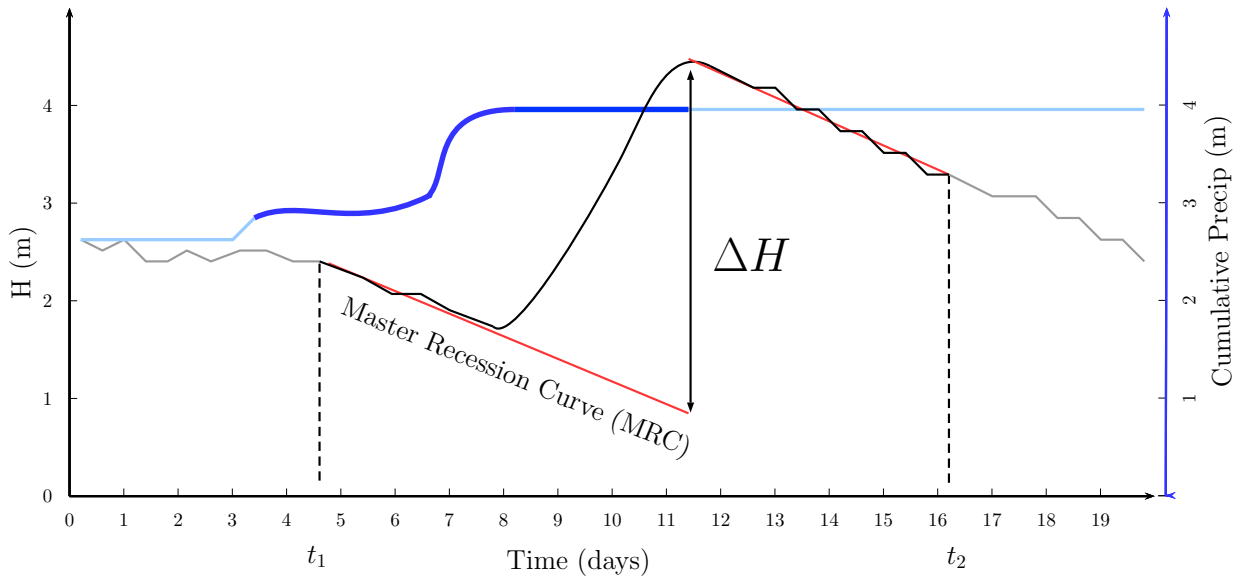

Figure 3.2: *Water table level behavior Ht representation. On the y-axis the level of the water table is shown in meters, while on the x-axis the time is represented. in the second axis of y the cumulative precipitation (meters; blue line) is instead represented, in which the dark blue color represents the precipitation event (storm) involved in the recharge episode. The red curves are the MRC fit extrapolations and distance between the two extrapolations gives the total recharge episode.*

3.1.4 Episodic master recession (EMR)

The Episodic Master Recession method (EMR) determines periods of significant water level rises. These periods are estimated using a MRC. This curve is a mathematical representation of the expected water table decline in the absence of episodic recharge as a function of hydraulic head [98]. If d_T is considered as an estimate of the maximum magnitude of water table fluctuations caused by factors other than recharge, a recharge event is identified by [92]:

$$\Delta H > d_t - \Delta H_{MRC} \tag{3.2}$$

where ΔH is the significant water table level change and ΔH_{MRC} represents the water table decline in the absence of recharge (obtained with the MRC extrapolation). Then, any recharge episode begins when this threshold is exceeded.

During a hydrographic analysis problems may arise related to the subjectivity in the hydrological perception of the variations, for example linked to the significance of fluctuations, which cannot be eliminated [99]. Despite this, thanks to an adequate parameter setting it is possible to limit this problem [2].

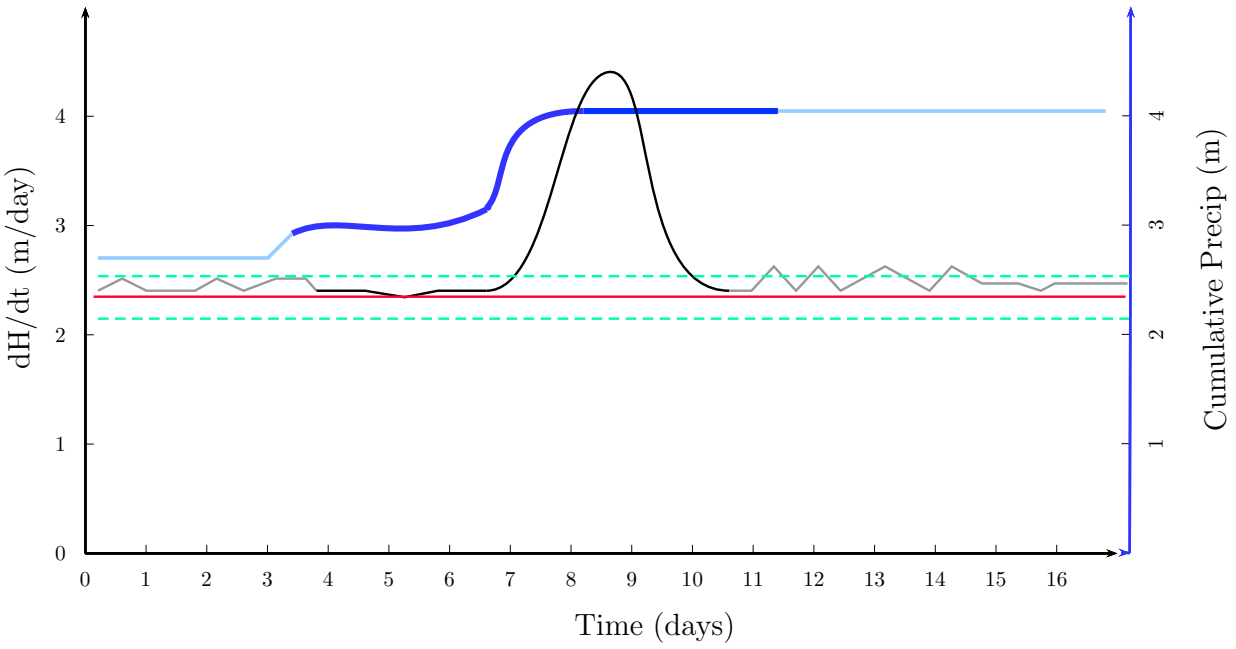

Figure 3.3: *Time rate of change dH/dt (black line) with MRC (red line) and tolerance bands (dashed green line).*

Thanks to MRC and EMR codes written for the open-source statistical software R [48], critical hydrological parameter values can be estimated and run using specifically designed packages available for RStudio (R's graphical user interface) [2,48,91]. In order to generate a good MRCfit and EMR outputs they both require an iterative process evaluation before-hand. The dataset used to generate MRCfit and EMR results is:

i. Time as a numerical quantity (e.g. daily time series)

ii. Water-table level (e.g daily time series)

iii. Cumulative precipitation(e.g daily time series)

The pure recession period is identified by a segment of the curve with a certain degree of slope (slope element). This element can be approximated to the length of a straight line and is adjustable through the use of the length parameter [2]. The *Resplimits* parameter defines the slope element within a range of values. With the *Mindrytime* parameter an input time period that is not significant for the system is considered. The *Maxtick* parameter indicates the maximum total value of the rises within the slope element. The amount of non-significant precipitation in the recession period is indicated with *Maxdelprec*. Within the recession period, data gaps must not be present and this period must not overlap with other selected inclination elements [2]. The inclined elements included are preferably taken as those representing the first parts of the recessive intervals [2,91].

Once the iterative process for the evaluation of the parameters indicated above has been carried out, the rate of decline of each slope element is calculated by linear regression of the data within it. The decline rates are coupled to the variable R from the midpoint of each slope element and

Table 3.1: *Master Recession Curve parameters in MRCfit [2].*

Name	Type	Meaning
Resplimits	numeric	min./max. limits values of slope elements
Tslength	numeric	duration of slope elements for linearization
Mindrytime	numeric	duration between significant precipitation and recession start
Maxdelprec	numeric	max. amount of precipitation considered negligible
Maxtick	numeric	max. total uptick within a linearized slope element
Throughorigin	true/false	force the fit through the origin
Binsize	numeric	bin size for lumping of dR/dt for fitting (0 for no binning)
Maxslope	numeric	max. allowable dR/dt for fitting

from their adaptation, the optimized parameters of the MRC are obtained. Other parameters that can be adjusted are the maximum *Maxslope* decline rate and the *Binsize*, with which you specify the number of bins (elevation interval [100]) thanks to which equidistant elevation bins (averaged values) are generated that range from the lowest to the highest altitudes. If the data are many and exhibit an irregular trend, the bins should be used [100]. Furthermore, it is possible to obtain a geometric meaning from several MRC estimates. In fact, by modifying *Resplimits* (response limits) one can take into account the lithology of the substrate, most likely connected to slope elements which show different slope [2]. From the analysis of the MRC the slope and intercept values are obtained which will define the line that represents the MRC adapted for the EMR analysis. During the execution of the EMR program the parameter to which particular attention must be paid is the *Fluctol*, through which the tolerance of the fluctuation is regulated in stationary conditions. A delay value should be determined to give a representation of the time needed for the amount of water that infiltrates the soil to reach the saturated area and generate a recharge event [2]. Furthermore, if the rain gauge is far from the well in which the stratum levels are measured, the difference between precipitation input and response may not follow the predicted relationship. The *Ependpar* parameter is useful for approximating the time needed to achieve the pre-event behavior, while the *Minprecip* parameter indicates the minimum quantity that will cause a real response.

Table 3.2: *Episodic master recession parameters [2].*

Name	Type	Meaning
Lagtime	numeric	lag time between start of input and response of hydrograph
Ependpar	numeric	parameter used in determining episode end
Fluctol	numeric	max. rate of change of response dR/dt, allowable as system noise
Minprecip	numeric	min. amount of precipitation to allow inclusion as an episode
Nsmooth	numeric	max. used for smoothing of the computed hydrograph slope

3.2 Geophysical estimation of Sy

3.2.1 Overview of methods for Sy calculation

For unconfined aquifers the most natural field method to estimate the value of Sy are pumping tests. However, it has been found that for many cases the Sy value obtained was an underes-

timation, reducing his efficiency [101–103]. To address this limitation, some authors have modified the starting conditions of the pumping tests. For example, observing the delayed yield when the interpretation of pumping tests [102, 103] or calculating the ratio between the cumulative volume of pumped water and the volume of the groundwater cone [104, 105]. The determination of Sy also has other difficulties: duration of the pumping test; geographical position of the test execution point and its observation point [106, 107], long times required for execution of the test, and high costs associated to the development of models that consider different phenomena (heterogeneity of the aquifer), even if they improve the estimate [108–111]. An alternative method to determine Sy involves using a neutron probe. In this method the whole interior of observation wells is used to determine the vertical profiles of the volumetric water content [112]. The major drawback of this method is that its use is extremely regulated and limited to the state laws in force at the moment. Another possibility to obtain Sy values is through the evaluation of the changes in gravity over time. These changes can be used to estimate variations in groundwater storage in unconfined aquifers [113]. This method allows for variations in hydraulic properties including Sy. However, a minimum variation of the water table equal to 0.3 m is required to be reliably detected [114]. Moreover, an integration of the vertical direction is obtained as a result. This prevents from discretization of the vertical variations in Sy. In addition to this drawback, field procedure and sand data processing are laborious [113, 114]. The Magnetic resonance sounding (MRS) method is a method used for large-scale data acquisition. This method allows to record magnetic resonance signals emitted by water molecules in aquifers. Consequently, many studies have turned towards this method with the aim of finding links between the hydraulic properties of the aquifer [115]. Finally, although geoelectrical methods are widely used for the characterization of aquifers and their main hydraulic properties [116, 117], few studies have been addressed to the evaluation of Sy. For example, good Sy values were obtained using vertical electric probes, deriving a modification of Archie's law [49, 118]. However, this approach implies ignoring the the lateral variations of resistivity. Finally, the time-lapse Electrical Resistivity Tomography (ERT) has also been used to map water content variations in response to phreatic level fluctuations [101] making ERT a possible approach for evaluating variability in the space of the Sy.

3.2.2 Electrical resistivity tomography (ERT) in DC current

Electrical Resistivity Tomography (ERT) in DC current has been proved as one of the most reliable and effective methods for groundwater exploration, since resistivity is influenced by lithology, pore fluid chemistry and water content. Electrical methods are very versatile, and can be applied in a wide range of survey configurations. The approach adopted will depend on:

- Objectives of the survey
- Expected spatial variability of electrical properties
- Access to suitable electrode sites
- Equipment availability
- Data processing capabilities

In surface applications, ERT can be used for 2D and 3D representations [119], depending on the spatial resistivity variation, the depth and the resistivity contrast between target and background values. Usually 2D profiles are performed by using a multi electrode configuration with automatic measurements of potential difference across couples of electrodes. In this manner one can obtain a profile of resistivity values along vertical and horizontal directions. This is one of the main strengths for the ERT method and it also allows the detection of subsoil changes in particularly complex environments. 3D applications are often used where targets are well defined, and restricted to a portion of subsoil (i.e. plumes or filtration paths). Moreover, multi temporal ERT surveys have also proven to be useful to highlight the changing of water content in the vadose zone.

3.2.2.1 Theory and basic principles

The purpose of an electrical resistivity survey is to individuate the soil spatial resistivity distribution. The resistivity of a medium is defined as follows:

$$\rho = R \times \frac{S}{L} \tag{3.3}$$

where R is the electrical resistance, L is the length of a cylinder and S is the area of its cross-section.

The electrical resistance R is defined by the Ohm's law as follows:

$$R = \frac{V}{I} \tag{3.4}$$

where V is potential and I is the current.

In a homogeneous half-space, with point source of current, the current flow is radial from this point and electrical equipotential surfaces are hemispherical.

In this configuration the potential can be expressed through the resistivity and the current:

$$V = \frac{\rho \times I}{2 \times \pi \times R} \tag{3.5}$$

In an elementary quadripolar configuration, on a homogeneous subsoil and with four electrodes called C1, C2, P1, P2, the injection of current from C1-C2 dipole produces a current flow and a correspondent potential field with equipotential surfaces, which can be measured through the P1-P2 dipole. The potential difference measurement between the P1-P2 dipole can be expressed in analytical way by the equation:

$$\Delta V = \frac{\rho \times I}{2 \times \pi} \times [\frac{1}{C1 \times P1} - \frac{1}{C2 \times P1} - \frac{1}{C1 \times P2} - \frac{1}{C2 \times P2}] \times \frac{\Delta V}{I} = K \times \frac{\Delta V}{I} \tag{3.6}$$

where C1P1, C2P1, C1P2 and C2P2 represent geometrical distances among every couple of electrodes C1, C2, P1, P2.

The electrical resistivity can then be calculated as follows:

$$\rho = [\frac{2 \times \pi}{(\frac{1}{C1 \times P1}) - (\frac{1}{C2 \times P1}) - (\frac{1}{C1 \times P2}) - (\frac{1}{C2 \times P2})}] \times \frac{\Delta V}{I} = K \times \frac{\Delta V}{I} \tag{3.7}$$

where K is a geometrical factor that depends on the relative disposition of the four electrodes (quadripolar configuration in figure 3.4).

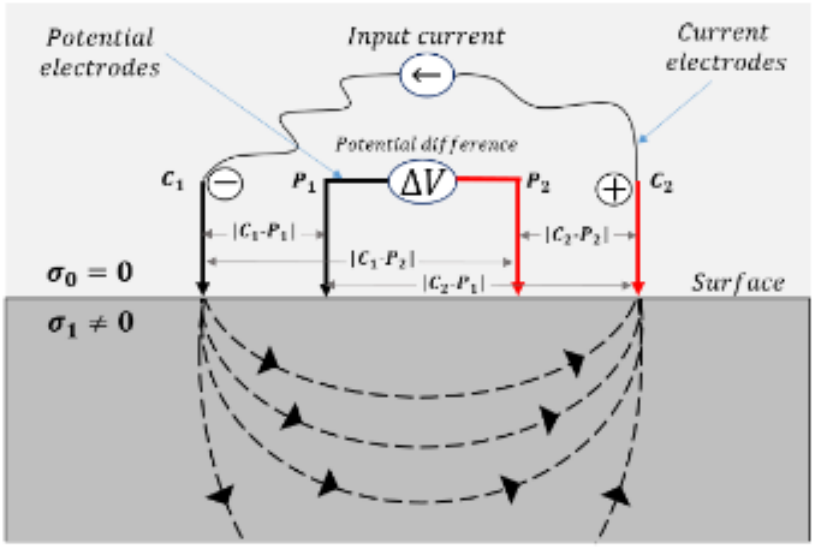

Figure 3.4: *Elementary quadripolar configuration in homogeneous half-space.*

For non-homogeneous subsoil, the current flow distribution depends on the resistivity of the medium, and the current flow is concentrated into the more conductive volume. Potential difference patterns provide information on the form of subsurface heterogeneities and of their electrical properties [120]. Subsurface electrical resistivity depends on textural and structural characteristics and is sensitive to the water content [121], therefore it can be considered as a proxy for the variability of soil physical properties. More in specific, the electrical resistivity is a grain size and mineralogy, voids intended as pore size distribution and connectivity, fluids content on pore and their resistivity properties and temperature. Electrical resistivity values for soils, range from a few Ωm to several tens of thousands Ωm. In terms of electrical conductivity, most of the soils are composed by insulating grain minerals, clayey conductive minerals and in minimum cases of metallic conductive minerals. The underlying electrical conductivity mechanisms are different depending on the prevalence of these minerals: if insulating grain minerals prevail, the current flow is mainly governed by electrolytic conductivity and takes place through the moisture-filled pores; in the case of clayey soils, resistivity depends of the electrical charge density at its surface and is related to the clay's cation exchange capacity Table 3.3. Finally when massive minerals are present without discontinuities, the current flow is a consequence of the displacement of free electrons.

Thus, both air and water content, as well as the resistivity variation in the subsoil are a consequence of the distribution of voids and their connections (i.e. grain size and textural structure), which depend on the depositional environment. Archie's law relates resistivity and porosity for

Table 3.3: *Exchange capacity of common clays.*

Clay	**Exchange Capacity**
Kaolinite	3 to 15 m-equiv/100 g
Halloysite $2H_2O$	5 to 10
Halloysite $4H_2O$	40 to 50
Montmorillonite	80 to 150
Illite	10 to 40
Vermiculite	100 to 150
Chlorite	10 to 40
Attapulgite	20 to 30

water saturated geological materials in absence of surface conductivity (i.e. without clay):

$$F = \frac{\rho}{\rho_w} = a \times \Phi^m \tag{3.8}$$

where F is the formation factor often assumed to be an indicator of hydraulic tortuosity, ρ and ρ_w are resistivity of formation and pore water, a and m are constants related to the coefficient of saturation and the cementation index respectively, and Φ is the porosity. Archie's law implicitly assumes that the effective porosity Φ_e is equal to the total porosity (Φ) of the sample, and that all electrical conductivity in a water-saturated rock or soil results from the migration of ions in the bulk pore-solution. If there are isolated pores through which ions cannot migrate, then $ne<n$, and Archie's law will over-predict sample conductivity [3]. Archie showed that m ranged from 1.3 for unconsolidated sands to approximately 2.0 for consolidated sandstones. Jackson et al. (1978) [122] made electrical conductivity measurements on natural and artificial sand samples, determining that m increased as the grains became less spherical while variations in grain size and sorting had little effect.

When electrical conductivity is only a consequence of the ionic content in the water, if the the resistivity of pore water is known as well as the resistivity of formation and empirical parameters a and m , is possible to calculate the porosity. Thus, Archie's law appears to be a powerful law to estimate the porosity Table 3.4, however its usefulness is limited when surface conductivity is not negligible and when applied to the vadose zone. Conductivity of an electrolyte is proportional to: the kind and total amount of dissolved ions, and water viscosity [123]. Thus, electrolytic conductivity has a large range of variations, which may change from soil to soil. Several ERT researches have been focused on studying these facts, aiming to delineate saline water intrusion areas into the coast [124,125]. Many studies were conducted about the estimation of water content focused on salinity variation. In some cases, it has been shown that, the volumetric water content relates to resistivity for different pore-water conductivity [126].

3.2.2.2 Geophysical data gathering

As previously mentioned, the ERT method has been applied in a wide range of survey configuration into the space, depending on target geometry and its spatial and temporal variability. Two-dimensional multi-electrodic arrays provide a 2D resistivity image of the subsoil. In this ar-

Table 3.4: *Archie law exponents (m) of different consolidated and non consolidated media [3].*

MEDIUM	**Porosity Range**	**Archie's Exponent**
clean sand	0.12-0.40	1.3
consolidates sandstones	0.12-0.35	1.8-2.0
glass spheres	0.37-0.40	1.38
binary sphere mixture	0.147-0.29	1.31
cylinders	0.33-0.43	1.47
disks	0.34-0.45	1.46
cubes	0.19-0.43	1.47
prisms	0.36-0.52	1.63
8 marine sands	0.35-0.50	1.39-1.58
glass beads (spheres)	0.33-0.37	1.20
quartz sand	0.32-0.44	1.43
rounded quartz sand	0.36-0.44	1.40
shaley sand	0.41-0.48	1.52
shell fragments	0.62-0.72	1.85
fused glass beads	0.02-0.38	1.50
fused glass beads	0.10-0.40	1.7
sandstone	0.05-0.22	1.9-3.7
ploydisperse glass beads	0.13-0.40	1.28-1.40
sandstones	0.07-0.22	1.6-2.0
limestones	0.15-0.29	1.9-2.3
Syporex	0.80	3.8
Bulgarian altered tuff	0.15-0.39*	2.4-3.3
Mexican altered tuff	0.50*	4.4
glass beads	0.38-0.40	1.35
quarz sand	0.40-0.44	1.45
tuff particles	0.60-0.64	1.66
*connected (inter-granular) porosity	-	-

ray, the current and potential electrodes are maintained at a regular fixed distance from each other and are progressively moved along a line at the soil surface. At each step, one measurement is recorded. The set of all these measurements, at this first inter-electrodic spacing gives a horizontal profile of resistivity values. Afterwards, the inter-electrode spacing is increased by a factor n = 2, and a second measurement level is done. This process (increasing factor n) is repeated until the maximum spacing between electrodes is reached. The larger n-values, the greater the depths of investigation in figure 3.5. As the distribution of the current also depends on the resistivity contrasts of the medium, the depth of investigation derived conventionally from the spacing, is also known as the "pseudo-depth".

The reciprocal position of each four electrodes for measurements, two for current and two for potential, leads to different configurations, which will be well explained later. Table 3.5 summarizes the different 2D array configurations and compares the following characteristics: the sensitivity of the array to horizontal and vertical heterogeneities, the depth of investigation, the horizontal data coverage, and the signal strength [4]. What configuration is chosen is crucial for the gathering of the geophysical data, since quadripolar configuration directly influences the results obtained. This choice strictly depends on: target geometry, sensitivity of the resistivity

Table 3.5: *Array configuration: Wenner, Wenner-Schlumberger, Dipole-Dipole, Pole-Pole, Pole-Dipole.*

	W	**W-S**	**D-D**	**P-P**	**P-D**
Structures horizontal array sensitivity	++++	++	+	++	++
Structures vertical array sensitivity	+	++	++++	++	+
Depth of investigation	+	++	+++	++++	+++
Horizontal data coverage	+	++	+++	++++	+++
Signal Strenght	++++	+++	+	++++	++

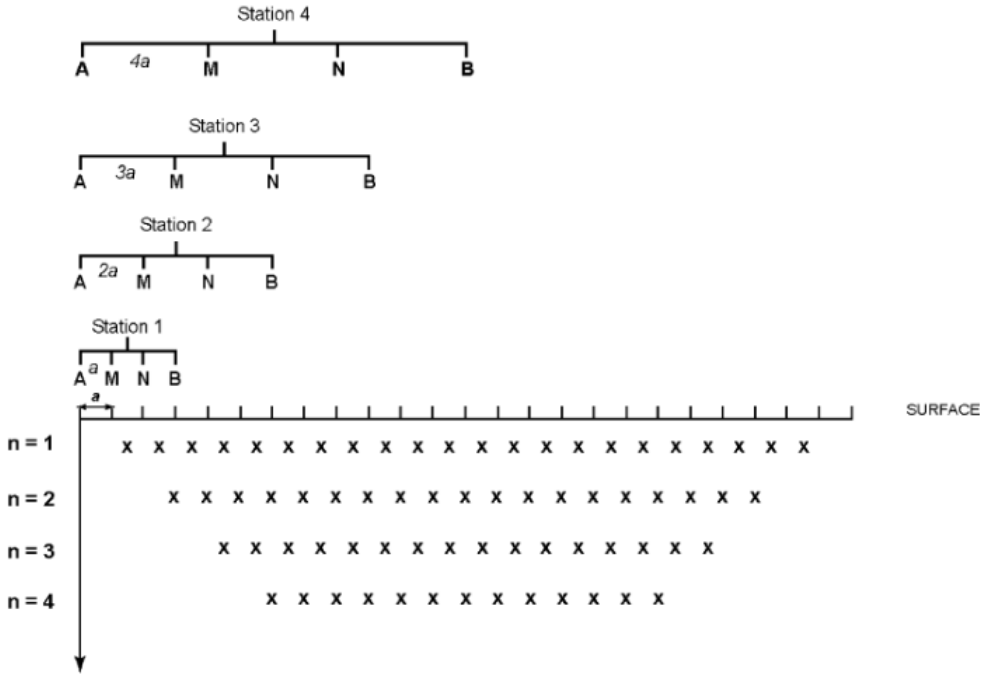

Figure 3.5: *Distribution of resistivity measurements on a 2D electrical resistivity pseudo section with n varying from 1 to 4.*

meter, and background noise level [127].

The Schlumberger reciprocal array is a manipulation of the classical Wenner-Schlumberger, where the current dipole is in the inner part of the quadripol. The larger distance of potential electrodes instead of the classical Wenner-Sclumberger makes it more sensible the telluric noise. One advantage of this configuration, in addition to the moderately sensitivity to both horizontal and vertical variations, is the possibility to use multi-channel optimization for simultaneous measurements. A drawback of this array is suffering possible effects of telluric currents in large dipole configurations [127] with respect to the Wenner-Schlumberger because of the reciprocal configuration. In presence of a high number of electrodes these features lead to a high-resolution, very low time-consuming configuration [128]. The high-resolution geoelectrical resistivity measurement were performed using the georesistivimeter Syscal-Pro Switch from IRIS Instruments (IRIS Instruments, 2003). The Syscal-Pro Switch is designed for intensive underground surveys, using the direct current method. It allows to automatically perform resistivity measurements (based on the voltage values, stacking number and Q factor) and record the resistivity variations

along the profile. Furthermore, it can measure the electrical chargeability of subsurface materials (Induced Polarization).

The Syscal-Pro Switch is composed of a single case containing:

- an internal switch that allows the employment of 96 electrodes;
- a georesistivimeter formed by a transmitter and a receiver.

The maximum output values are 800 V in the switch mode and 1000 V in the manual mode, 2.5 A and 250 W with the internal transformer and battery 12 V, which can be increased up to 1200 W with an external generator and AC/DC (IRIS Instruments, 2003). The system of acquisition (up to 10 channels) allows to carry out a maximum of 10 simultaneous readings, remarkably reducing the time of acquisition. The time of injection/measurement is variable between 0.25 and 8 seconds. The maximum configuration is 96 metallic electrodes with galvanic connection subdivided in 4 multi-conductor cables.

3.2.2.3 Inversion method

As explained in section 3.2.2.1, the immediate result of a 2D and 3D is either a resistivity pseudo section (2D) or a resistivity pseudo volume (3D). Thus, to obtain an electrical resistivity image, the conversion from the apparent resistivity values to the resistivity model is necessary. To obtain this conversion, it is necessary to apply the RES2DINV [129] routine. The distribution of the data points in the pseudo-section is loosely tied to the arrangement of the blocks. The distribution and size of the blocks is automatically generated by the program using the distribution of the data points as a rough guide. The depth of the bottom row of blocks is set to be approximately equal to the equivalent depth of investigation of the data points with the largest electrode spacing [130]. A forward modelling subroutine is used to calculate the apparent resistivity values, and a non-linear least-squares optimization technique is used for the inversion routine [131, 132]. The program supports both the finite-difference and finite-element forward modelling techniques. The smoothness-constrained least-squares method (L2–norm) is based on the following equation:

$$(\mathbf{J}^t \times \mathbf{J} + \lambda \times \mathbf{J}) \times \Delta\mathbf{q}_k = \mathbf{J}^t \times \mathbf{g} \tag{3.9}$$

where:

- I = identity matrix
- λ = Marquardt or damping factor
- $\mathbf{J}$ = matrix of partial derivates (or Jacobian matrix)
- $\Delta\mathbf{q}$ = model parameter change vector
- g = discrepancy vector between observed data and model response data

One advantage of this method is that the damping factor and flatness filters can be adjusted to suit different types of data. The purpose of this program is to determine the resistivity of the rectangular blocks that will produce an apparent resistivity pseudo section that agrees with the actual measurements. The layer discretization depends on the array configuration applied to carry out the survey and in general the thickness of each subsequent layer is increased by a value ranging from 10% to 25% with the depth. The depths of the layers can also be changed manually by the user. The optimization method basically tries to reduce the difference between the calculated and measured apparent resistivity values by changing the resistivity of the model blocks. This difference can be assessed by the root-mean squared error (RMS). Iterations stop when reached a defined number or the variation in terms of RMS is lower than a threshold value; on other hand additional iterations don't give substantial improvement at the results. However the model with the lowest possible RMS error can sometimes show large and unrealistic variations in the model resistivity values and might not always be the "best" model from a geological perspective [127]. In general the most prudent approach is to choose the model at the iteration after which the RMS error does not change significantly. This usually occurs between the 3rd and 5th iterations [127].

The conventional smoothness-constrained least squares method (L2-norm) [131] attempts to minimize the square of the changes in the model resistivity values. This formulation is given by:

$$(\mathbf{J}^t \times \mathbf{J} + \lambda \times \mathbf{W}^t \times \mathbf{W})\Delta\mathbf{q}_k = \mathbf{J}^t \times \mathbf{g} - \lambda \times \mathbf{W}^t \times \mathbf{W}) \times \mathbf{q}_k \tag{3.10}$$

where q is the model resistivity vector.

The resulting resistivity image is a model with a smooth variation in the resistivity values and is suitable in the case of subsurface resistivity varies in smooth manner. In presence of sharp boundaries with high resistivity contrast the smoothness-constrained method produces images far from the real distribution of resistivity, that will change in a too smooth manner with respect to the real distribution. When the robust model constrain inversion method (L1-norm) is applied for the processing of the resistivity model, the program will attempt to minimize the absolute changes in the resistivity values. His formulation is:

$$(\mathbf{J}^t \times \mathbf{R}_d \times \mathbf{J} + \lambda \times \mathbf{W}^t \times \mathbf{R}_w \times \mathbf{W})\Delta\mathbf{q}_k = \mathbf{J}^t \times \mathbf{R}_d \times \mathbf{g} - \lambda \times \mathbf{W}^t \times \mathbf{R}_m) \times \mathbf{W} \times \mathbf{q}_k \tag{3.11}$$

This constrain tends to produce models with sharp interfaces between different regions with high contrast of resistivity values, and within each region the resistivity value is almost constant. This might be more suitable for areas where such a geological situation exists, such as the soil-bedrock interface over a homogeneous bedrock.

3.2.3 Specific yield (Sy) calculation

Specific yield (Sy) is defined as the average volume of water that can be drained, per unit surface of aquifer per unit drop of head, from the column of soil or rock extending from the water table to the ground surface [101]. The main purpose of interpretation of resistivity data is to determine the true resistivities and thicknesses of different layers purely from theoretical

considerations. These results were subsequently used to obtain a realistic picture of the geological framework. The geoelectrical method can contribute substantially towards obtaining initial measures that allow the estimation of the aquifer transmissivity and hydraulic conductivity from geophysical resistivity data. This method can greatly reduce the number of necessary pumping tests, which are both expensive and time consuming [118]. When the aquifer resistivity of saturated media and unsaturated layers is known, the specific yield of the aquifer can be calculated as follows [49]:

$$S_y = \left(\frac{\rho_w}{\rho_{sat}}\right)^{\frac{1}{m}} \times \left[1 - \left(\frac{\rho_{sat}}{\rho_{unsat}}\right)^{\frac{1}{n}}\right] \tag{3.12}$$

where ρ_{sat} is the aquifer resistivity (Ωm); ρ_w is water resistivity (Ωm); ρ_{unsat} is resistivity of unsaturated zone (Ωm); m is a coefficient that reflects the degree of cemented grains forming porous media; finally n is a parameter like m which is considered for aquifers and in most cases is equal to 2.

3.3 Statistical approach for hydroclimatic analysis

3.3.1 Hydroclimatic dataset reconstruction

The hydroclimatic analysis was conducted using the precipitation and temperature records available at the Tuscany regional hydrological database. The first step was to locate all the stations that fell within the study area. Afterwards, only those stations that had the greatest amount of daily records for the time period needed (1951-2018) were used to construct the time series to be analyzed. The stations selected using this criteria, as well as their location and ID are listed in table 3.6.

Table 3.6: *Geographic coordinates and altitude of raingaudges used to historical rainfall reconstruction.*

Weather station	**Latitude (°)**	**Longitude (°)**	**Altitude (m)**	**ID**
Bibbona	43.266	10.596	70.00	Bibbona1
Bibbona	43.262	10.597	70.00	Bibbona2
Bolgheri	43.247	10.553	9.62	Bolgheri
Castagneto Carducci	43.163	10.622	195.25	Carducci1
Castelluccio	43.226	10.618	70.11	Castelluccio
Donoratico	43.152	10.582	39.00	Donoratico1
San vincenzo	43.052	10.556	14.00	S.vincenzo2
Sassetta	43.131	10.646	320.00	Sassetta1
Sassetta	43.124	10.640	351.00	Sassetta2

Thus, the study area fell within the Bibbona and San Vincenzo villages at the North and South, respectively; while from East to West, it comprised from the coastline to the hills (figure 3.7).

A first review of the precipitation data showed a great amount of missing records. This hampered the construction of a 50 year time series [133] to conduct climatic change studies. One way to fill these gaps, is to perform data interpolation [47]. A time series can be reconstructed using precipitation records from nearby stations [47], as long as they show similar precipitation trends and that they have high correlation values. This approach also requires selecting one station to be completed. Taking into account both its location and the amount of gaps that needed to be filled, the station Carducci1 was the one selected for the reconstruction. This operation was possible thanks to the use of the package hyfo [134].

3.3.2 Change point and trend test

Change point analysis is useful to determine sudden changes in the mean and/or variance of the time series evaluated. Thus, this analysis is also known as discontinuity analysis, since from that point on the series behaves in a different manner. The change point analysis was carried out using an algorithm present in the R software libraries *Changepoint* [135]. In the first package, algorithm calculates the optimum position and the number of discontinuity points within the data through a user-defined method. For this research, the method selected involved the detection of changes using the mean and the variance of the data. On the other hand. The evaluation of the time series trends was done using both the Mann-Kendall and the Sen's Slope tests [136]. The Mann-Kendall test, is a non-parametric statistic method that evaluates the trend in a time series, taking as a null hypothesis that the samples that make up the complete dataset do not have any correlation and are independent between them. The Mann-Kendall test was designed to detect a monotonical data change (either increase or decrease), failing to detect sudden events and it is more sensitive to gradual changes in the evaluated trends. For the Mann-Kendall test, the m statistic is calculated using the equation shown in 3.13 where a_ij and b_ij are either the precipitation or the temperature values in the i and j times. A positive or negative value of m reflects increasing or decreasing trends respectively, where a_ij and b_ij are obtained using 3.14 and 3.15.

$$m = \sum_{i=1}^{n-1} \sum_{j=i+1}^{n} a_{ij} b_{ij} \tag{3.13}$$

$$a_{ij} = sign(y_i - y_j) \begin{cases} 1, \text{if} & y_i > y_j \\ 0, \text{if} & y_i = y_j \\ -1, \text{if} & y_i < y_j \end{cases} \tag{3.14}$$

$$b_{ij} = sign(t_i - t_j) \begin{cases} 1, \text{if} & t_i > t_j \\ 0, \text{if} & t_i = t_j \\ -1, \text{if} & t_i < t_j \end{cases} \tag{3.15}$$

In an erratic series that is, one where H_o is true, it is expected an m value equal to zero and with a variance equal to 3.16.

$$var(m) = \frac{n(n-1)(2*n+5)}{18} \tag{3.16}$$

The standard normal distribution (Z) statistic is calculated through the equation 3.17, for which Kendall proved that if n $\leq$ 10, the approximation to a Gaussian distribution can be considered acceptable.The results from the Mann-Kendall test are analyzed using the p-value, accepting the null hypothesis (H_o) if this value is below the 0.05 significance level. A positive value of Z reflects an upward trend (increase) while a negative value is associated to a downward trend (decrease).

$$z = \frac{m}{\sqrt{\frac{n(n-1)(2*n+5)}{18}}} \tag{3.17}$$

Finally, the trends evaluation shown by a time series can be carried out using Sen's non-parametric method. Sen's test uses a linear model fitted to the data to estimate real slope of the model and, with this, analyzes trends. The calculated slope represents the speed of the linear variation shown by the data. A series of linear slopes is calculated using equation:

$$d(k) = \frac{x_j - x_i}{(j-i)} \tag{3.18}$$

where ($1 \leq i < j \leq n$); d equals the slope; x is the variable to be evaluated; n the number of observations and i and j indexes. Sen slope (b) is then calculated as the median of all the slopes calculated, through equation: b = median (d(k)).

3.3.3 Local regression model

Local regression model represents relationship between an independent variable and a dependent variable by local weighted adaptation of polynomials in space. It represents "local" relationship between a response variable and a predictor variable on parts of their intervals, which may differ from a "global" relationship determined using the entire data set with favorable statistical and computational properties. A first approach proposed by Stones suggests a weight function that assigns positive values only to k observations with values x_0 closer to point of interest x, where "closer" is determined using a pseudo-metric p, which is subject to the conditions of regularity [137]. The weight function *"nearest k"* (kNN) is defined for each x_0, where $W_i(x)$ is a function such that $W_i(x) > 0$ if and only if $I \in I_k$, where I_k is a set index defined so that $I \in I_l$ if and only if less than k of points $X_1, X_2, ..., X_n$ are closer x_0 than X_i using the metric p. So $W_i(x)$ is a kNN weight function. It start with a local polynomial fit [138] that adapts to least squares so as to obtain the final adaptation. In particular, is possible to start with polynomial regression in a neighborhood of x, find $\beta \in \mathbb{R}^{p+1}$ which minimizes:

$$n^{-1} \sum W_{ki}(x) \left(y_i - \sum_{i=1}^{n} \beta_j x^j \right)^2 \tag{3.19}$$

where $W_{ki}(x)$ indicates the weights kNN. Calculate the residuals ϵ_i and the scale parameter $\sigma = median(\epsilon_i)$. Define robustness weights $i = K(\epsilon_i/6\sigma)$, where $K(u) = (15/16)(1-u)^2$, if $|u| \leq 1$ and $K(u) = 0$. And then adapt a polynomial regression, but with weights ($\sigma_i W_{ki}(x)$).

The curve (black line) properties smooth and minimize the variance of the residuals or the prediction errors. It is known as "lowess" or "loess" curve. The acronyms are intended to represent the notion of locally weighted regression: a technique of adapting curves or functions that provides a smooth curved behavior, whose value in a given position along the x axis is determined only by the neighborhood points (the size of the neighborhood can be controlled using the "span" argument, which controls the degree of smoothing. So, the greater the value of span, more smooth is the fitted curve.). Consequently, the method does not hypothesize about the form of the relationship and allows to discover the form using the data itself. Here below, we have also a representation of 95% confidence interval.

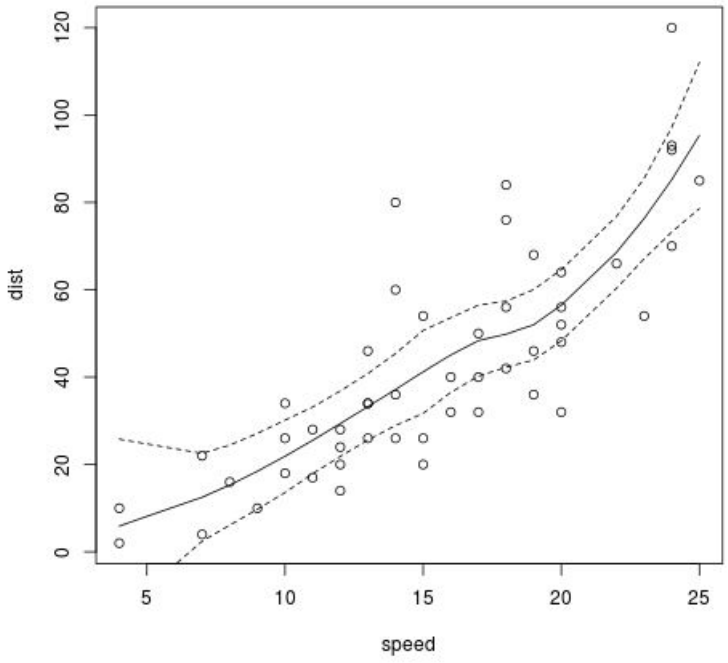

Figure 3.6: *An exemple of lowess fit using r.*

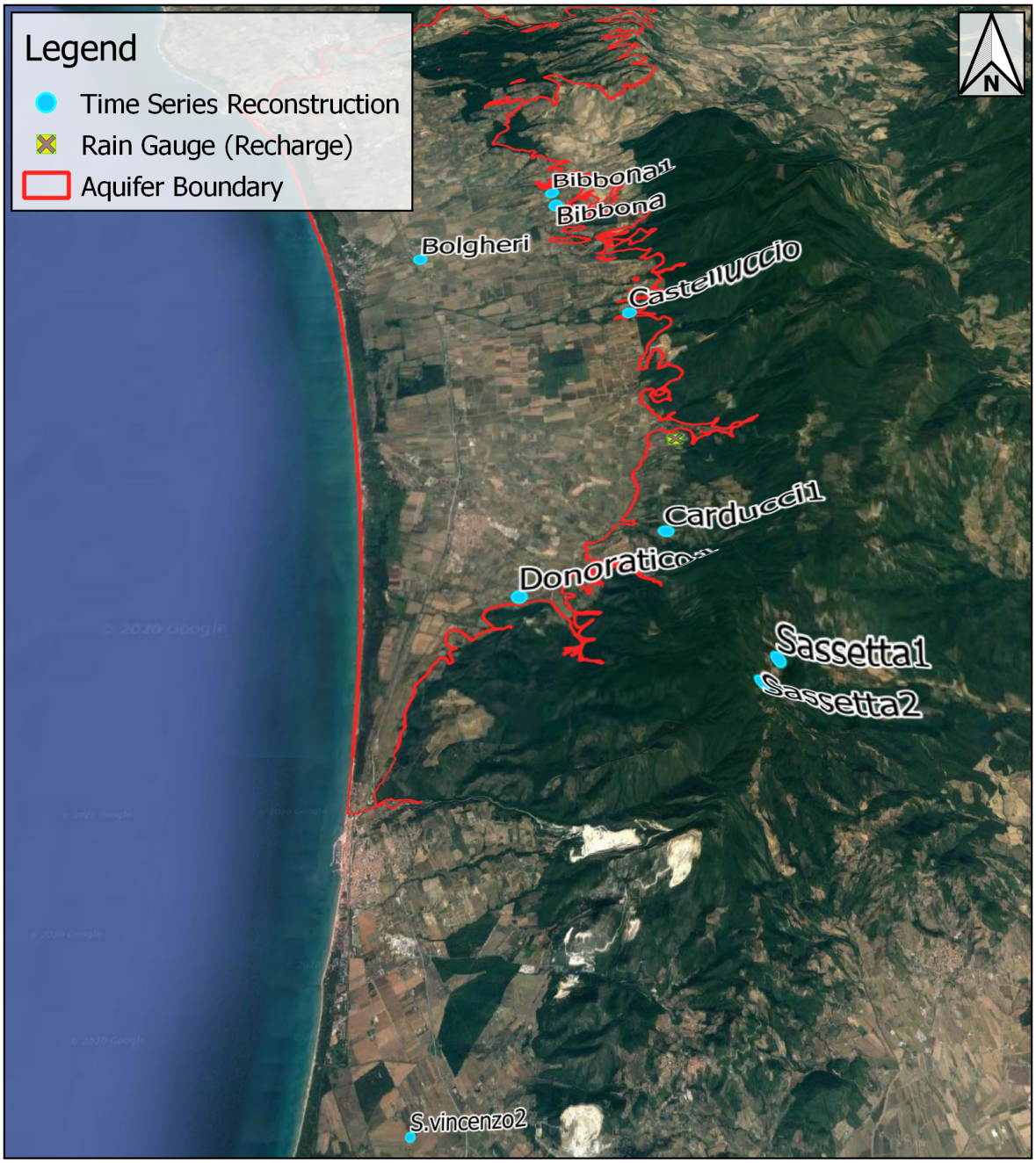

Figure 3.7: *Weather stations used for time series rainfall reconstruction based on table 3.6.*

Chapter 4

Results

"The world is changing:
I feel it in the water, I feel it in the earth, and I smell it in the air"
J. R. R. Tolkien in The Return of the King

The proposed methods have been applied to described and understand phenomenon of natural recharge in study area. This hydrogeological parameter is currently unknown in this area. In particular, for proposed objectives, I applied an integrated analysis of time series recorded from 2011 to September 2019 in Regional Monitoring well P.10745 located in the municipal area of Castagneto Carducci and subjected to daily monitoring by Hydrology Tuscany Region Agency. The drilling dept is 36 meters and its coordinates are Est 1628204 North 4783711 ("Monte Mario Italy zone 1" Projected Coordinate Reference System, EPSG Geodetic Parameter: 3003).

In 2018 (last complete year) annual average precipitation (referred to the rain gauge considered for the recharge calculation) is of 2.2 mm. The following table 4.1 summarizes descriptive statistics relating to the years considered complete (years whose non significant gaps have been interpolated will also be considered).

Table 4.1: *Statistical summary of rainfall and piezometric levels for years 2011-2012-2013-2017-2018.*

year	**2011**	**2012**	**2013**	**2017**	**2018**
rain-cum max (mm)	572	742.8	856	417.4	806.4
rain max (mm)	61.6	41.8	77.8	66	47.2
piezo min (m)	4.59	3.58	4.58	3.69	4.27
piezo max (m)	8.03	6.52	7.69	6.36	6.32

During 2018 piezometric levels observed varied between 4.27 ad 6.32 meters with an average level of 5.28 meters. The minimum level of 3.69 was recorded on 2017 that coincides with drier year of the considered years. The maximum value was detected on 2011 with 8.03 meters above sea level. Soil is mainly composed of vegetable soil in the first meter (verification of stratigraphy) and is often around 0.5 m. At the topographical level, the well is located 9 meters above sea level and the land is flat and not characterized by steep slopes. A targeted survey was carried out on site for verification of hole position and hole casing/filtering. With video inspection carried out it was not possible to visualize well filtered sections, due to the short distance between the tube and the camera that did not allow to catch opportune differences. The electrical conductivity log

was also carried out along the entire depth of the well to check for any differences in conductivity. The results do not show any particular differences in the electrical conductivity values (except the first half meter of water with a value of 950 micro Siemens).

Table 4.2: *The Electrical conductivity log for profiling conductivity and temperature studies in well was conducted with TLC meter, ideal for profiling conductivity and temperature in wells. The conductivity range is from 0-80.000 $\mu S/cm$. Conductivity and temperature measurements are displayed on a LCD screen on the face of the reel. Conductivity accuracy is 5% of reading or 100 μ. A light and buzzer are briefly activated when the zero point of the probe enters water. The depth to water and depth of displayed readings are read off the tape.*

Electrical conductivity (mS)	**Water table level (m)**	**Temperature** (C)
950	-4.76	20
1080	-5.76	18.3
1103	-6.76	17.5
1110	-7.76	17.3
1114	-8.76	17.1
1113	-9.76	17.1
1115	-10.76	17.1
1114	-11.76	17.1
1114	-12.76	17.1
1113	-13.76	17.1
1113	-14.76	17.1
1113	-15.76	17.1
1113	-16.76	17.1
1113	-17.76	17.1
1113	-18.76	17.1
1112	-19.76	17.1
1112	-20.76	17.1
1112	-22.76	17.1
1112	-24.76	17.1
1112	-26.76	17.1
1112	-28.76	17.1
1112	-30.76	17.1
1112	-32.76	17.1

It is therefore assumed that the well is filtered for all its depth. The water level was checked and compared to the daily level recorded in the regional database 4.2, which turned out to be corresponding and equal to -4.49 m. In the study area, no studies were carried out to identify the quantification of the recharge. Some indications for the present study can be taken from Mubarak 2017 [38], where, using water table fluctuation method, they identified 13 cases in different areas of the globe, taking into account the humid, semi-arid and arid climate. The results obtained derive from a careful review of the sources of error attributable to methods used 4.3. Specifically, a strong evapotranspiration due to diurnal fluctuations was not possible to verify this effect because daily time series downloaded from regional databases provide the daily average value, although this effect is probably to be excluded given the agricultural characteristics of the land. Absence of heavy groundwater pumping by neighboring wells was confirmed by field verification 4.46 (respect distance of 200 m [1] from well studied). Changes in atmospheric pressure, pressure changes due to entrapped air and rapid conversion of capillary water to phreatic water where water table is

near the ground surface are inherently minimized by application of the EMR method [91, 92]. Hence, before recharge episodes calculation, a first cross correlation analysis was carried out between precipitation and fluctuation of the water levels [91]. To do this, water table levels and rainfall events related to the 2018 were used. Regional rain gauge station used for specific site rainfall events evaluation is located in municipal area of Castagneto Carducci. Its coordinates are Est 1632296 North 4783121 ("Monte Mario Italy zone 1" Projected Coordinate Reference System, EPSG Geodetic Parameter: 3003), has an altitude of 95 meters above sea level and is located 4 kilometers from studied well. One of the main challenges of this study was to verify the correlation between precipitation events and groundwater fluctuations [2, 86, 91, 100, 139]. Subsequently, according to Knapp 2015 [140], the episodes of precipitation considered "storm" have been identified: that is all rainy events developed in consecutive days or with at most two days of difference, with a quantity equal to or greater than 99 percentile (in our case 29.76 mm for daily rainfall time series of 2018). This has allowed me to identify 6 characteristic storms. In order to determine the water-table-response time to rainfall events, the cross-correlation method, which is a time series technique, has been used to reveal the significance of the water-table response to rainfall [2,92,139]. In particular, cross correlation was set to the period of time over which there is a correlation between groundwater level and rainfall at the 95% confidence level, assuming that it is homogenous in the study. For example, the figure 4.6 shows that the vertical bars are above the 95% confidence level for selected days, thereby indicating that it takes 1 day for the groundwater level inside the period in the study area to fully respond to the daily storm event. Hence, a first cross correlation analysis between pure daily precipitation values and associated water table levels was studied. Having obtained low correlations between daily groundwater levels and daily rainfall values (figure 4.3), groundwater levels rate of change against daily precipitation were correlated. In this way, significant correlations were obtained for one lag of difference (in one case 2 lag).

Table 4.3: *Sources of error considered for the calculation of the recharge based on the bibliographic indications.*

Water Table level Fluctuation Error Source	Literature reference	Action
Atmospheric changes	*Coock 2002, Nimmo 2015*	Solved
Air pressure changes	*Coock 2002, Nimmo 2015*	Solved
Water rapid conversion	*Coock 2002, Nimmo 2015*	Solved
Correlation rain water table level	*Mubarak 2017, Nimmo 2018*	Verified
Specific yield estimation	*Coock 2002, Mubarack 2017*	Calculated
Evapotraspiration (diurnal fluctuation)	*Coock 2002, Nimmo 2018*	Verified
Other wells pumping activities	*Coock 2002, Tashie 2016*	Verified

Specifically, the six events identified in the periods of March, May, October and November were studied. For each events was produced a daily time series representation of rainfall and water table level, water table level rate of change over time and finally a graph relating to cross correlation between groundwater table levels and rate of change of levels for considered period. Time series graph for March 2018 (figure 4.4) identify a rain event of 7 days, with a total of 60.4 mm. Rain peaks correspond to increase in groundwater levels, while the maximum peak as rate of change is 0.15 m/d (figure 4.5). In order to establish water table response time respect

rainfall events, cross-correlation has been used to reveal significance of the water-table response to rainfall. The Cross correlation graph in March shows a significant peak for a lag equal to 1, with a value of 0.88 (figure 4.6). First storm event identified in May is equal to 4 days, for an amount of 47.6 mm (figure 4.7). The identified rain peaks tend to increase in groundwater levels with a maximum peak in the rate of change of 0.13 m/d (figure 4.8). Cross correlation graph for first storm recorded in May shows a significant peak for a lag equal to 1, with a value of 0.94 (figure 4.9). Rainy event identified in the second storm of May consists of 2 days for an amount of 36 mm (figure 4.10). The identified rain peaks correspond to an increase in groundwater levels with a maximum peak rate of change of 0.04 m/d (figure 4.11). Cross correlation of second storm recorded in May shows a significant peak for a lag equal to 1, with a value of 0.67 (figure 4.12). Rainy event identified on third storm of May consists of 6 days, with 4 days without precipitation and an amount of 70.6 mm (figure 4.13). In this case, it was considered a single rainy event due to the increase in the level of groundwater on the first day and a non significant decrease in the remaining days without rain. The identified rain peaks correspond to an increase in groundwater levels with a maximum peak rate of change of 0.09 m/d (figure 4.14). Third cross correlation shows a significant peak for a lag equal to 2, with a value of 0.5 (figure 4.15). The rainy event identified between October and November 2018 consists of a total of 9 days, interspersed with 1 days without precipitation for an amount of 146.6 mm (figure 4.16). In this case, it was considered a single rainy event given the increase in the level of groundwater on the only day without rain. First three rainy days do not correspond to increases in the groundwater level, the identified rain peaks correspond to an increase in groundwater levels with a maximum peak rate of change of 0.07 m/d (figure 4.17). Cross correlation graph for recorded storm shows a significant peak for a lag equal to 1, with a value of 0.63 (figure 4.18). The rainy event in November 2018 consists of a total of 3 days, for an amount of 57.8 mm (figure 4.19). Rain peaks identified correspond to increases in groundwater levels with a maximum peak of the rate of change of 0.10 m/d (figure 4.20). Cross correlation chart for recorded storm shows a significant peak for a lag equal to 1, with a value of 0.76 (figure 4.21).

Figure 4.1: *Site investigation for Regional Monitoring well P.10745 located in the municipal area of Castagneto Carducci. The instrumentation used for field investigations consists of: interface probe for water table level measurements, weight for well depth measuring, interface probe for measuring electrical conductivity, video underwater camera for inspection of the well.*

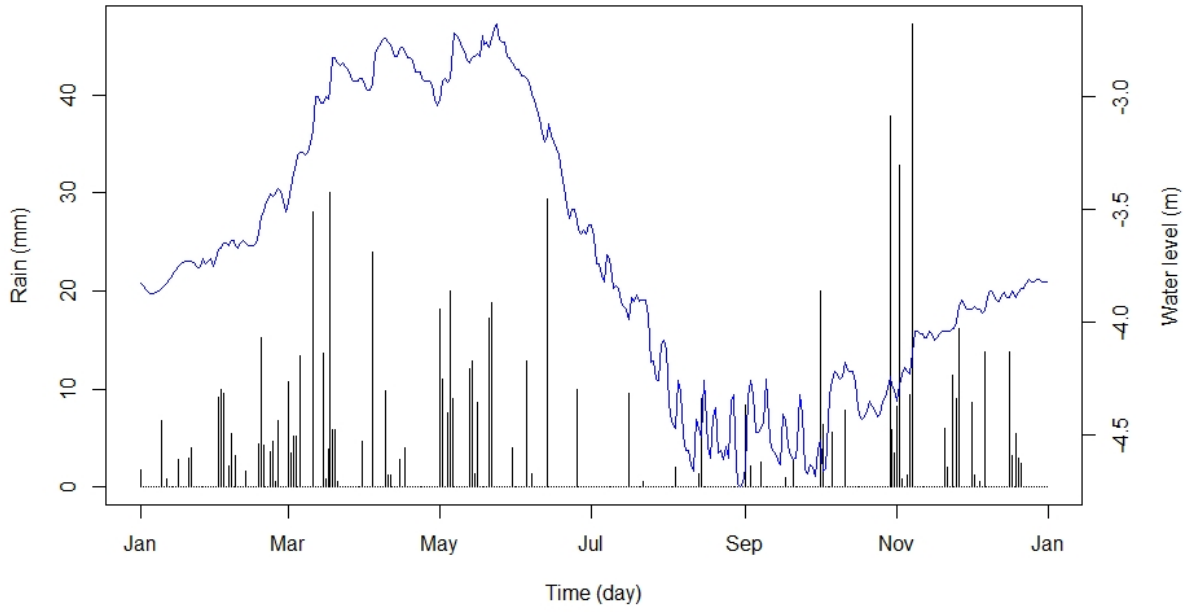

Figure 4.2: *Time series graph where daily rainfall (black lines) and water table level (blue lines) are represented on 2018.*

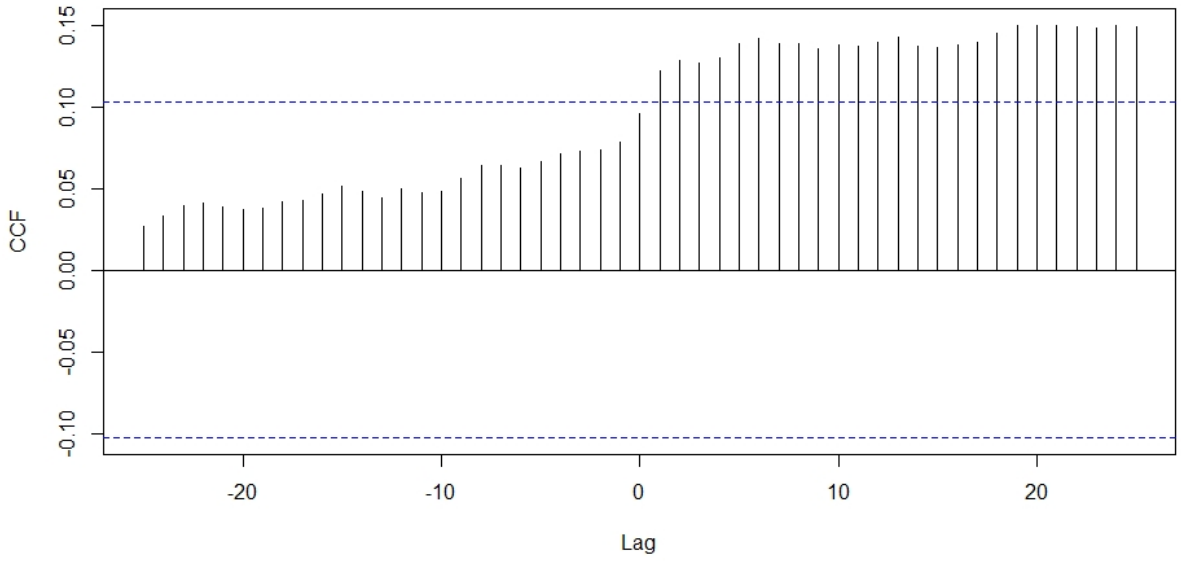

Figure 4.3: *An example of Cross Correlation between daily water table level and rainfall on 2018. Results presents a maximum correlation value of 0.15, proving in this case a low correlation.*

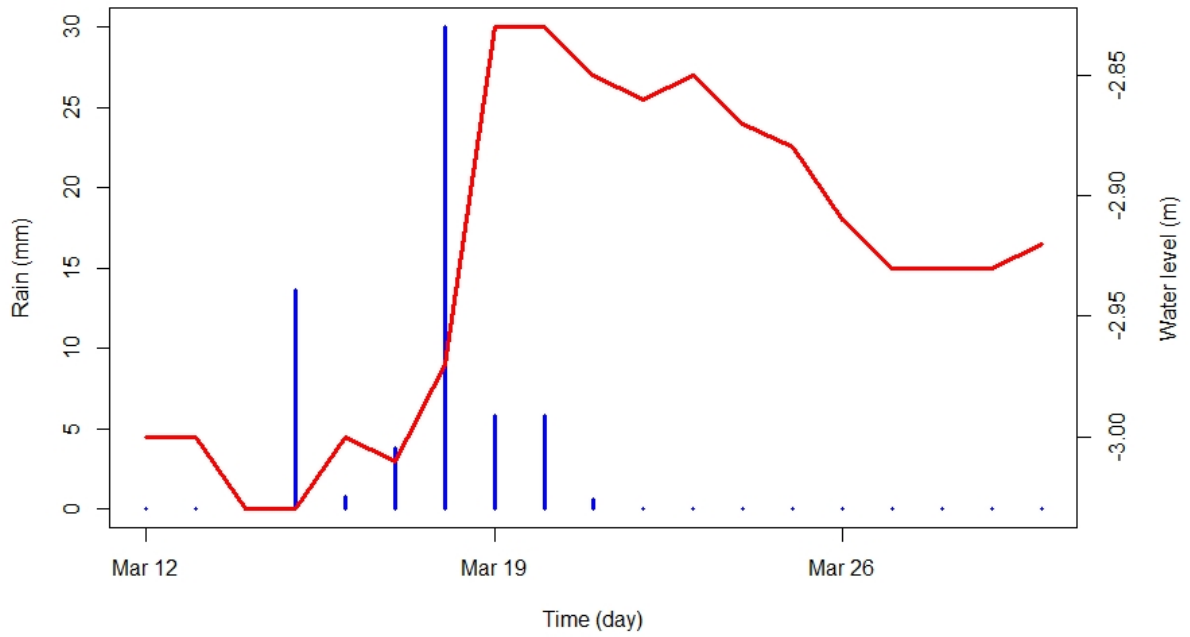

Figure 4.4: *Time series storm event on March 2018.*

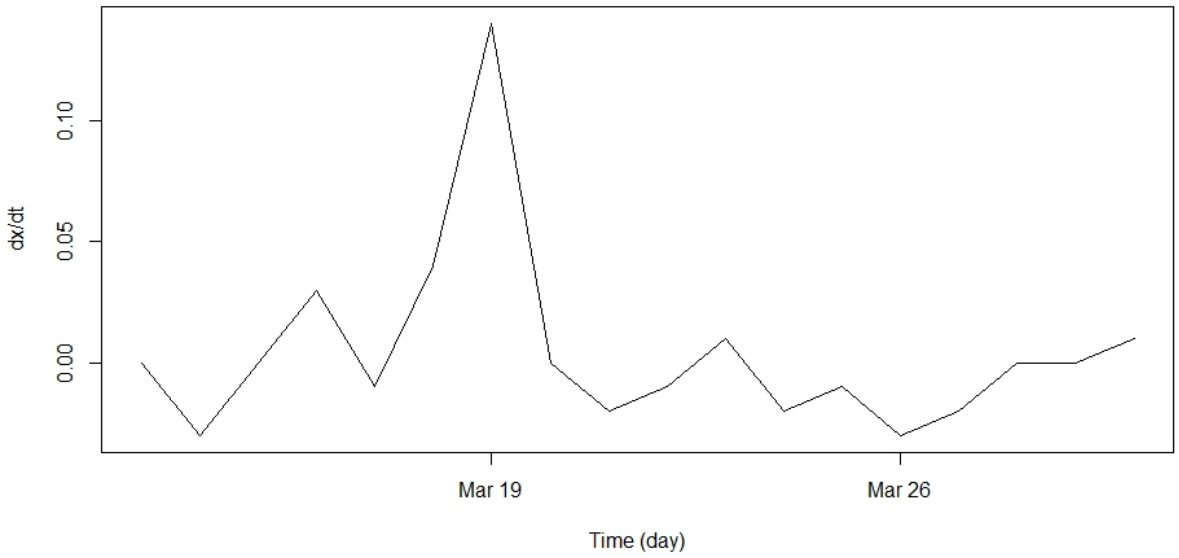

Figure 4.5: *Rate of change of groundwater level during storm event on March 2018.*

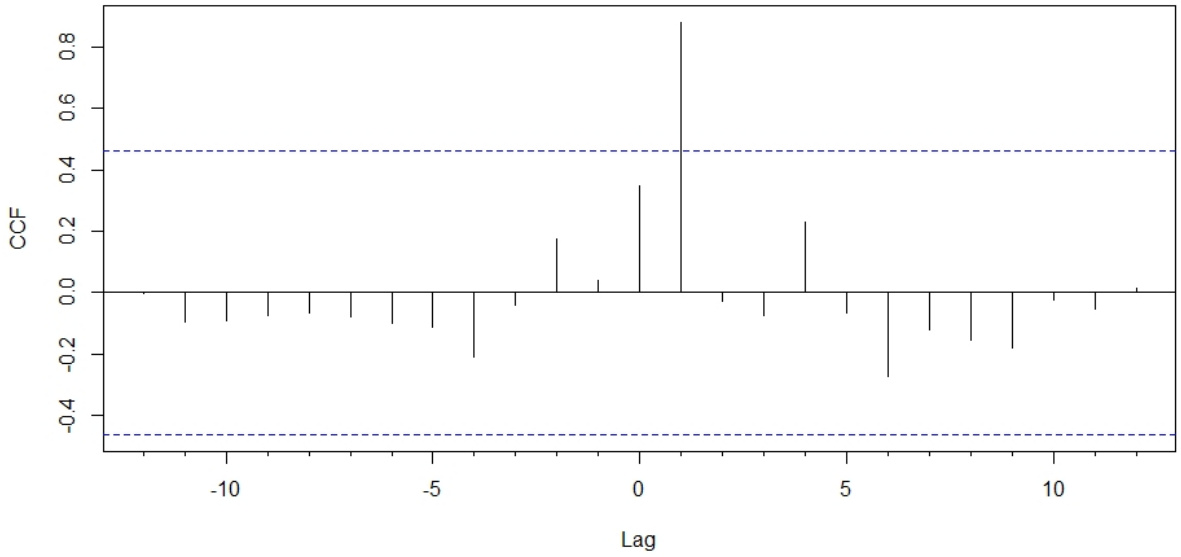

Figure 4.6: *Cross correlation analysis between rate of change groundwater level and rainfall storm event studied on March 2018.*

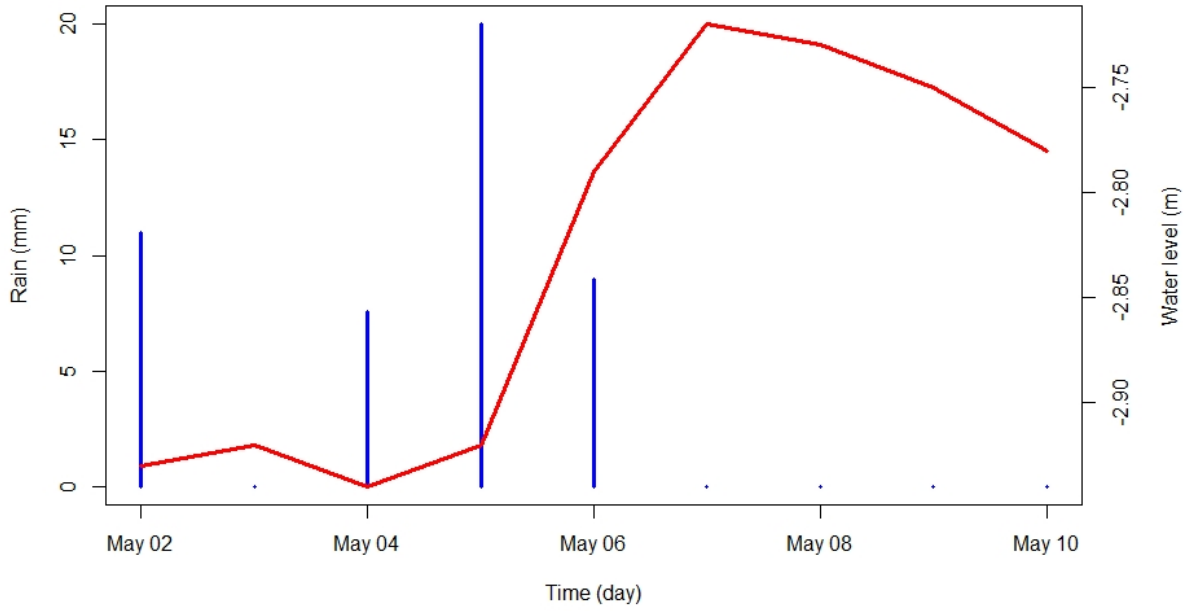

Figure 4.7: *First time series storm event with groundwater level behavior on May 2018.*

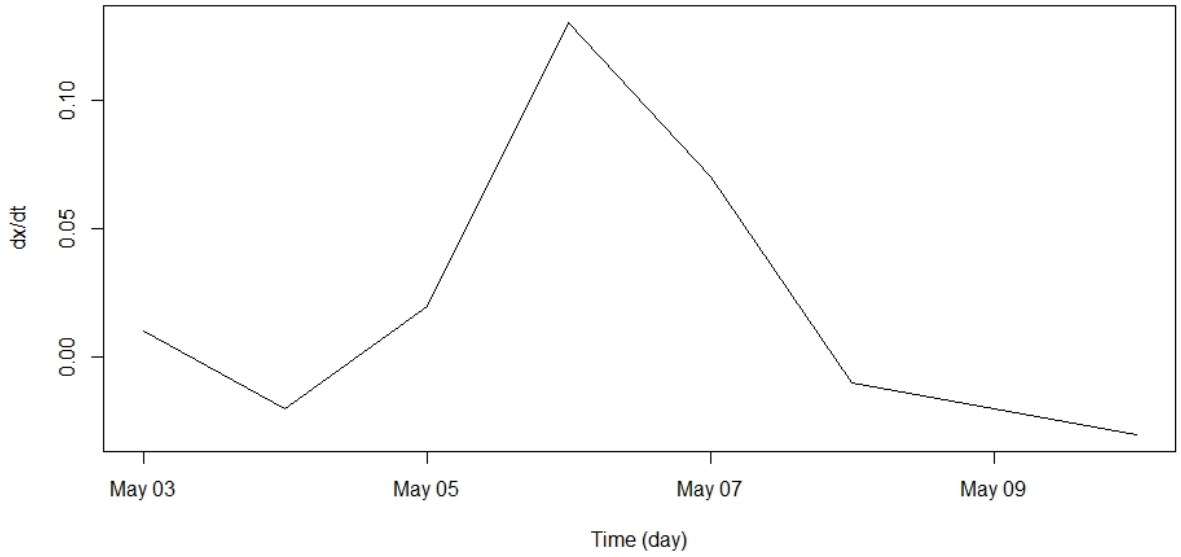

Figure 4.8: *Rate of change of groundwater level during first storm event on May 2018.*

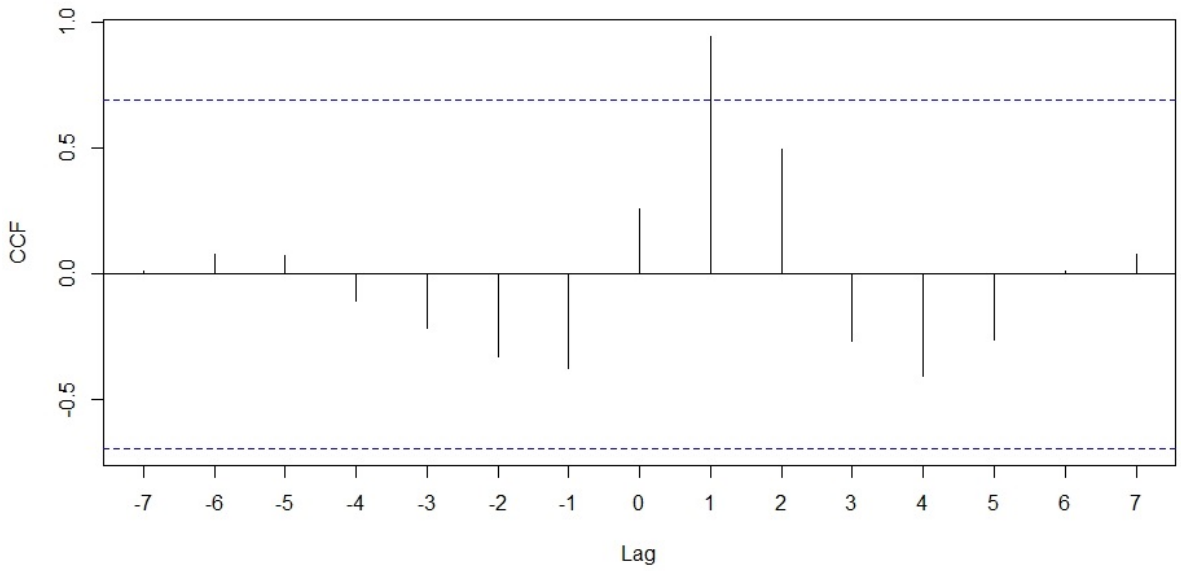

Figure 4.9: *Cross correlation analysis between rate of change groundwater level and rainfall storm event studied on May 2018.*

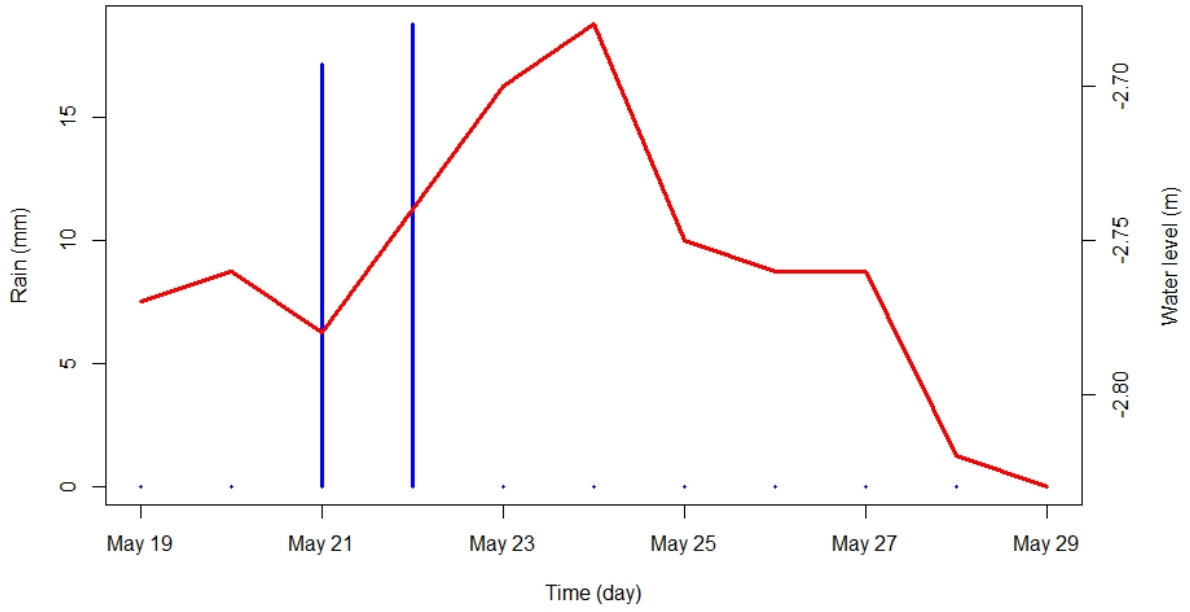

Figure 4.10: *Second time series storm event with groundwater level behavior on May 2018.*

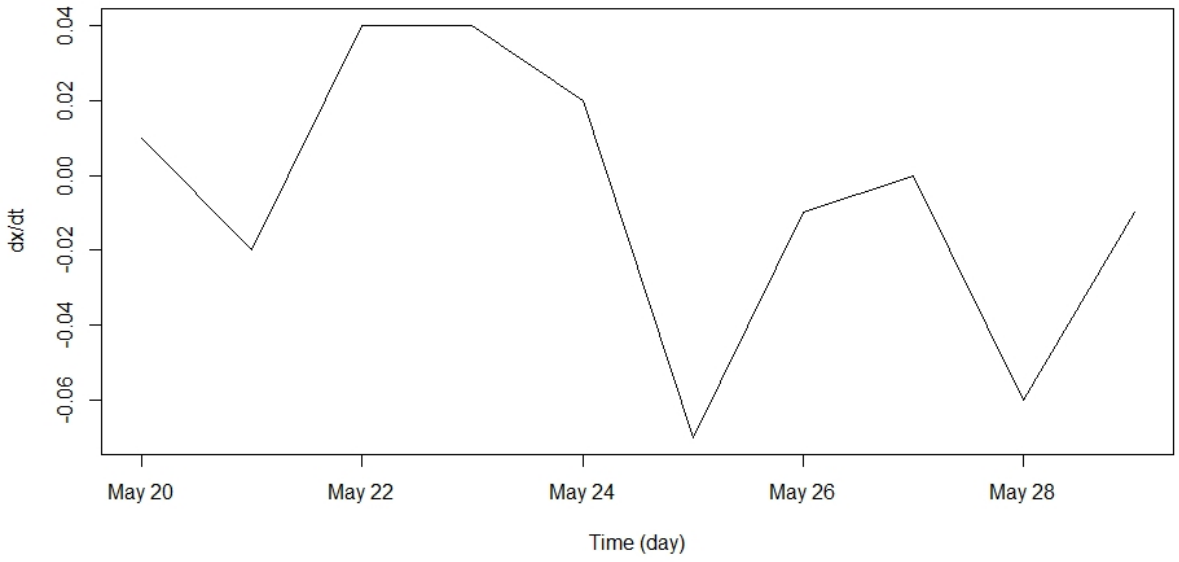

Figure 4.11: *Rate of change of groundwater level during second storm event on May 2018.*

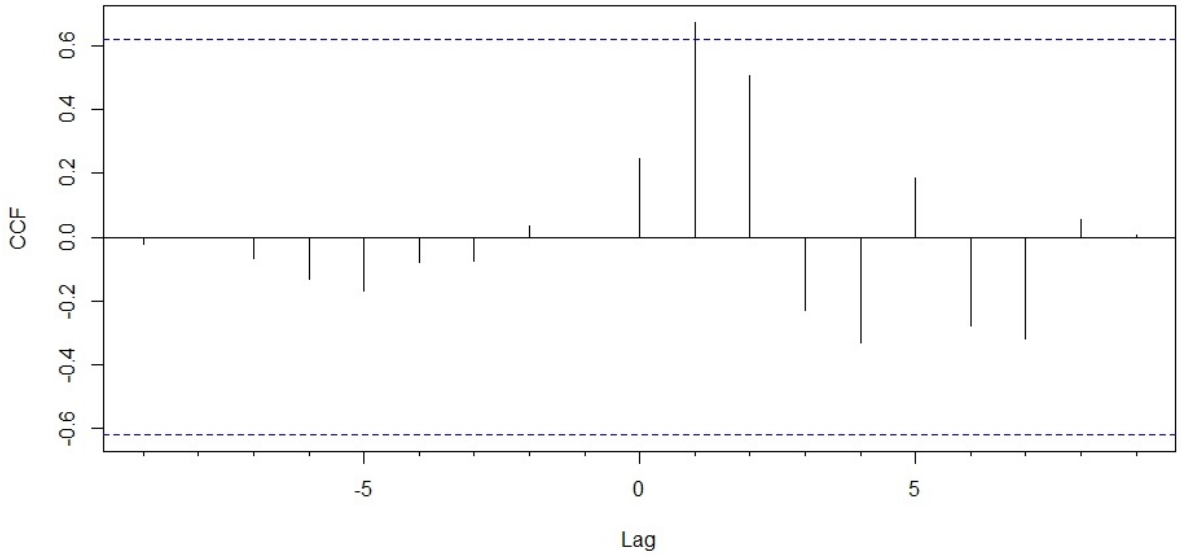

Figure 4.12: *Cross correlation analysis between rate of change groundwater level and rainfall storm second event studied on May 2018.*

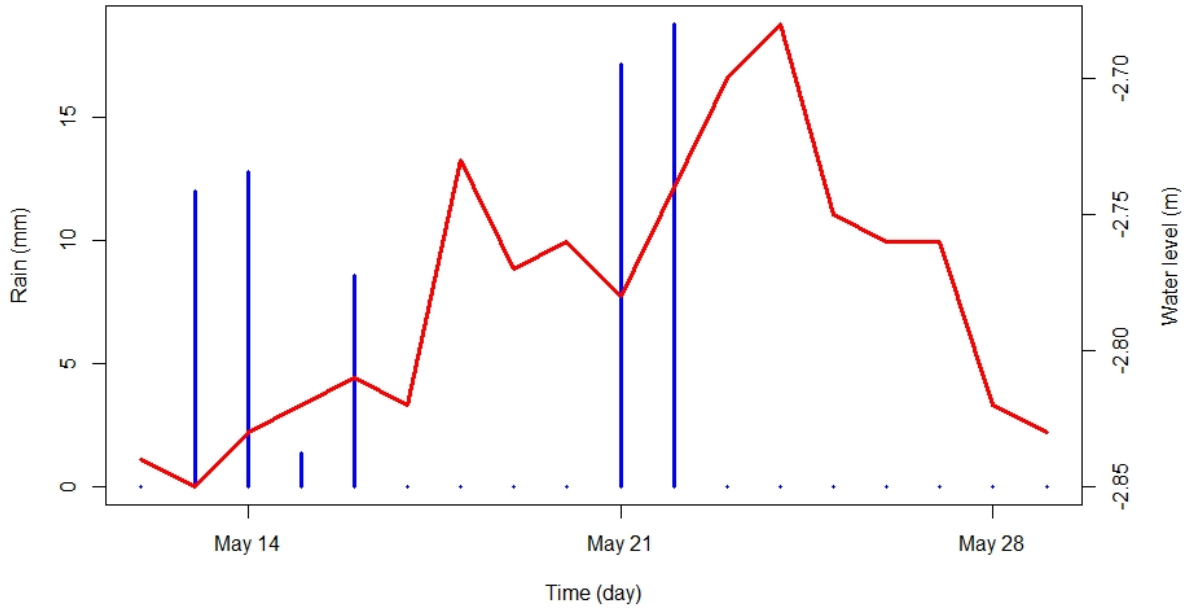

Figure 4.13: *Third time series storm event with groundwater level behavior on May 2018.*

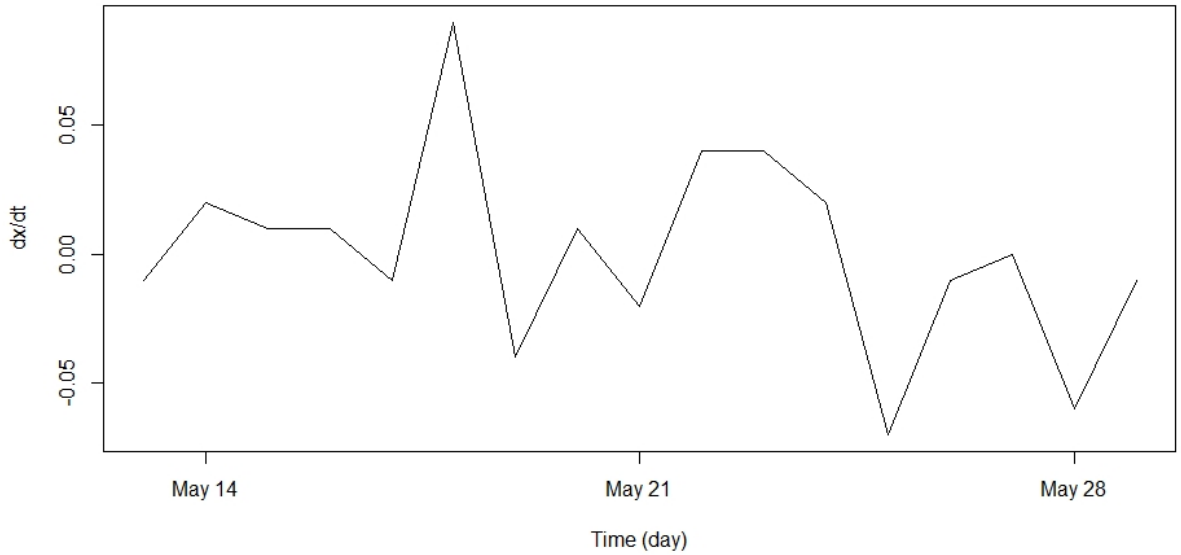

Figure 4.14: *Rate of change of groundwater level during third storm event on May 2018.*

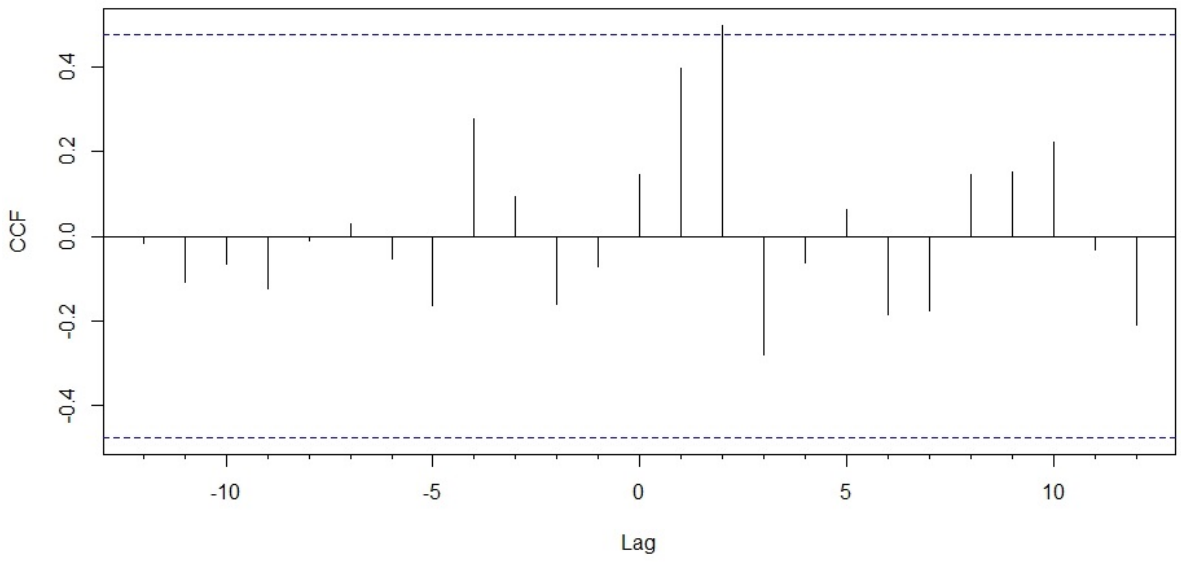

Figure 4.15: *Cross correlation analysis between rate of change groundwater level and rainfall storm third event studied on May 2018.*

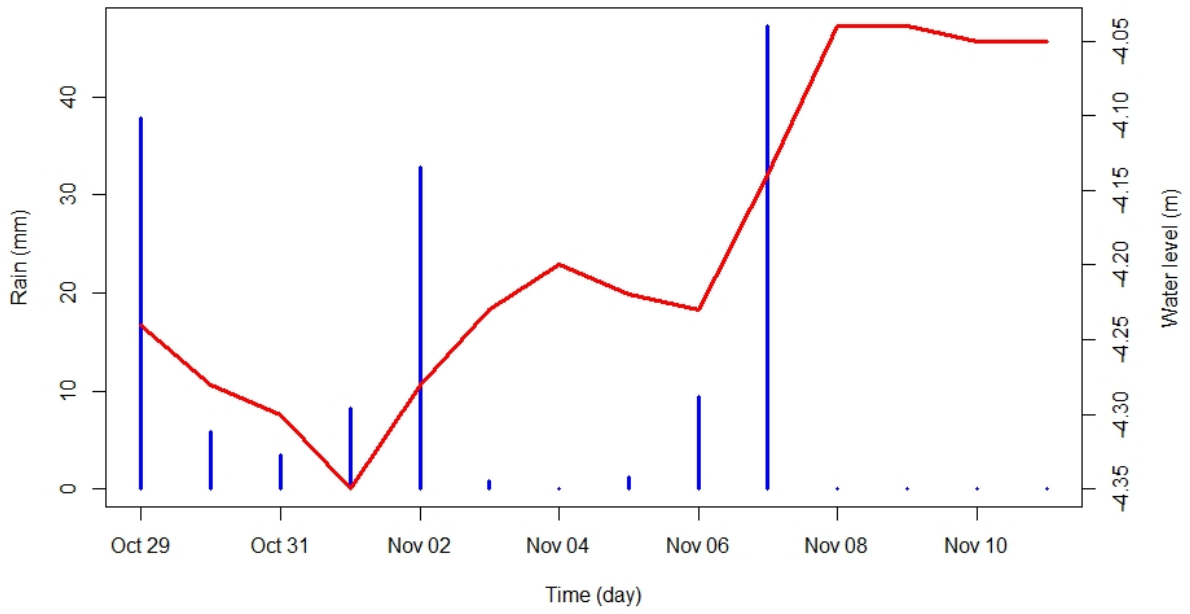

Figure 4.16: *Time series storm event with groundwater level behavior on October 2018.*

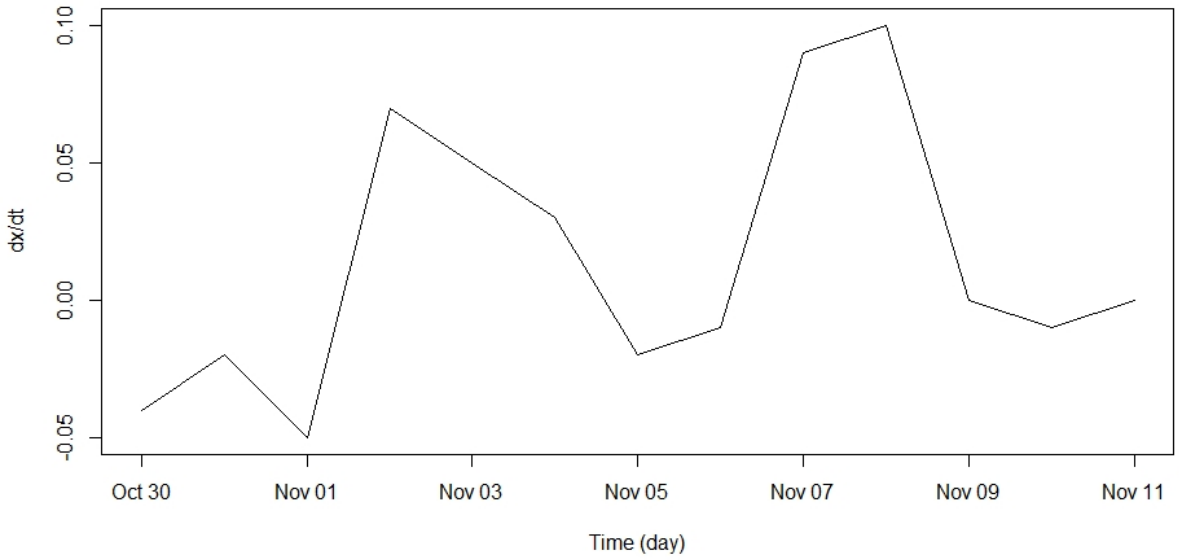

Figure 4.17: *Rate of change of groundwater level during storm event on October 2018.*

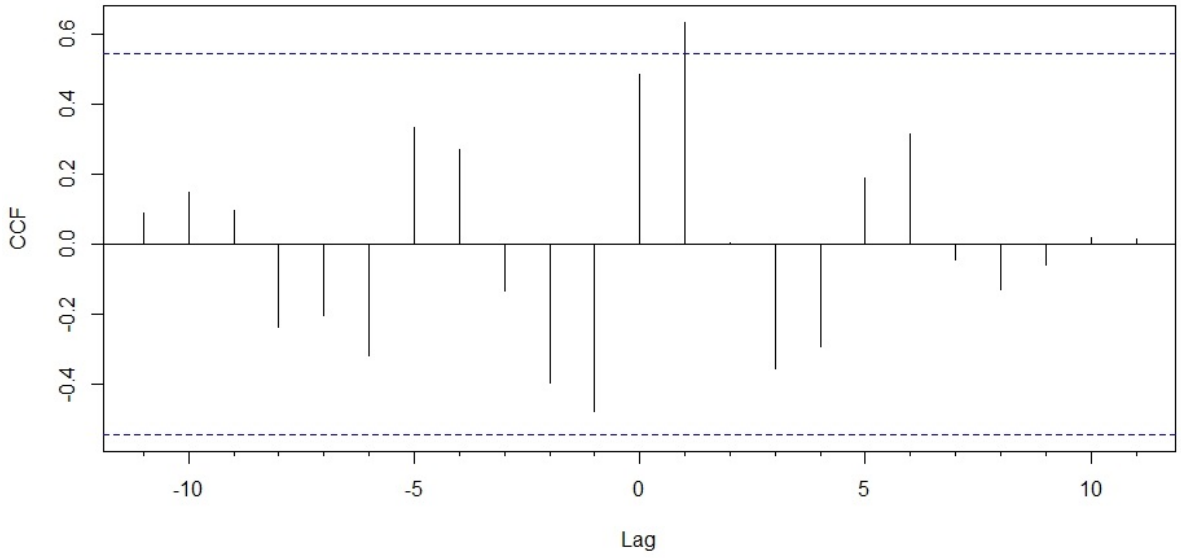

Figure 4.18: *Cross correlation analysis between rate of change groundwater level and rainfall storm event studied on October 2018.*

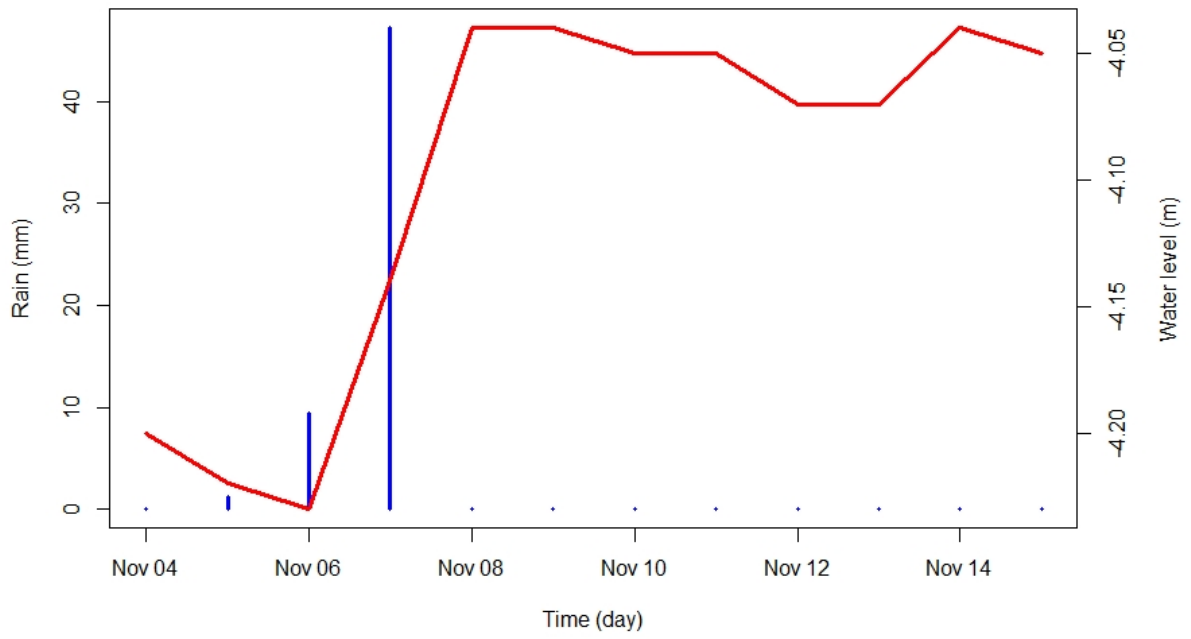

Figure 4.19: *Time series storm event with groundwater level behavior on November 2018.*

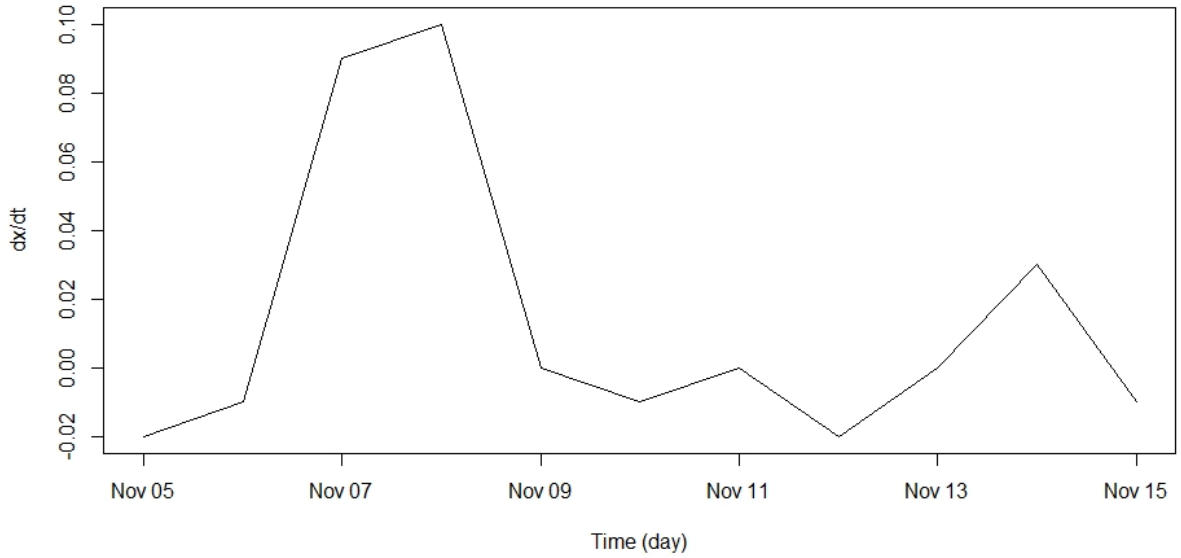

Figure 4.20: *Rate of change of groundwater level during storm event on November 2018.*

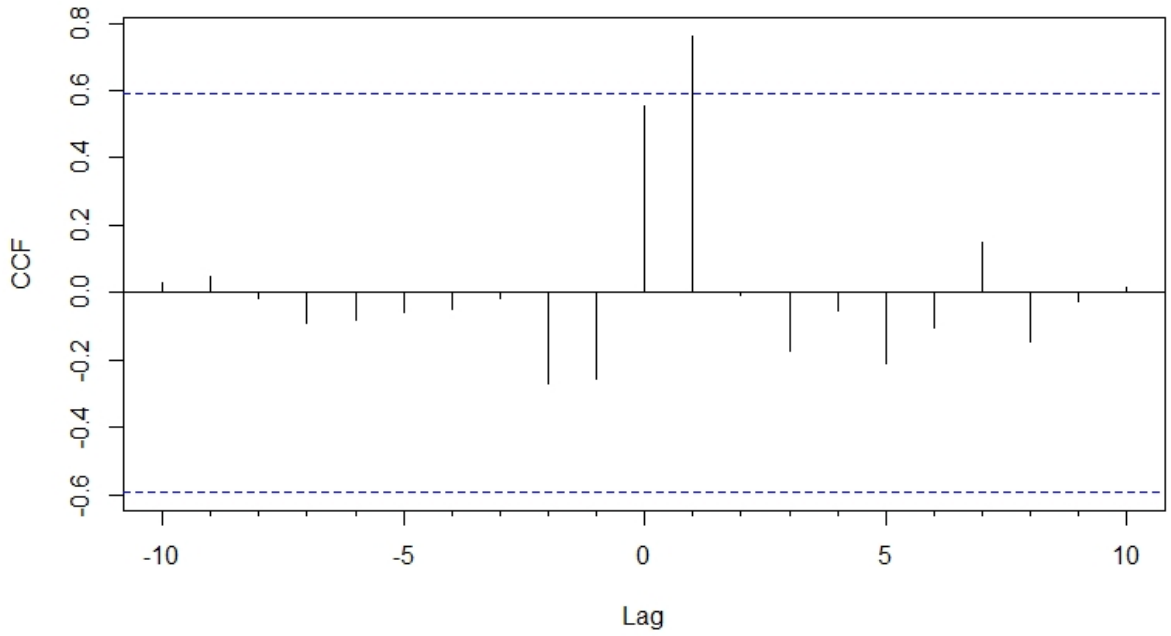

Figure 4.21: *Cross correlation analysis between rate of change groundwater level and rainfall storm event studied on November 2018.*

4.1 Master recession curve setting

Time series relating to years recorded from 2011 to 2019 were initially assessed on the basis of existing gaps. For this reason it was decided to interpolate only those small gaps (to be determined how small) and those that were part of the recessions due to the summer season (see example 2011 year). Furthermore, original data were filtered using second-order moving media to reduce or eliminate white noise and apparent diurnal fluctuation (another possible source of error [2,86,139]) present in the daily series. Finally, phreatimetric data have been transformed into piezometric levels. One of the most important steps was to identify days of pure recession within time series, so as to identify the characteristic slope element length (a short segment of recession that can be considered as a straight line case by case) [2,94]. This parameter has generally been settled for 3 days because in some cases a setting lower led to the recession points at the time of the curve's rise (see 2017). For complete series, i.e. for the years 2011, 2012, 2013, 2017, 2018 and 2019, winter period was considered as representative for master recession curves parameterization. For years relating to 2014 and 2015 instead, it was necessary to use only short time series cuts, while few data belonging to 2016 were considered unusable.

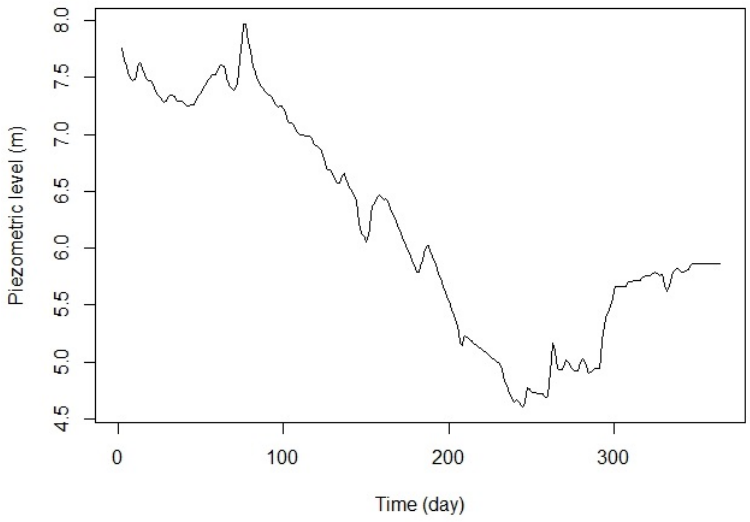

Figure 4.22: *Piezometric time series related to 2011 after moving averaged application. Interpolation effect is visible between day 130 and day 230.*

Throughorigin parameter was set false because zero piezometric value is not present in all time series. Minimum duration of interval between significant precipitation and beginning of recession (*Mindrytime*, 1 or 2 days depending on cases studied in 2018) was set at 3 days for the years 2017, 2018, 2019. This because a lower setting brought recession points identified (recession start) in a rising moment curve (see 2017). Rainfall quantity that can be considered as zero in recession period was generally set to 1 mm. *Maxtick* parameter has been set to 0.1 (default value), having already applied a moving average filter. Averages points rates identified by Master Recession Curve (*Binsize*) were not used, as they did not improve final coefficients results. Finally, maximum angle of increase-response in a slope recession element has always been set to -0.01 value.

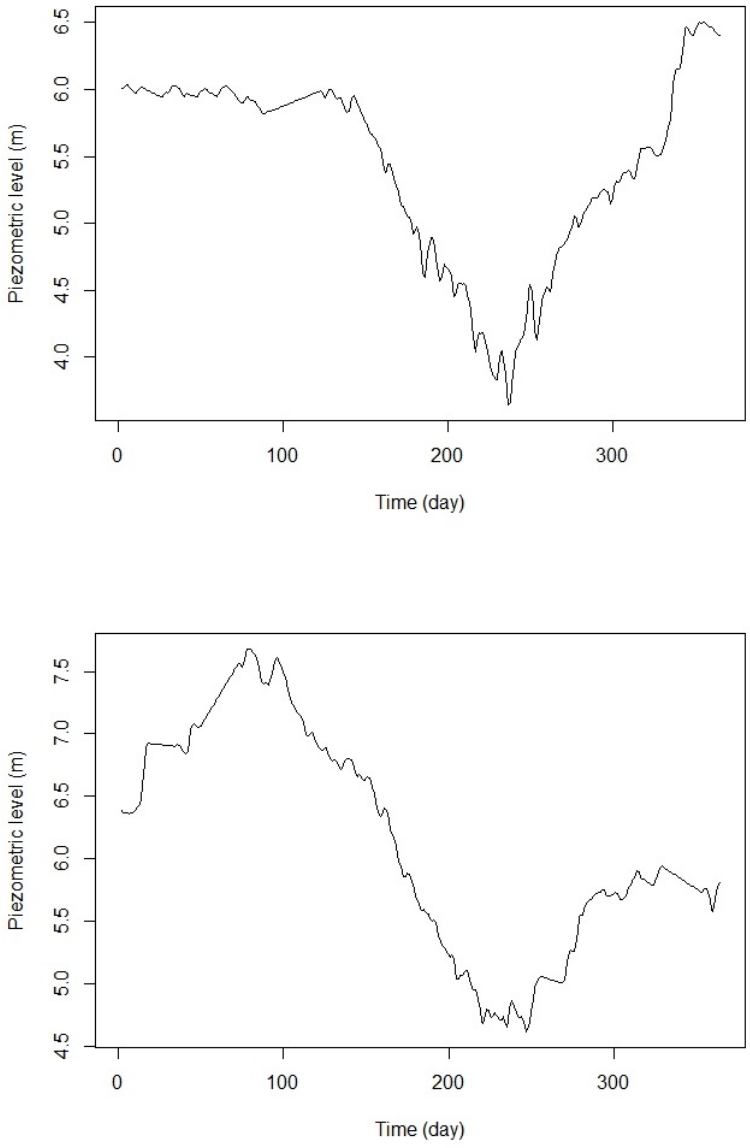

Figure 4.23: *Piezometric time series of 2012 (upper figure) and 2013 (lower figure) after moving averaged application. For 2012 interpolation effect is visible between day 100 and day 130, while for 2013 while for 2013 it is visible in the initial and final part of the year.*

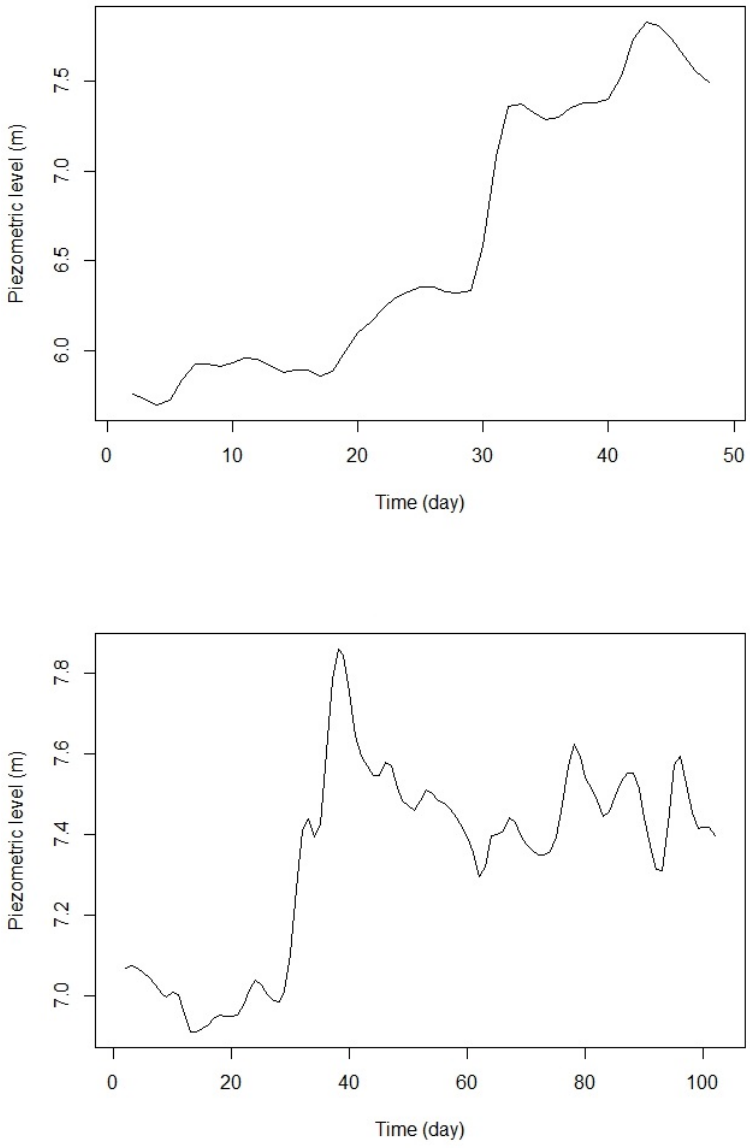

Figure 4.24: *Piezometric time series of 2014 (winter; upper figure) and 2015 (winter-spring; lower figure) after moving averaged application. For both time series, temporal interpolations were not applied due to incompleteness of original data.*

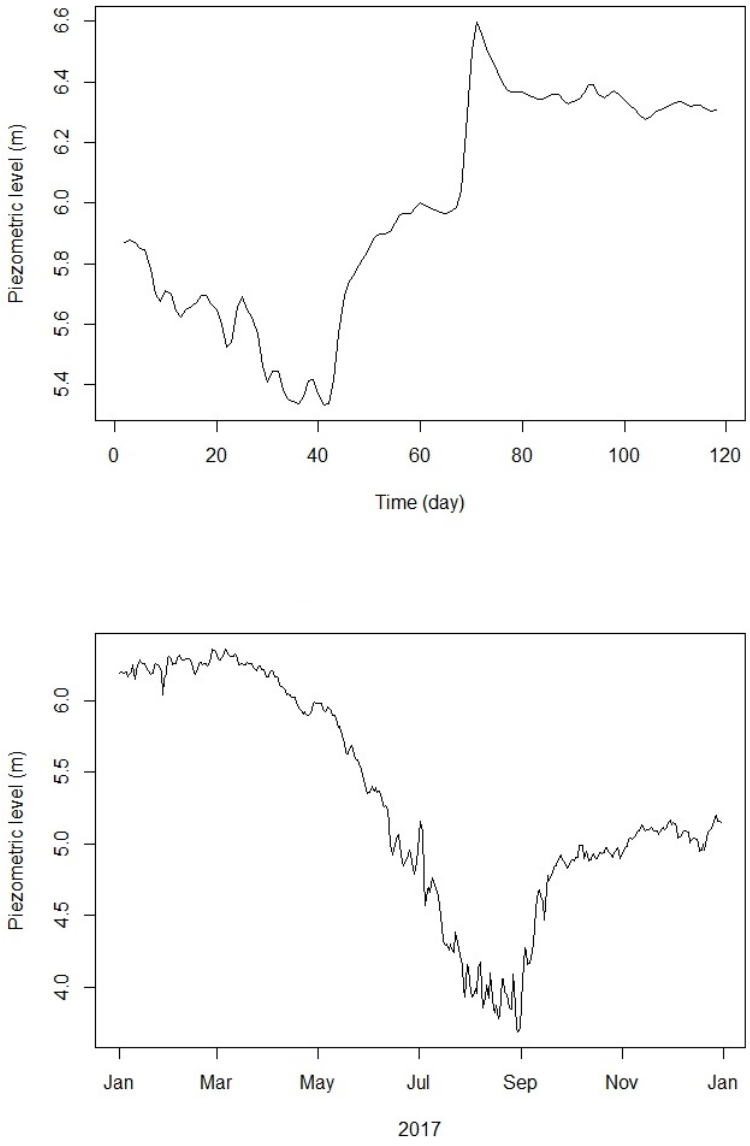

Figure 4.25: *Piezometric time series of 2015 (summer-autumn; upper figure) and 2017 after moving averaged application. For second part of 2015, linear interpolation was not applied due to incompleteness of original data; while for 2017 linear interpolation was not applied (no gaps in original data).*

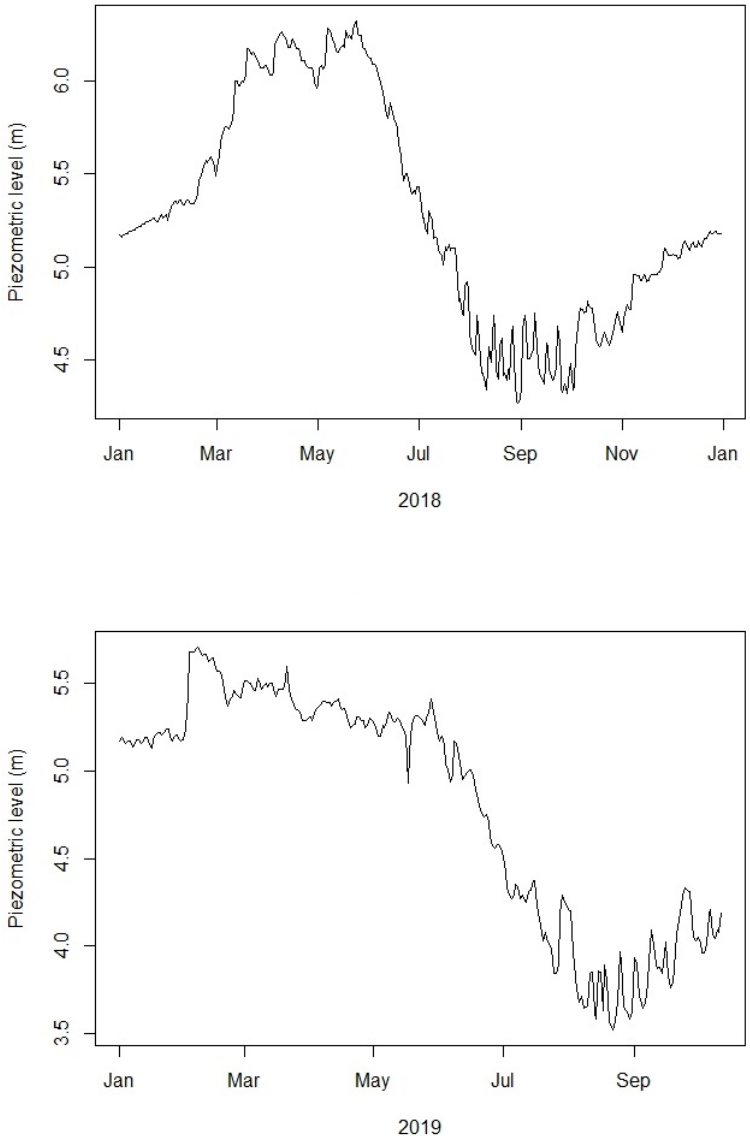

Figure 4.26: *Piezometric time series of 2018 and 2019 after moving averaged application. For both time series, temporal interpolations were not applied (no gaps in original data).*

Time series relative to 2011 was partial complete respect groundwater level values. Linear interpolations have been applied to 5 short periods. First one when water level was growing and others when level was in recession, during the summer period. Relative hydrograph shows selected slope elements that are represented with the cumulative precipitation in the background and where blue crosses are starting point of selected recession moments. Remaining points in each slope are highlighted by red symbols. Most peaks are linked with each rainy event, indicating a direct response between water table level and rainy events. In table 4.4 all parameter values are expressed and they are used to derive coefficients of the main master recession curve. Hydrograph chart shows selected recession slopes characterized into winter season and in which groundwater levels are more superficial over time. First selection process of MRC parameter values was closely linked to visual assessment of interaction between cumulative rainfall values and groundwater level reaction. After this, test and error parameter values evaluation based on Goodness Of Fitness [141] was applied to identify best results, considering a negative inclination of MRC fitting curve from distribution of the identified slope points. The computed regression visible in figure 4.27 shows slope points of selected elements, presenting a Goodness Of Fit index (GOF) equal to 0.43. *Mindrytime* and *tslenght* parameter were set in 3 days. The *maxdelprec* parameter was set to 1 mm, while *binaverage* operations were not managed. For year 2012 (figure 4.29), linear interpolations of groundwater levels were carried out (they were not so large as to compromise the hydrological evaluation). Best fitting was obtained by evaluating recession periods during first part of the year. Parametrization process is characterized by a *midrytime* of 2 days, which is only one differs from the previous analysis conducted on 2011. Computed regression visible in figure 4.29 shows selected slope points elements and presents a GOF value of -0.05. In 2013 linear interpolations were applied to the first and last part of the year (these interpolations will be taken into greater consideration in Episodic Master Recession evaluation, figure 4.31). These made it impossible to evaluate recession curves at initial period of the year (was the case for the years 2011 and 2012). For this reason, *mrcfit* was calculated from mid-March to late August, where no interpolations were performed. The *mrcfit* parameters were found to be the same as 2012 and have returned a GOF of -0.05 (figure 4.32). In order to obtain more information regarding the amount of top-up, the first part of 2014 (figure 4.33) was considered (wettest year compared to others years considered for this study, for a total of 1323.2 mm). In this case the time series of the first 50 days of the year shows a clear correspondence between rainy events and the raising of the groundwater level. The best possible parameterization has identified four recession points and an *tslenght* equal to 2 days. The *mindrytime* was increased to 1 day compared to previous years, while the GOF value was equal to 0.79 (figure 4.34). Time series for 2015 (figure 4.35) is characterized by a first part from January to May and a second part from September to December. Consequently the *mrcfit* was calculated only for these two series, without taking into account central period of the year (too large to interpolate). Regarding to first time series, relative hydrogram shows a clear dependency between rainy events and groundwater levels, while characterization of recession periods the whole series was considered (figure 4.36). The value of *mindrytime* was set to 2 days, as well as *tslength*, but *mindrytime* was set to 2 days. calculated GOF value was of 0.13. To *mrcfit* second time series characterization of 2015, final part of the series was considered (figure 4.37). This because consideration of the whole series would have produced a positive inclination regression line. For this reason settings have been kept unchanged with respect to previous series,

and only *resplimits* number has been changed to identify best recession points (GOF = 0.98, figure 4.38). Year 2017 (figure 4.39) was analyzed without preliminary interpolations. Recession periods studied also concerned here first part of the year. Through the try and error process the *mindrytime* value was reset to 3 days as well as *tslength*. Relative *mrcfit* chart shows identified recession points with a calculated GOF equal to -0.06 (figure 4.40). Interpolations were also applied for time series relative to 2018 (figure 4.41). The period from mid-March to June was considered a useful period for the recession points assessment. The *mrcfit* setting was kept equal to 2017 and returned a GOF of 0.5 (figure 4.42). The same analysis has also been carried out on year 2019 although it is not naturally terminated (analysis conducted until mid-October). Also in this case there was no need to interpolate groundwater values and *mcfit* parameters were kept constant with respect to the 2017 and 2018 series. In this case the fitting GOF was 0.07.

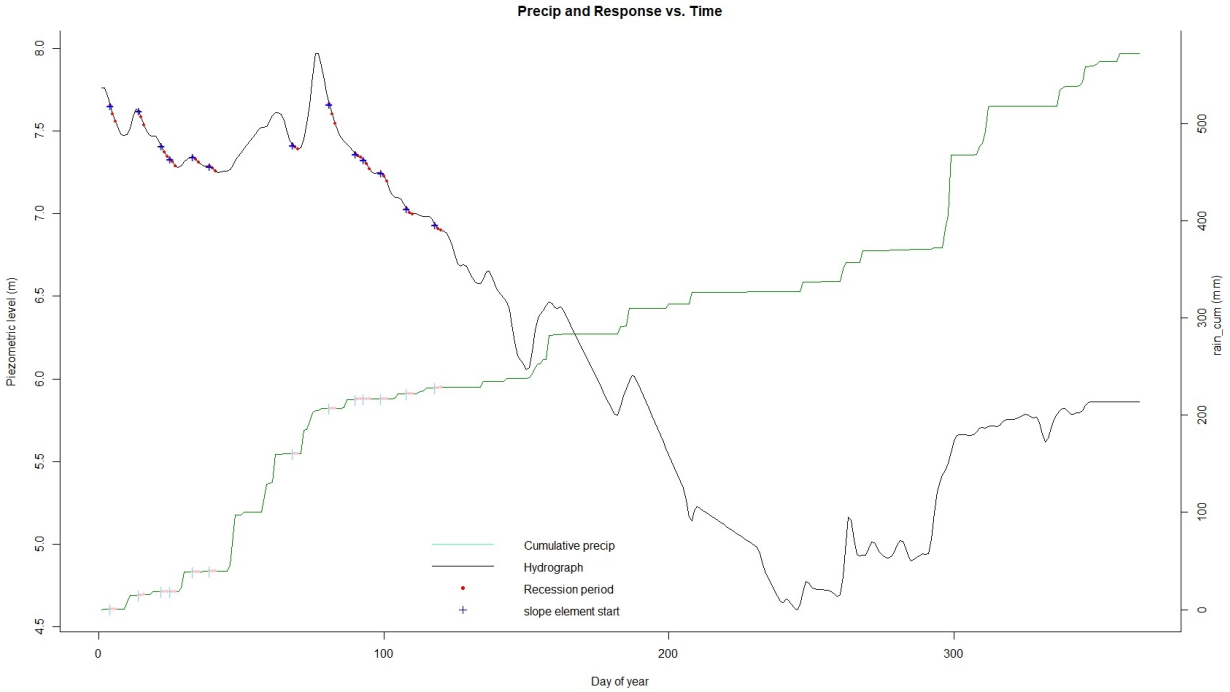

Figure 4.27: *Hydrograph with piezometric level (where H_0 = 9 m a.s.l.) where start points (blue points) and pure recessional data (red points) are selected for 2011. In background, the cumulative precipitation and selected slope element are also identified as representing of characteristic recession piezometric level.*

Table 4.4: *MRC parameter values for 2011.*

Parameter	**value**
resplimits	6.9 to 7.97 m
throughorigin	false
mindrytime	3 d
maxdelprec	1 mm
tslength	3 d
maxtick	0.1 m
binsize	0
maxslope	-0.01

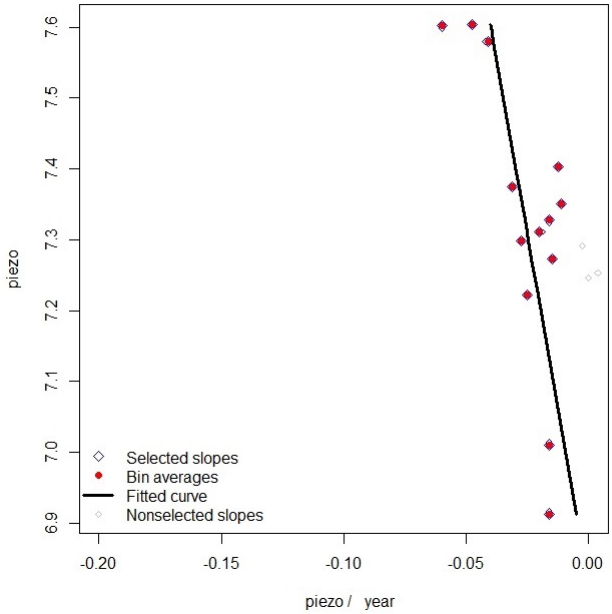

Figure 4.28: *Master Recession Curve (MRC) for 2011. Points representing slope elements determined by regression, with fitted master recession curve as a black line.*

Table 4.5: *MRC parameters values for 2012.*

Parameter	**value**
resplimits	5.5 to 6.5 m
throughorigin	false
mindrytime	2 d
maxdelprec	1 mm
tslength	3 d
maxtick	0.1 m
binsize	0
maxslope	-0.01

Table 4.6: *MRC parameters values for 2013.*

Parameter	**value**
resplimits	4.6 to 6.6 m
throughorigin	false
mindrytime	2 d
maxdelprec	1 mm
tslength	3 d
maxtick	0.1 m
binsize	0
maxslope	-0.01

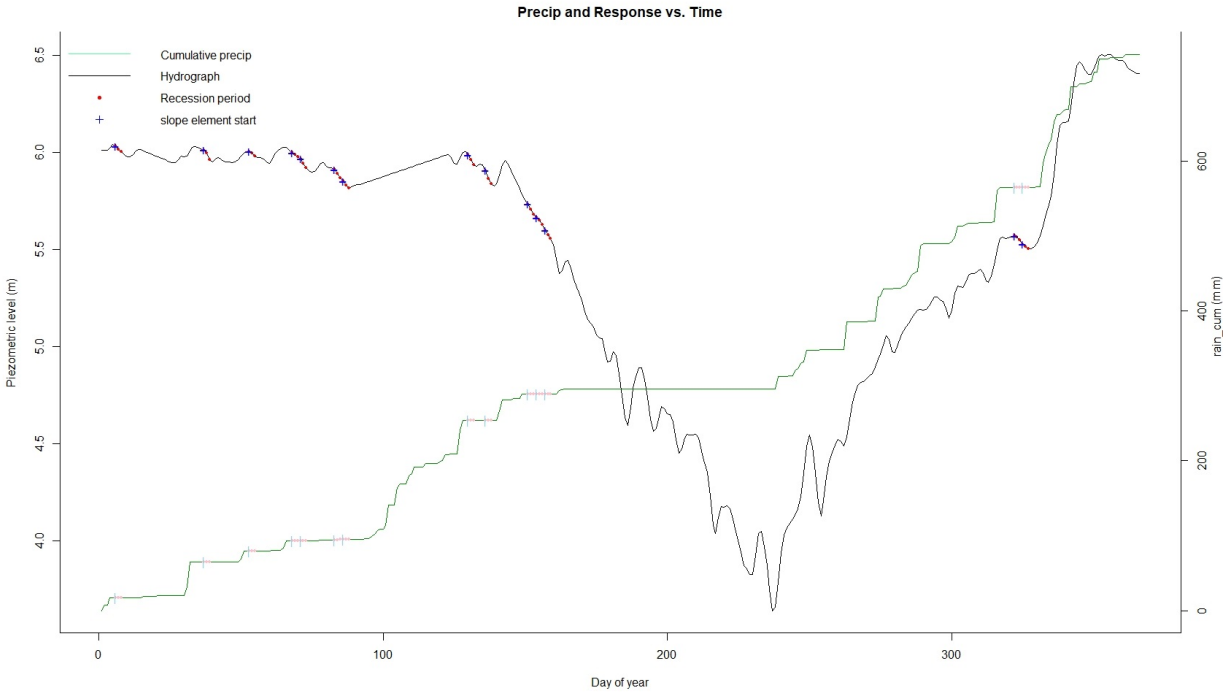

Figure 4.29: *Hydrograph with piezometric level (where H_0 = 9 m a.s.l.) where start points (blue points) and pure recessional data (red points) are selected for 2012. In background, the cumulative precipitation and selected slope element are also identified as representing of characteristic recession piezometric level. In this case with the exception of two points identified at the end of the distribution. This because* resplimits *parameter selects only the depth range of the recession levels to be analyzed.*

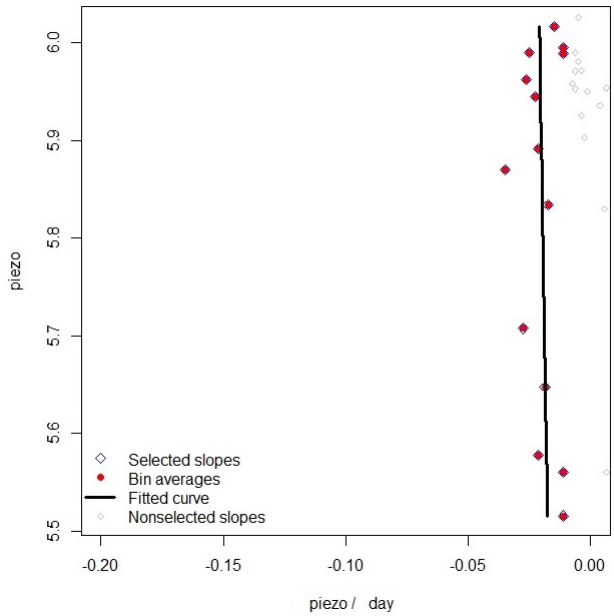

Figure 4.30: *Master Recession Curve (MRC) for 2012. Points representing slope elements determined by regression, with fitted master recession curve as a black line.*

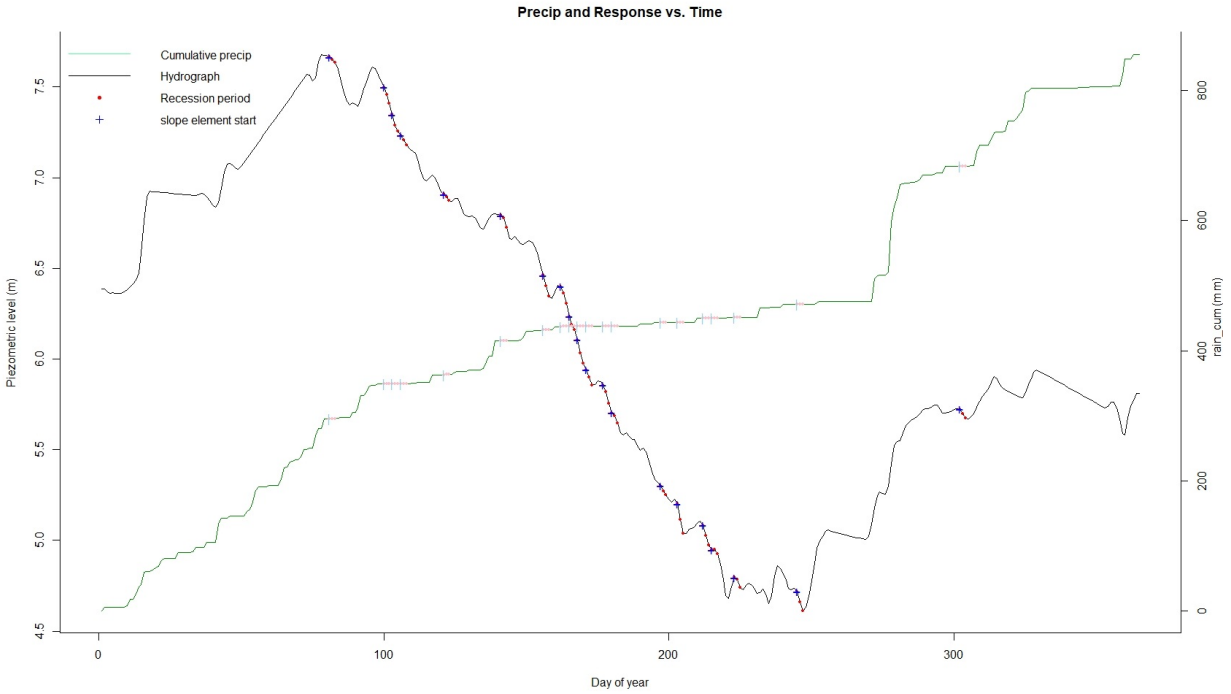

Figure 4.31: *Hydrograph with piezometric level (where H_0 = 9 m a.s.l.) where start points (blue points) and pure recessional data (red points) are selected for 2013. In background, the cumulative precipitation and selected slope element are also identified as representing of characteristic recession piezometric level. Evaluation of the recession period for this time series was performed by excluding the initial period (first 80 days) due to the presence of significant interpolations.*

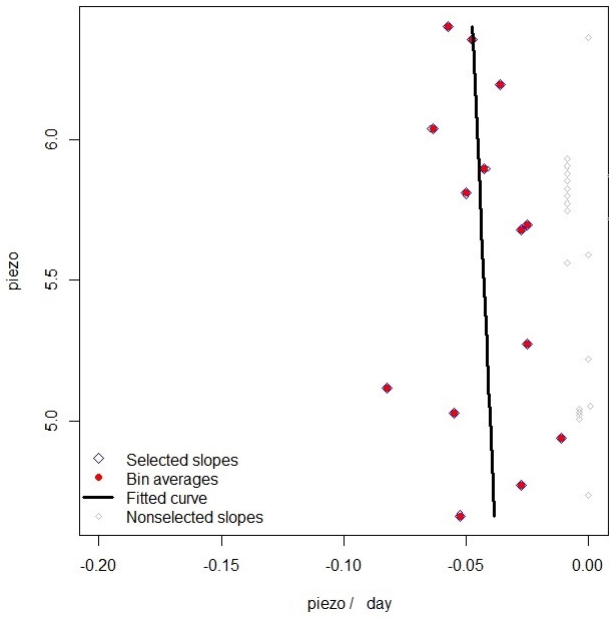

Figure 4.32: *Master Recession Curve (MRC) for 2013. Points representing slope elements determined by regression, with fitted master recession curve as a black line.*

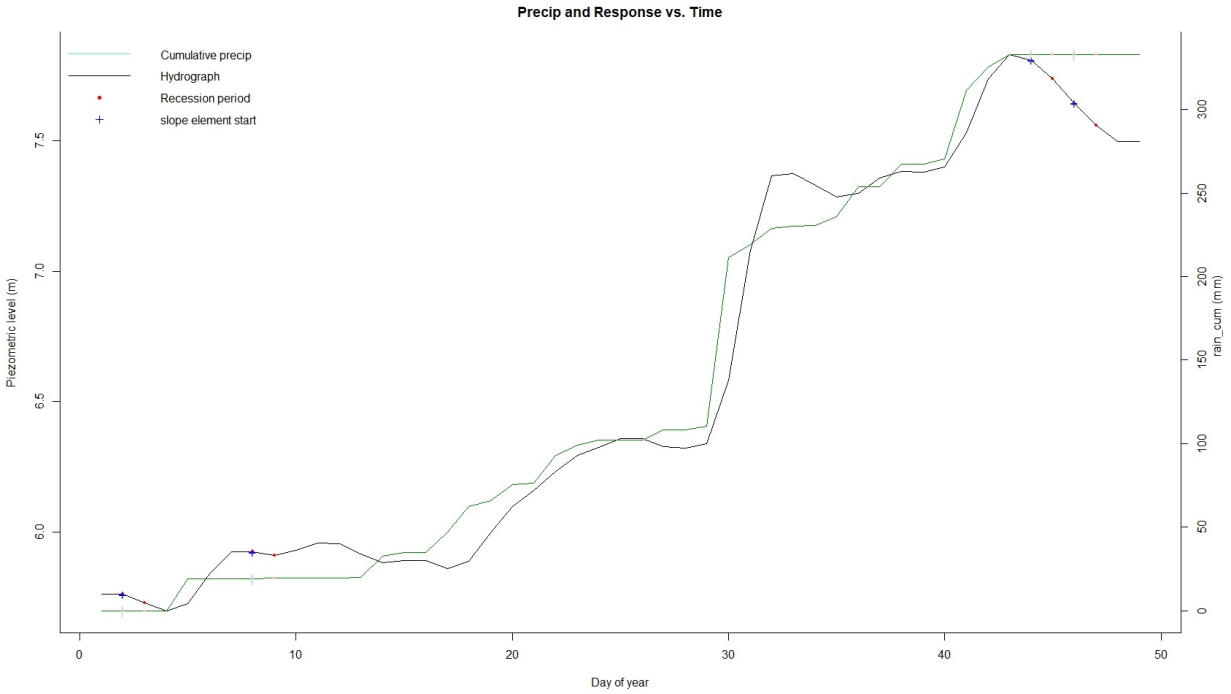

Figure 4.33: *Hydrograph with piezometric level (where H_0 = 9 m a.s.l.) where start points (blue points) and pure recessional data (red points) are selected for 2014. In background, the cumulative precipitation and selected slope element are also identified as representing of characteristic recession piezometric level. It was possible to study only first part of the year.*

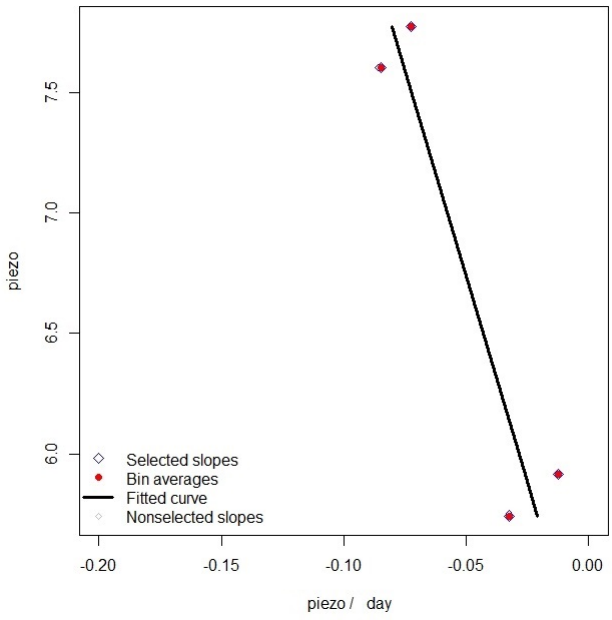

Figure 4.34: *Master Recession Curve (MRC) for 2014. Points representing slope elements determined by regression, with fitted master recession curve as a black line.*

Table 4.7: *MRC parameters values for 2014.*

Parameter	**value**
resplimits	5.7 to 7.8 m
throughorigin	false
mindrytime	2 d
maxdelprec	1 mm
tslength	2 d
maxtick	0.1 m
binsize	0
maxslope	-0.01

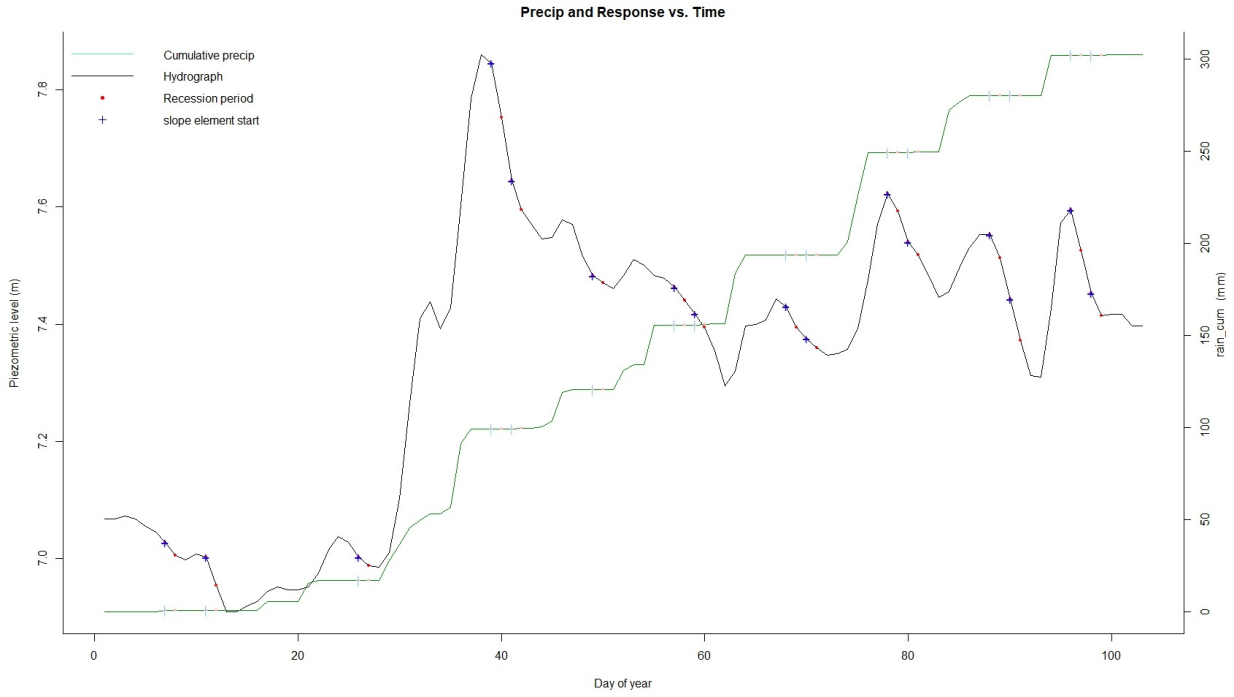

Figure 4.35: *Hydrograph with piezometric level (where H_0 = 9 m a.s.l.) where start points (blue points) and pure recessional data (red points) are selected for winter-spring of 2015. In background, the cumulative precipitation and selected slope element are also identified as representing of characteristic recession piezometric level.*

Table 4.8: *MRC parameters values for winter-spring of 2015.*

Parameter	**value**
resplimits	6.91 to 7.86 m
throughorigin	false
mindrytime	2 d
maxdelprec	1 mm
tslength	2 d
maxtick	0.1 m
binsize	0
maxslope	-0.01

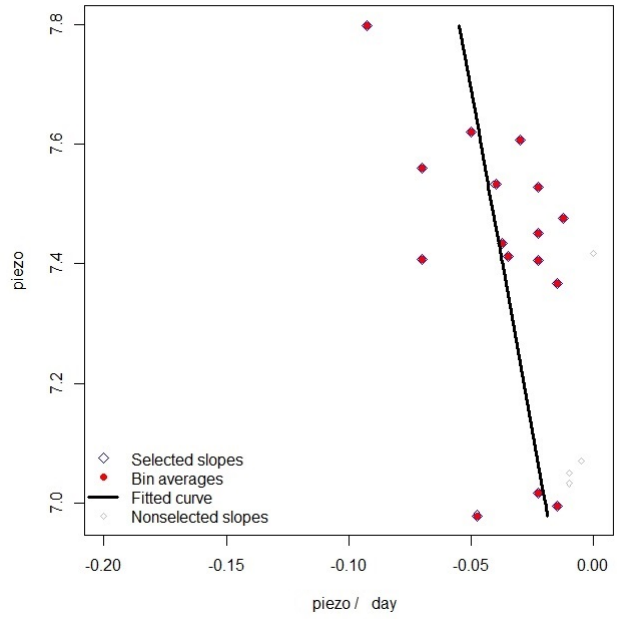

Figure 4.36: *Master Recession Curve (MRC) for winter-spring period of 2015. Points representing slope elements determined by regression, with fitted master recession curve as a black line.*

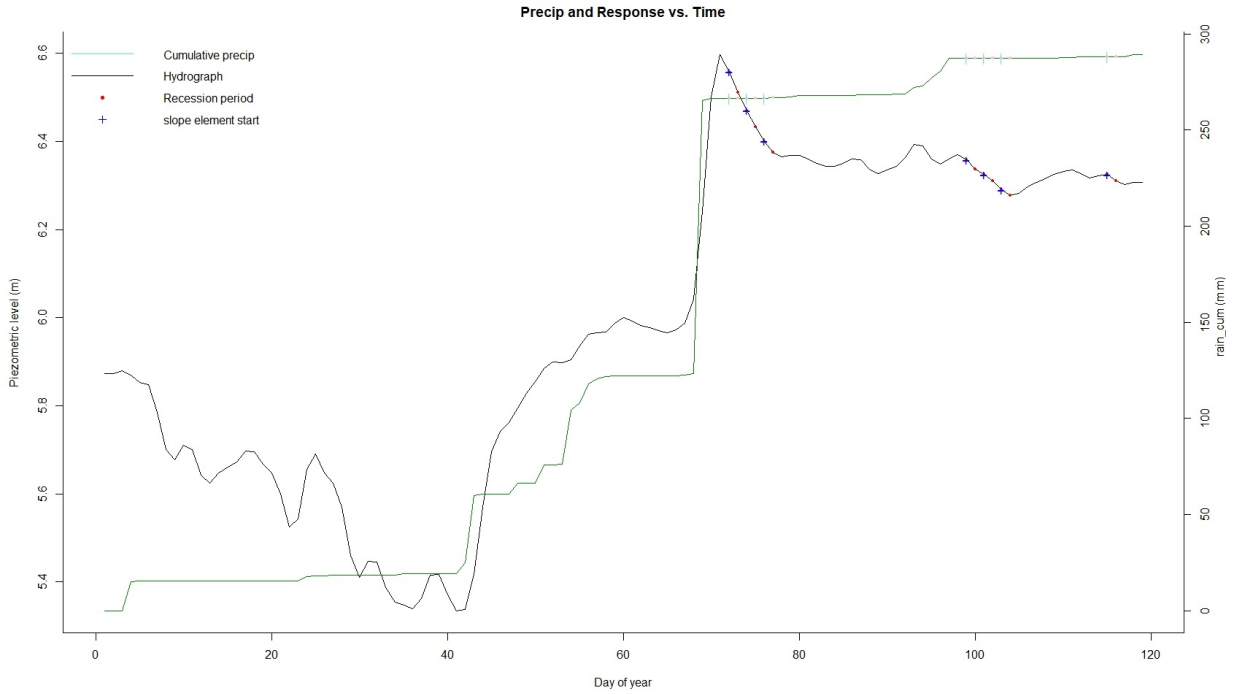

Figure 4.37: *Hydrograph with piezometric level (where H_0 = 9 m a.s.l.) where start points (blue points) and pure recessional data (red points) are selected for summer-autumn of 2015. In background, the cumulative precipitation and selected slope element are also identified as representing of characteristic recession piezometric level.*

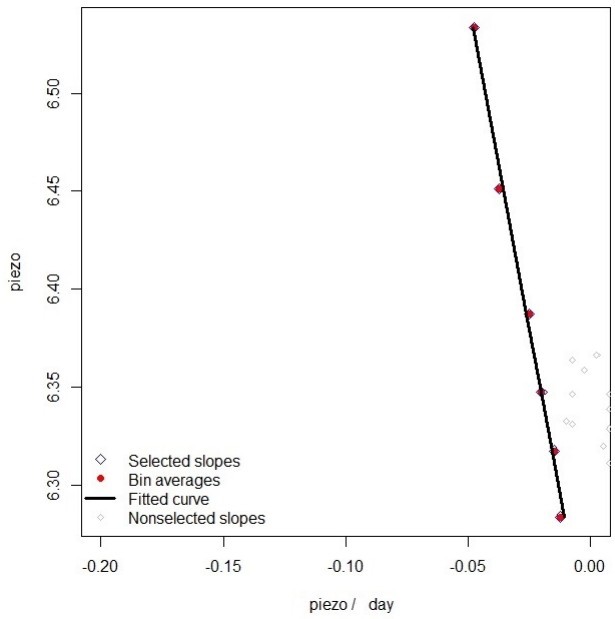

Figure 4.38: *Master Recession Curve (MRC) for summer-autumn period of 2015. Points representing slope elements determined by regression, with fitted master recession curve as a black line.*

Table 4.9: *MRC parameters values for summer-winter of 2015.*

Parameter	**value**
resplimits	6.2 to 6.59 m
throughorigin	false
mindrytime	2 d
maxdelprec	1 mm
tslength	2 d
maxtick	0.1 m
binsize	0
maxslope	-0.01

Table 4.10: *MRC parameters values for 2017.*

Parameter	**value**
resplimits	5.9 to 6.35 m
throughorigin	false
mindrytime	3 d
maxdelprec	1 mm
tslength	3 d
maxtick	0.1 m
binsize	0
maxslope	-0.01

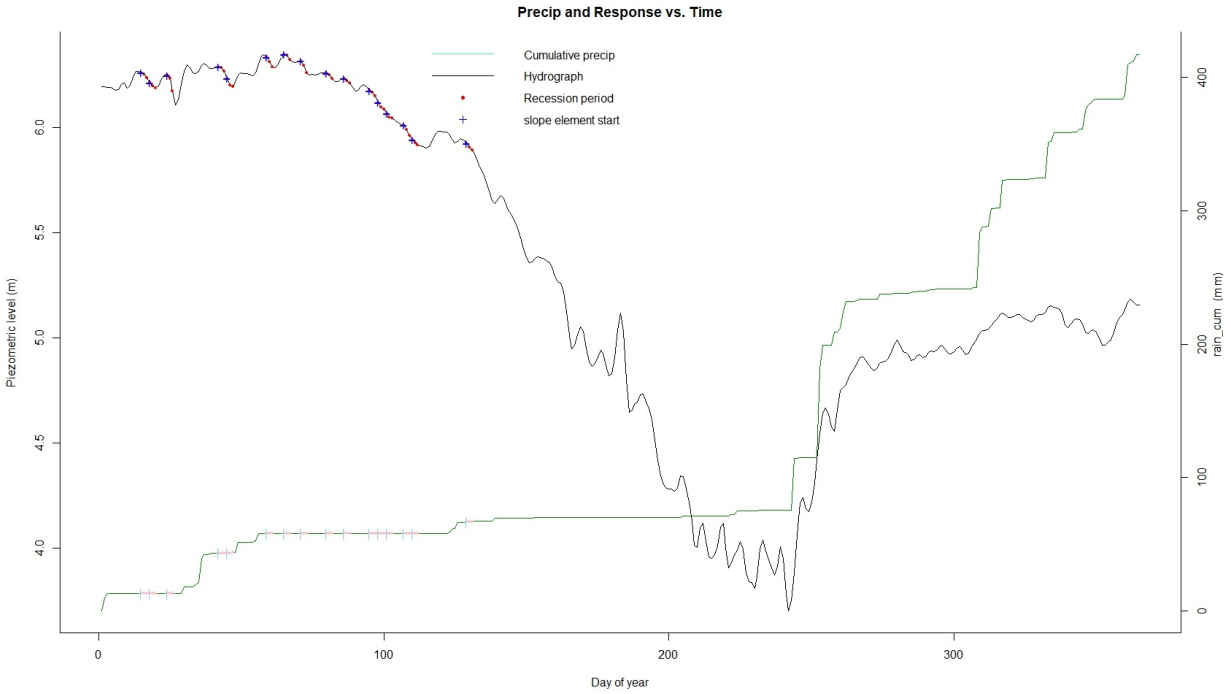

Figure 4.39: *Hydrograph with piezometric level (where H_0 = 9 m a.s.l.) where start points (blue points) and pure recessional data (red points) are selected for 2017. In background, the cumulative precipitation and selected slope element are also identified as representing of characteristic recession piezometric level.*

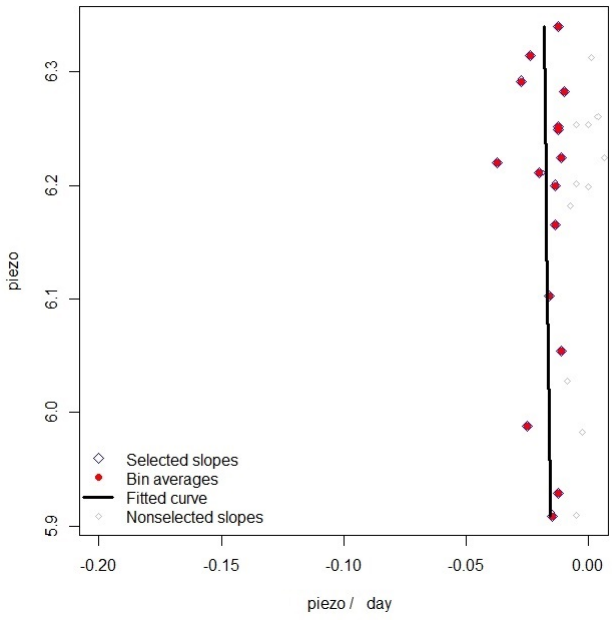

Figure 4.40: *Master Recession Curve (MRC) for 2017. Points representing slope elements determined by regression, with fitted master recession curve as a black line.*

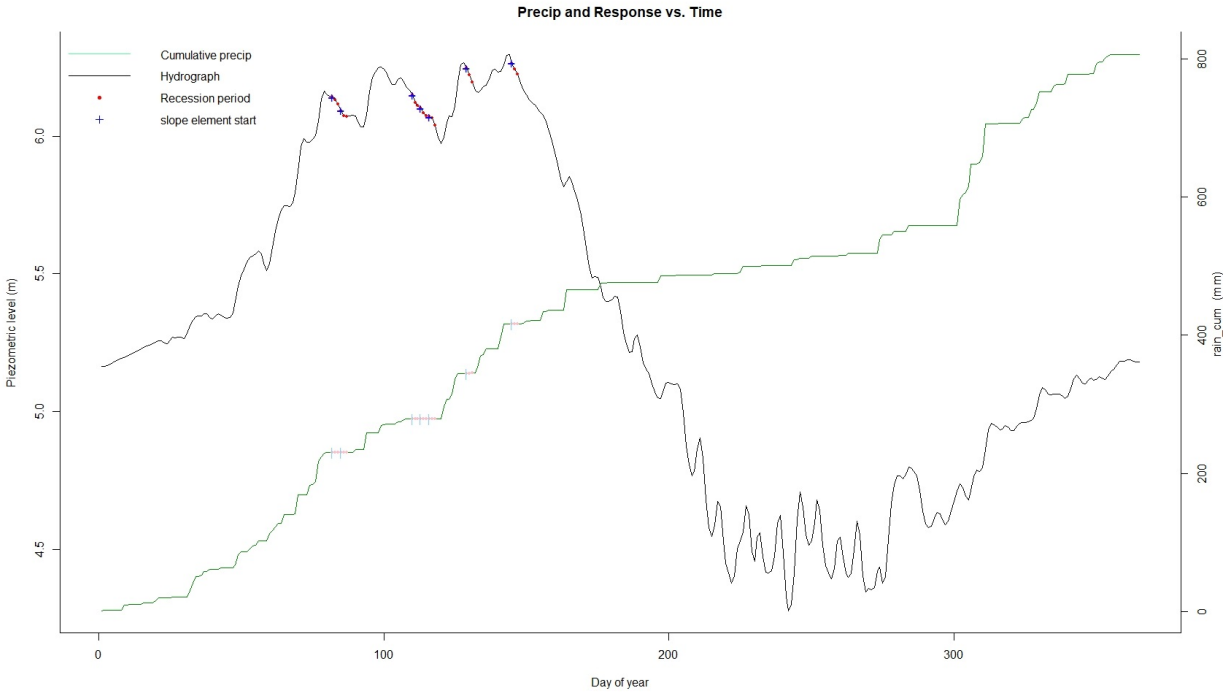

Figure 4.41: *Hydrograph with piezometric level (where H_0 = 9 m a.s.l.) where start points (blue points) and pure recessional data (red points) are selected for 2018. In background, the cumulative precipitation and selected slope element are also identified as representing of characteristic recession piezometric level.*

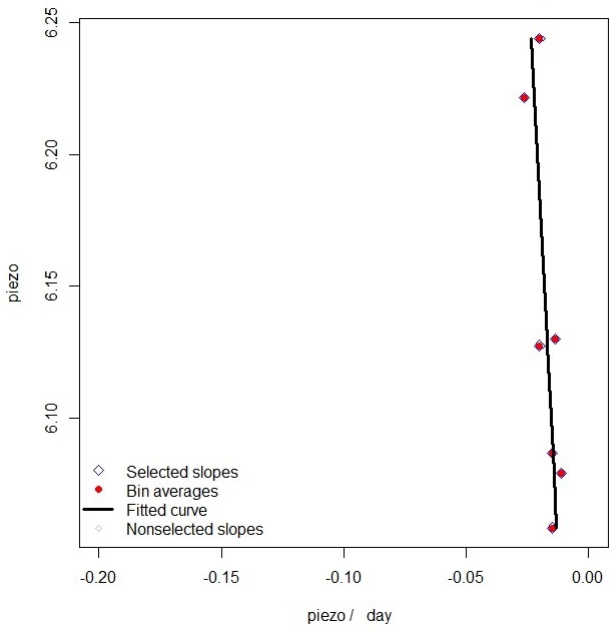

Figure 4.42: *Master Recession Curve (MRC) for 2018. Points representing slope elements determined by regression, with fitted master recession curve as a black line.*

Table 4.11: *MRC parameters values for 2018.*

Parameter	**value**
resplimits	5.9 to 6.23 m
throughorigin	false
mindrytime	3 d
maxdelprec	1 mm
tslength	3 d
maxtick	0.1 m
binsize	0
maxslope	-0.01

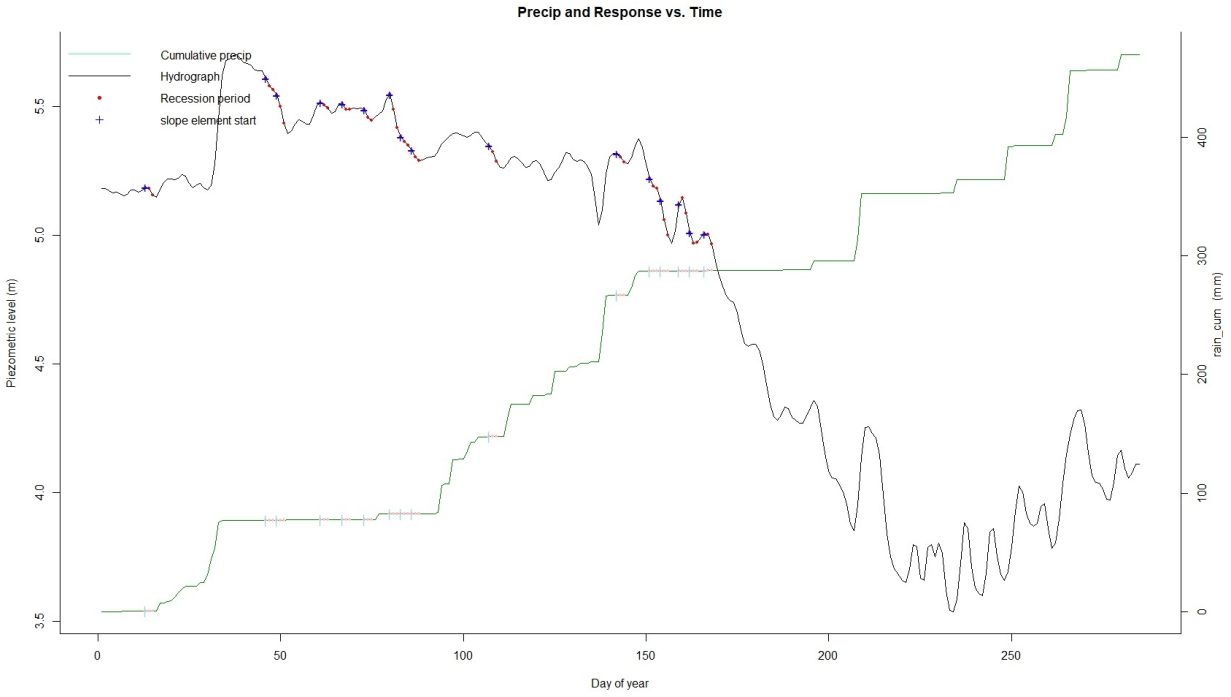

Figure 4.43: *Hydrograph with piezometric level (where H_0 = 9 m a.s.l.) where start points (blue points) and pure recessional data (red points) are selected for 2019. In background, the cumulative precipitation and selected slope element are also identified as representing of characteristic recession piezometric level.*

Table 4.12: *MRC parameters values for 2019.*

Parameter	**value**
resplimits	5.9 to 6.35 m
throughorigin	false
mindrytime	3 d
maxdelprec	1 mm
tslength	3 d
maxtick	0.1 m
binsize	0
maxslope	-0.01

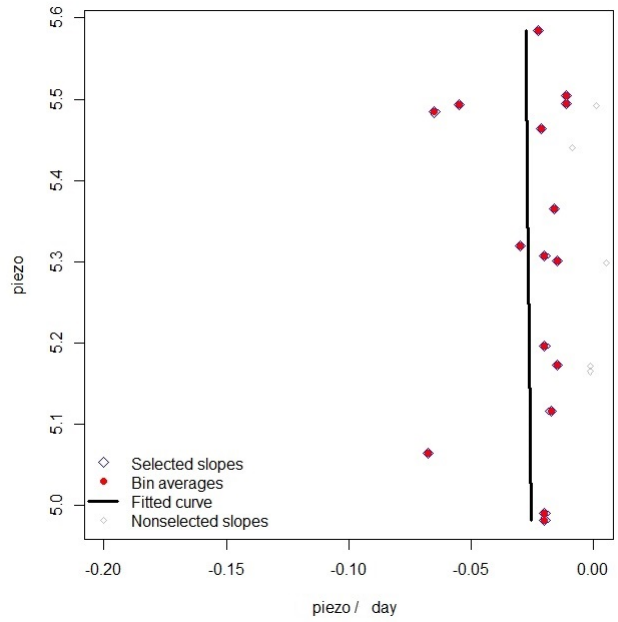

Figure 4.44: *Master Recession Curve (MRC) for 2019. Points representing slope elements determined by regression, with fitted master recession curve as a black line.*

4.2 Determination of the specific yield by electrical resistivity tomography

Geophysical data acquisition campaign was performed from 22 to 27 January 2017 and following were performed: two geophysical surveys in geoelectrical arrays, electrical resistivity. The geoelectrical lines EL04 and EL05 were 166 m and 237.5 m respectively, with a spacing of 2m and 2.5 meters. Geoelectrical prospecting were carried out using the method of electrical resistivity using Syscal Pro georesistimeter by IRIS Instruments which allows for fully automatic measurements. For acquisitions in the study area, carried out using a reciprocal Schlumberger quadripolar configuration, from a minimum of 84 to a maximum of 96 galvanic-coupled metal electrodes were used. The distance from the monitoring well and the geoelectrical lines are 54 m for the EL04 line and 24 m from the beginning of the EL05 line. The first step in processing data acquired during the campaign carried out in the study site was to define a 2D block model, for each profile, that divided the investigation zone into a number of rectangular cells with strictly arranged and size linked to the distribution of the measurement points in the acquisition phase and to the electrode spacing. For all the profiles a model was used in which the cells have equal width equal to half of the electrode spacing.

The program used for data processing uses an inversion process based on the technique of optimizing least squares using mathematical analysis with finite differences and finite element. The purpose is to determine the resistivity value of each single block of the model such as to produce an apparent resistivity as far as possible according to the measured value. Iterative process stops when the difference between the minimum is reduced to a set minimum resistivity measured in the field and that calculated by the set model. The quantification of the deviation of

Figure 4.45: *Syscal Pro georesistivimeter by IRIS Instruments.*

the two measurements is indicated by the standard deviation returned by the model. The water level measured during the data acquisition campaign was 6.9 m a.s.l in agreement with the values recorded by the electronic monitoring system in the same period. This evaluation has allowed us to identify the boundary between the unsaturated and saturated subsoil horizon. From here it was possible to derive the average resistivity values for the two horizons (table 4.13), used in the equation 3.12. Considering the inconsistent nature of the lithologies found on site, a value of 1.3 was placed on the m coefficient and a value of 2 on the n coefficient [118]. The water resistivity ρ_w of the site was calculated using the mean value determined on site through the conductivity log (table 4.2). From the equations 4.1 and 4.2 a value of ρ_w equal to 9.85 Ωm was obtained. Finally, a value of Specific Yield of 0.12 was obtained, in accordance with the values obtained in the literature [118] for the same lithologies.

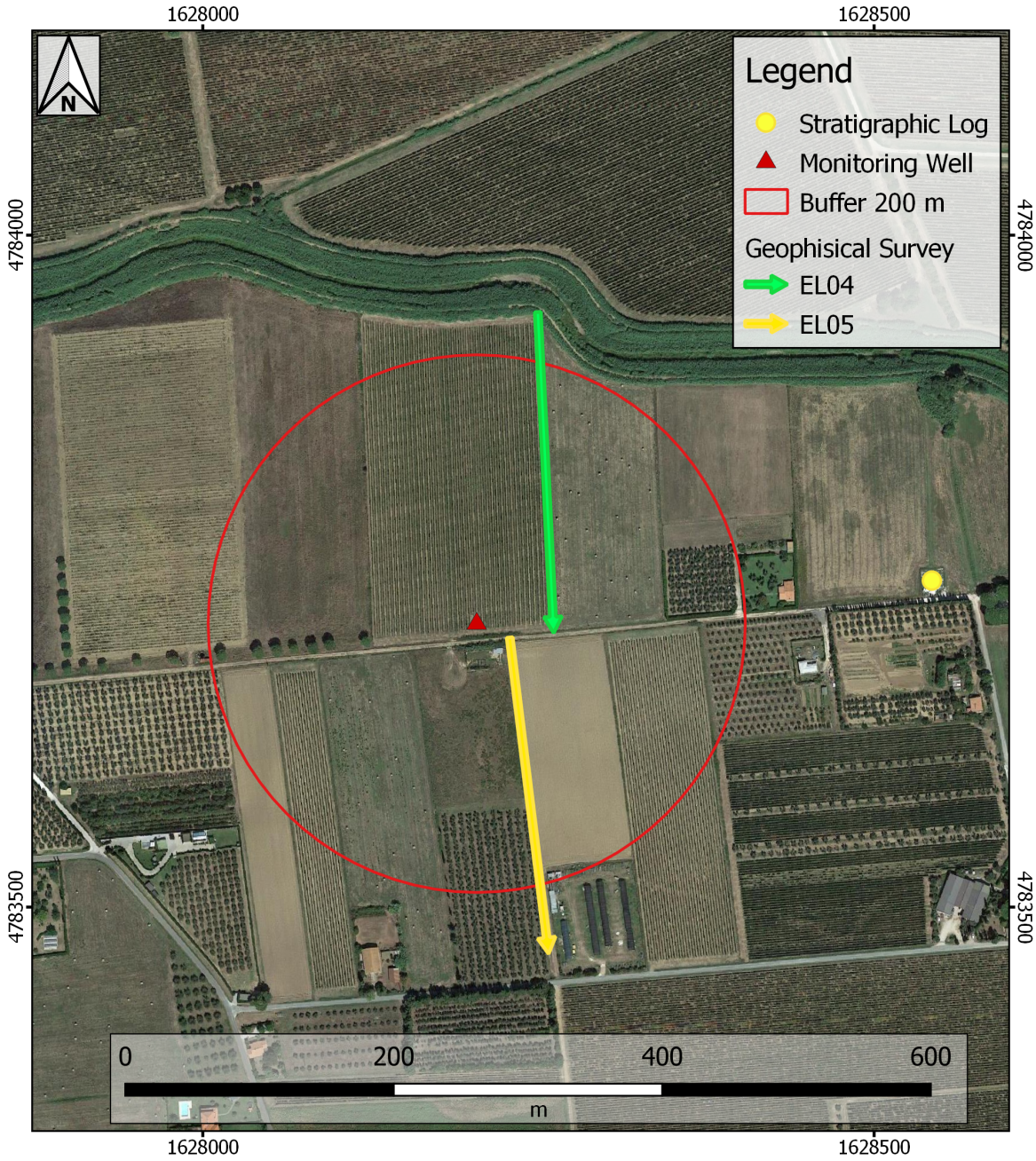

Figure 4.46: *Map of Geophysical survey: Electrical profile El04 (green line); Electrical profile El05 (yellow line); Monitoring well (red triangle); Perforation stratigraphic log (yellow circle); Well pumping area verification [1].*

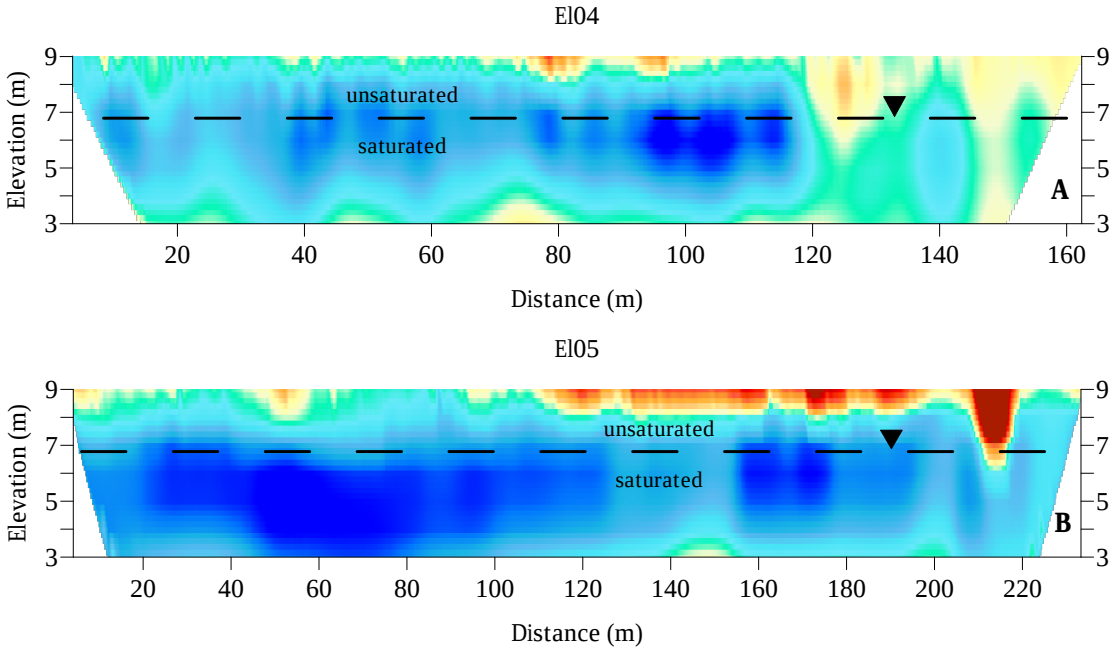

Figure 4.47: *2D Electrical Resistivity Tomography carried out with Schlumberger reciprocal quadripolar configuration. Electrical tomography sections: (A) Electrical profile El04; (B) Electrical profile El05.*

Table 4.13: *Calculated values of resistivity.*

Level	**Mean (Ωm)**	**St. Dev. (Ωm)**	**Altitude (m)**
Unsaturated	28.2	19	Altitude $>$ 6.9
Saturated	18.1	4.10	3.5 $<$ Altitude $<$ 6.9

$$\sigma(S/cm) = \frac{1}{\rho(\Omega cm)} \Rightarrow \rho(\Omega cm) = \frac{1}{\sigma(S/cm)} \tag{4.1}$$

$$\rho(\Omega cm) = \frac{1}{1.015 * 10^{-3}(S/cm)} = 985.22\ \Omega cm = 9.85\ \Omega m \tag{4.2}$$

$$S_y = \left(\frac{9.85}{18.1}\right)^{\frac{1}{1.3}} \times \left[1 - \left(\frac{18.1}{28.2}\right)^{\frac{1}{2}}\right] = 0.12 \tag{4.3}$$

Table 4.14: *Parameters of equation 3.12.*

Parameter	Value
$\rho Unsat$	28.2
ρSat	18.1
ρw	9.85
m	1.3
n	2

Figure 4.48: *First figure on the left represents electrical cables for the El04 line. The relative metric cable is visible in white, useful for establishing the electrodes spacing at a distance of 2 meters. Second image on the right shows the detail of the electrode into the ground during the acquisition of the El05 line.*

4.3 Episodic master recession parameter setting

The EMR method was applied to the time series of the water table using the coefficient of the curved master recession obtained. Regarding to physical parameter setting for recharge episodes calculation, they are discussed in chapter 5.1.

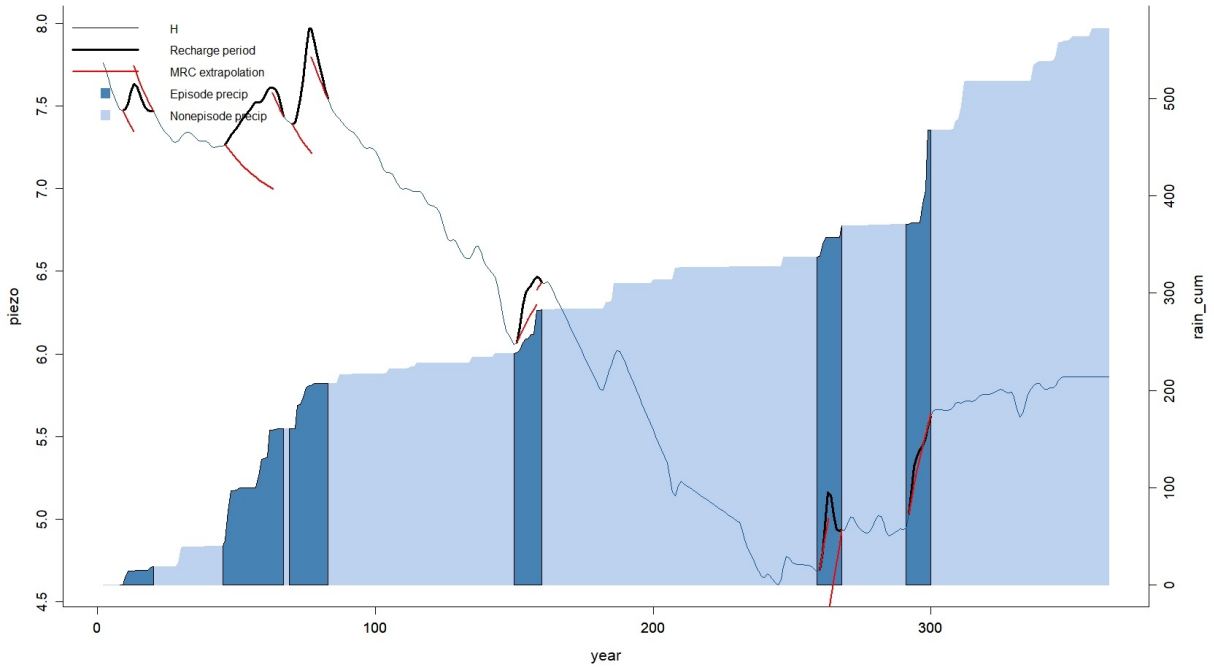

Figure 4.49: *Hydrograph with recharge episodes distinguished for 2011: quantitative identifications are classified in table 4.16.*

Table 4.15: *EMR parameters values for 2011.*

Parameter	**value**
capacity	0.12 m
lagtime	1 d
fluctol	0.06 m/d
minprecip	1 mm
ependpar	3 d

The numerical results of calculated recharge episodes have been summarized in tables 4.16, in which are reported number of identified episodes, their duration in days, total precipitation input that generated the single event, Delta H width generated by the event, the recharge episode expressed in meters and the recharge-precipitation ratio RPR as a ratio between the groundwater recharge for the j^{th} recharge episode. Graphical result of the EMR application is visible for example in figure 4.61 in which cumulative precipitation and groundwater levels expressed as piezometric levels over time are illustrated. The hydrograph shows precipitation record with recharge episodes, which are indicated by a bold hydrograph trace. The red curves represents MRC extrapolations from the episode start and end points. Figure 4.62 shows the computed derivative of water-table

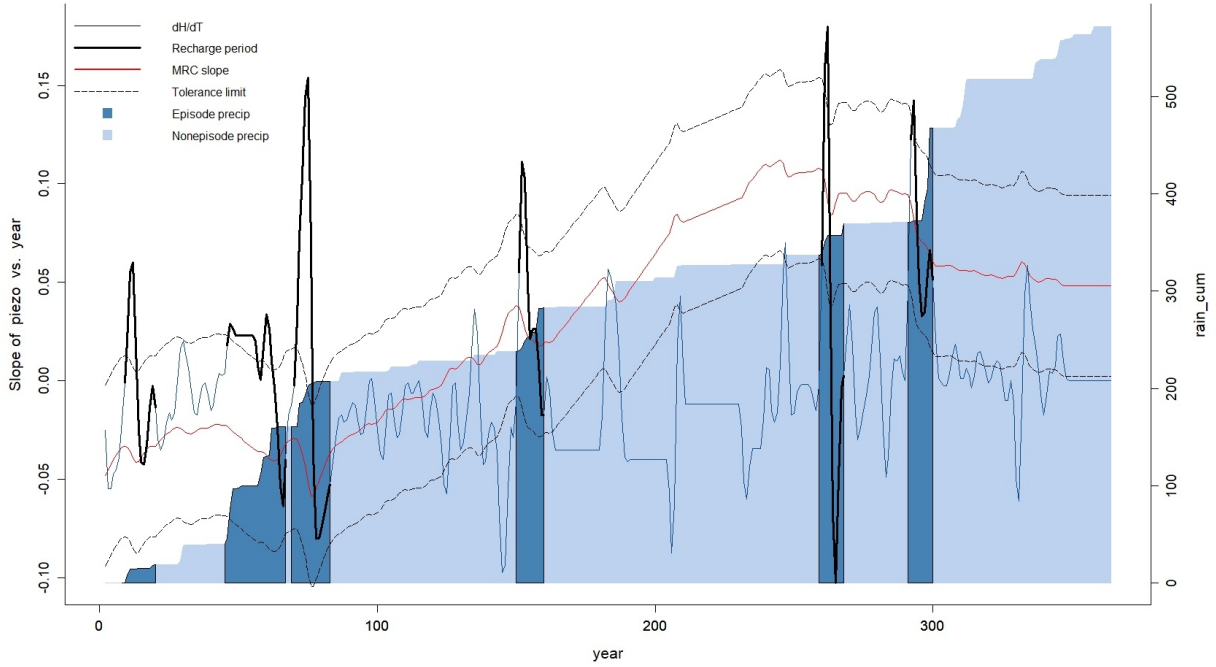

Figure 4.50: *Time derivative hydrograph where instantaneous slope are represented for 2011.*

Table 4.16: *EMR results for 2011.*

Episode	Duration (d)	Water Input (m)	Episode δH (m)	Episode Recharge (m)	RPR (m)
1	11	0.0182	0.39	0.05	2.570
2	21	0.1208	0.57	0.07	0.571
3	13	0.0464	0.58	0.07	1.502
4	9	0.0454	0.09	0.01	0.247
5	8	0.032	-0.59	-0.07	-2.235
6	8	0.097	-0.02	-0.002	-0.020

on time that identifies the same episodes shown in figure 4.61. Finally, the dashed black line indicates a tolerance band determined using *fluctol* parameter, useful to establish a threshold of dR/dt rate above which a recharge episode is detected.

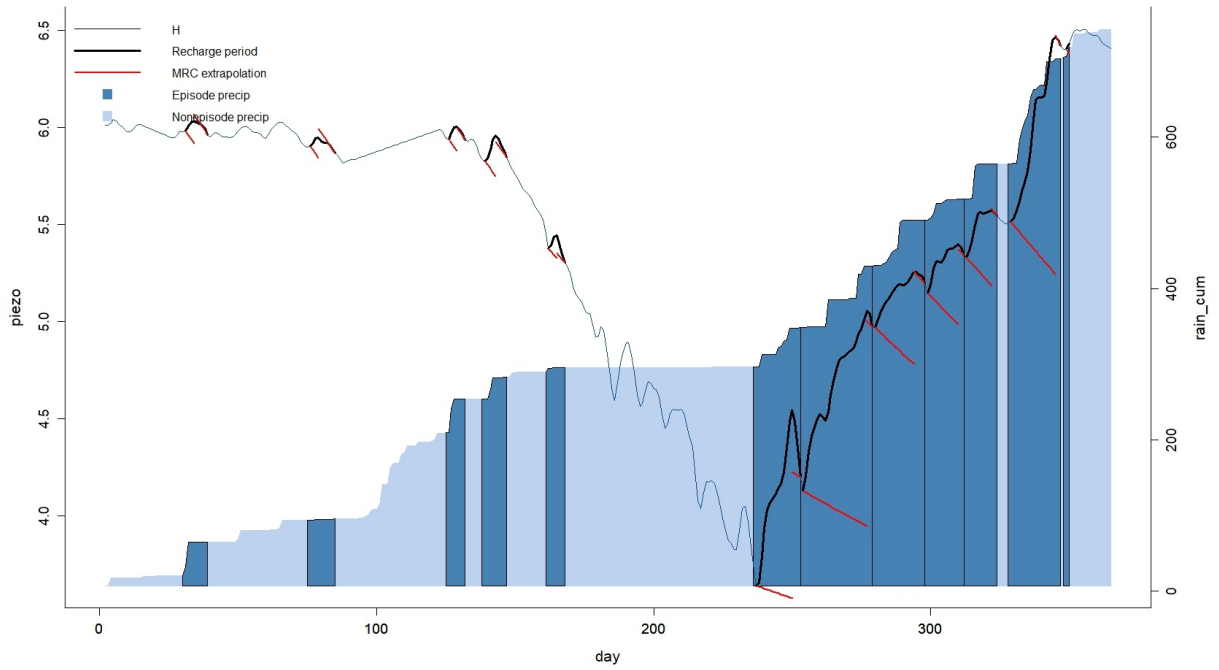

Figure 4.51: *Hydrograph with recharge episodes distinguished for 2012: quantitative identifications are classified in table 4.18.*

Table 4.17: *EMR parameters values for 2012.*

Parameter	**value**
capacity	0.12 m
lagtime	1 d
fluctol	0.04 m/d
minprecip	1 mm
ependpar	4 d

Table 4.18: *EMR results for 2012.*

Episode	Duration (d)	Water Input (m)	Episode δH (m)	Episode Recharge (m)	RPR (m)
1	8	0.045	0.15	0.02	0.396
2	9	0.002	0.15	0.02	9.963
3	6	0.045	0.12	0.01	0.0312
4	8	0.029	0.17	0.02	0.728
5	6	0.006	0.03	0.003	0.490
6	16	0.052	0.65	0.08	1.508
7	25	0.082	1.05	0.13	1.544
8	18	0.060	0.47	0.06	0.946
9	13	0.028	0.39	0.05	1.634
10	11	0.047	0.40	0.05	1.017
11	18	0.139	1.22	0.15	1.059
12	1	0.013	0.05	0.006	0.494

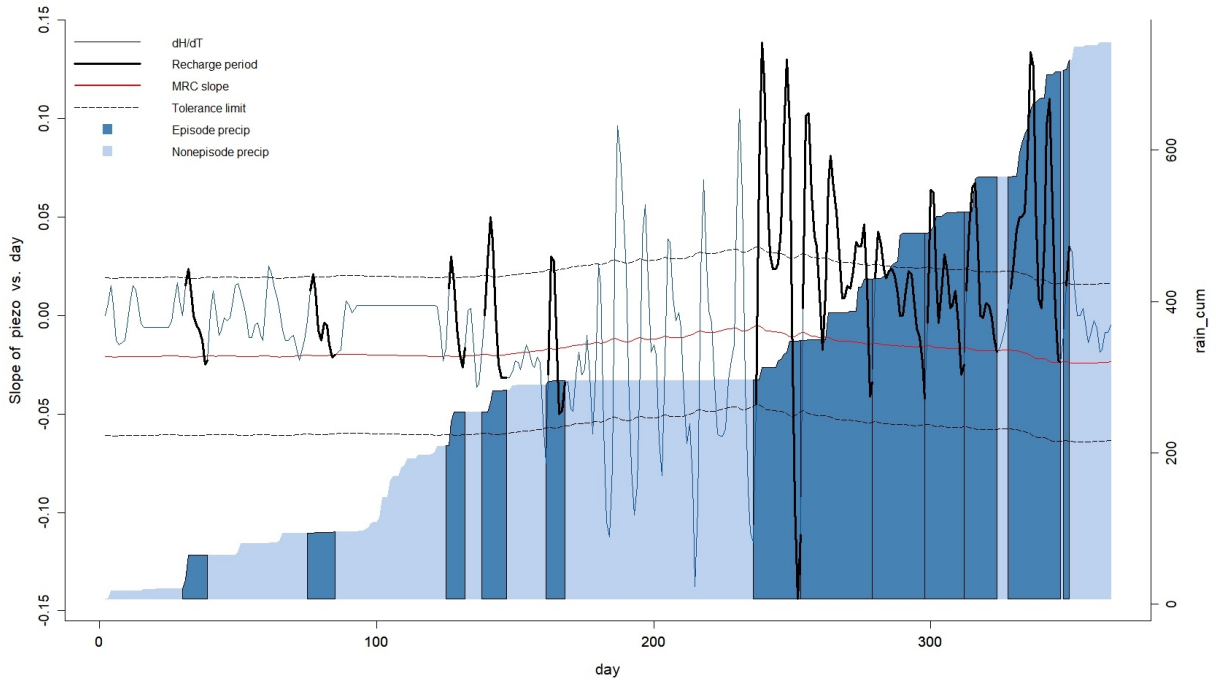

Figure 4.52: *Time derivative hydrograph where instantaneous slope are represented for 2012.*

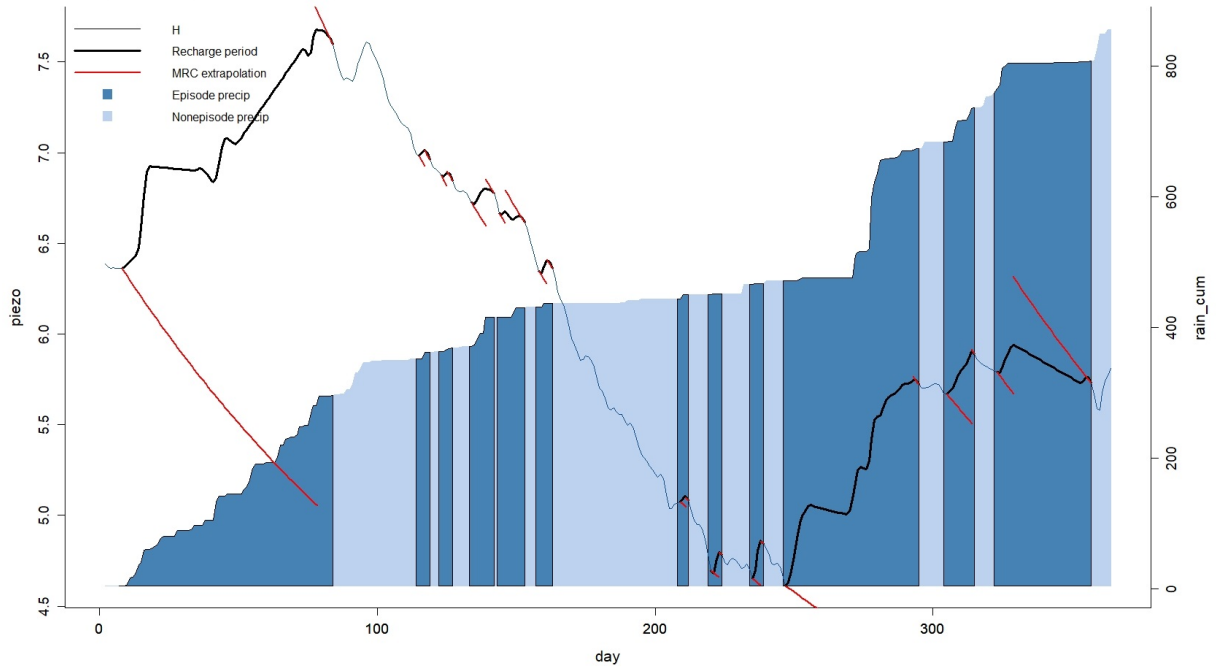

Figure 4.53: *Hydrograph with recharge episodes distinguished for 2013: quantitative identifications are classified in table 4.20.*

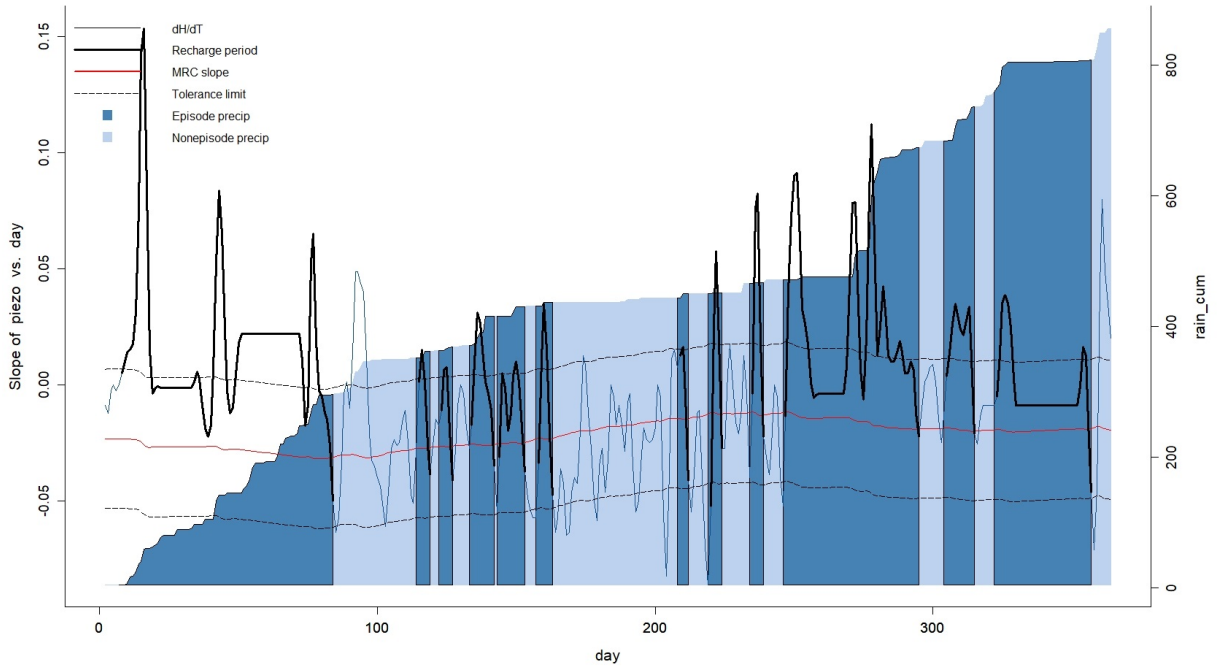

Figure 4.54: *Time derivative hydrograph where instantaneous slope are represented for 2013.*

Table 4.19: *EMR parameters values for 2013.*

Parameter	**value**
capacity	0.12 m
lagtime	1 d
fluctol	0.03 m/d
minprecip	1 mm
ependpar	4 d

Table 4.20: *EMR results for 2013.*

Episode	Duration (d)	Water Input (m)	Episode δH (m)	Episode Recharge (m)	RPR (m)
1	76	0.291	2.73	0.33	1.128
2	4	0.011	0.09	0.01	0.963
3	4	0.005	0.08	0.009	1.889
4	8	0.045	0.26	0.03	0.690
5	9	0.015	0.18	0.02	1.408
6	5	0.006	0.13	0.01	2.799
7	3	0.006	0.05	0.006	0.965
8	4	0.001	0.14	0.02	16.368
9	4	0.001	0.24	0.03	23.846
10	48	0.202	1.61	0.19	0.958
11	10	0.052	0.4	0.05	0.937
12	34	0.049	0.64	0.08	1.560

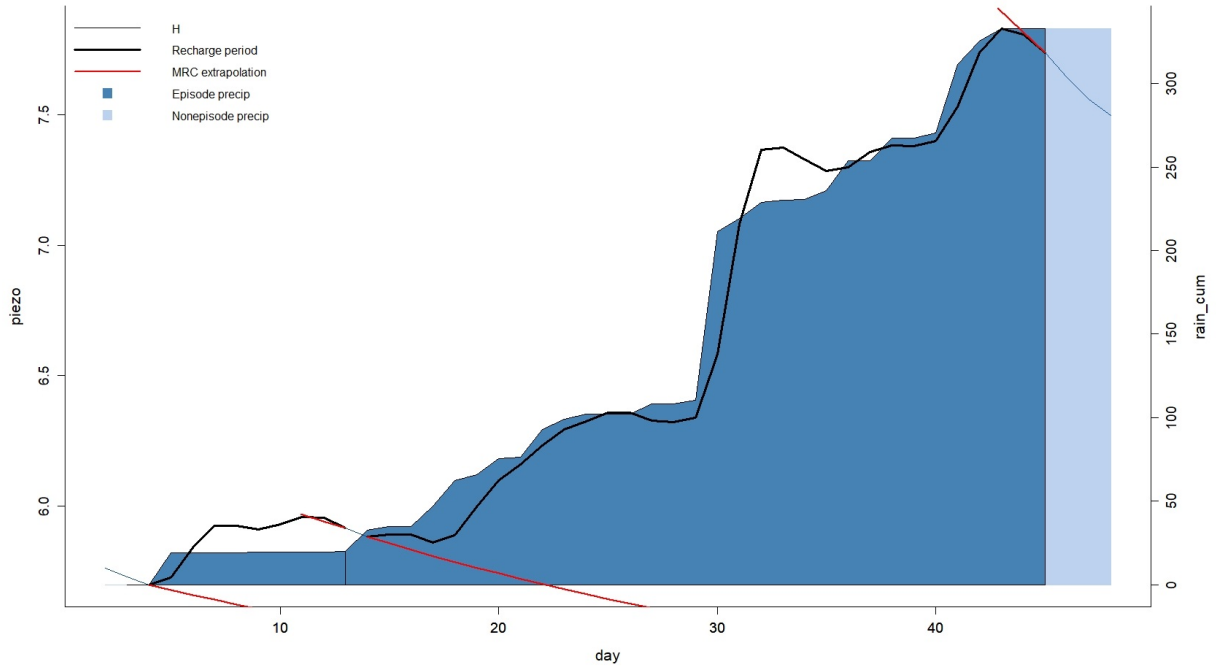

Figure 4.55: *Hydrograph with recharge episodes distinguished for 2014: quantitative identifications are classified in table 4.22.*

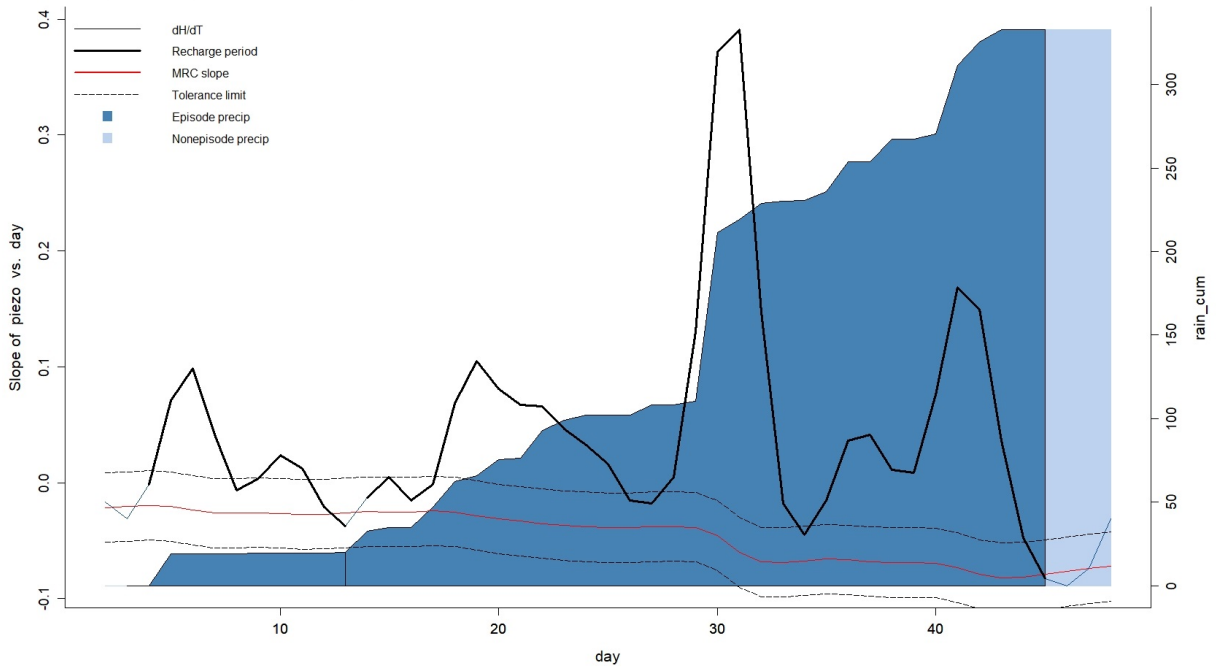

Figure 4.56: *Time derivative hydrograph where instantaneous slope are represented for 2014.*

Table 4.21: *EMR parameters values for 2014.*

Parameter	**value**
capacity	0.12 m
lagtime	1 d
fluctol	0.03 m/d
minprecip	1 mm
ependpar	1 d

Table 4.22: *EMR results for 2014 from January to February.*

Episode	Duration (d)	Water Input (m)	Episode δH (m)	Episode Recharge (m)	RPR (m)
1	9	0.02	0.4	0.05	2.400
2	31	0.31	2.51	0.3	0.962

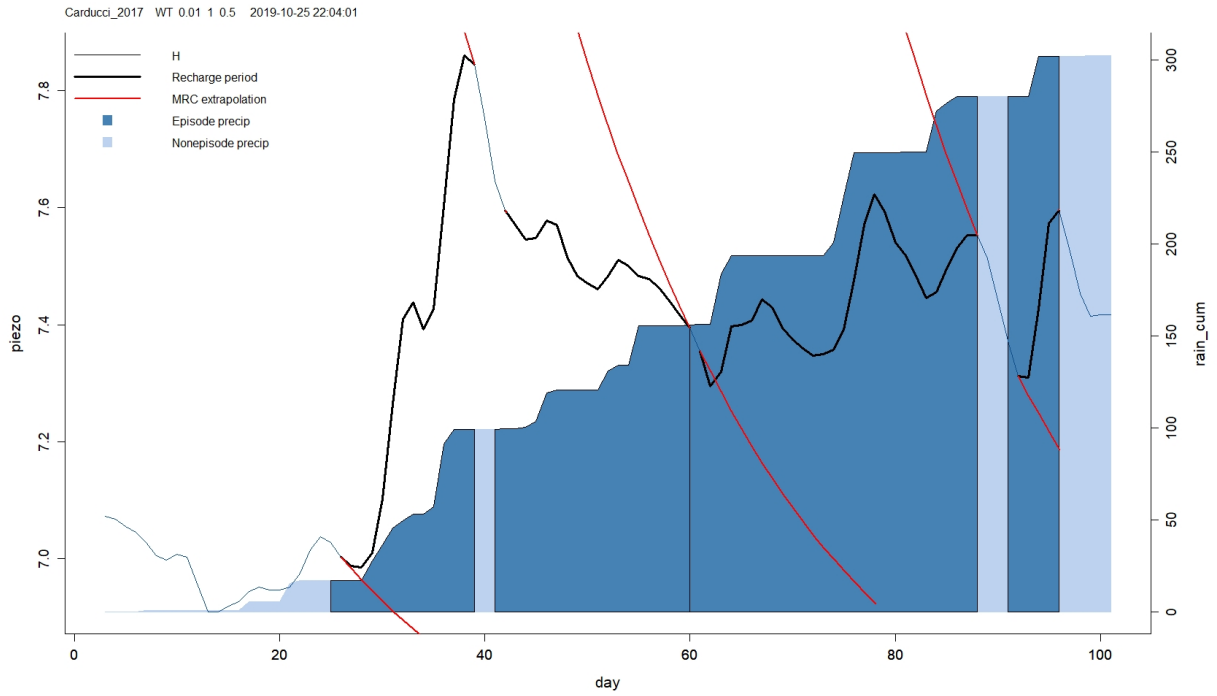

Figure 4.57: *Hydrograph with recharge episodes distinguished for 2015 (from Winter to Spring): quantitative identifications are classified in table 4.24.*

Table 4.23: *EMR parameters values for 2015 from Winter to Spring.*

Parameter	**value**
capacity	0.12 m
lagtime	1 d
fluctol	0.03 m/d
minprecip	1 mm
ependpar	1 d

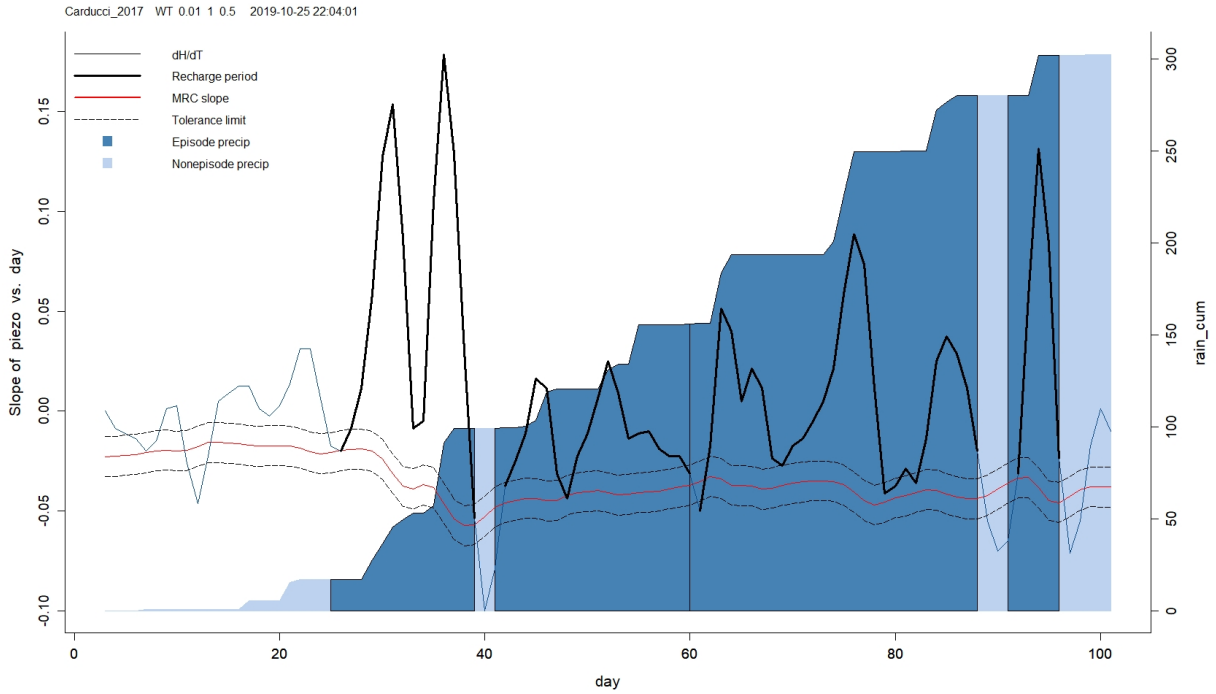

Figure 4.58: *Time derivative hydrograph where instantaneous slope are represented for 2015 (from Winter to Spring).*

Table 4.24: *EMR results for 2015 from Winter to Spring.*

Episode	Duration (d)	Water Input (m)	Episode δH (m)	Episode Recharge (m)	RPR (m)
1	13	0.082	1.09	0.13	1.583
2	18	0.057	0.78	0.09	1.660
3	27	0.124	1.16	0.14	1.126
4	4	0.022	0.41	0.05	2.223

Table 4.25: *EMR parameters values for 2015 from Summer to Autumn.*

Parameter	**value**
capacity	0.12 m
lagtime	1 d
fluctol	0.025 m/d
minprecip	1 mm
ependpar	1 d

Table 4.26: *EMR results for 2015 from Summer to Autumn.*

Episode	Duration (d)	Water Input (m)	Episode δH (m)	Episode Recharge (m)	RPR (m)
1	3	0.015	0.03	0.004	0.267
2	6	0.003	0.33	0.04	13.127
3	43	0.248	4.86	0.58	2.350

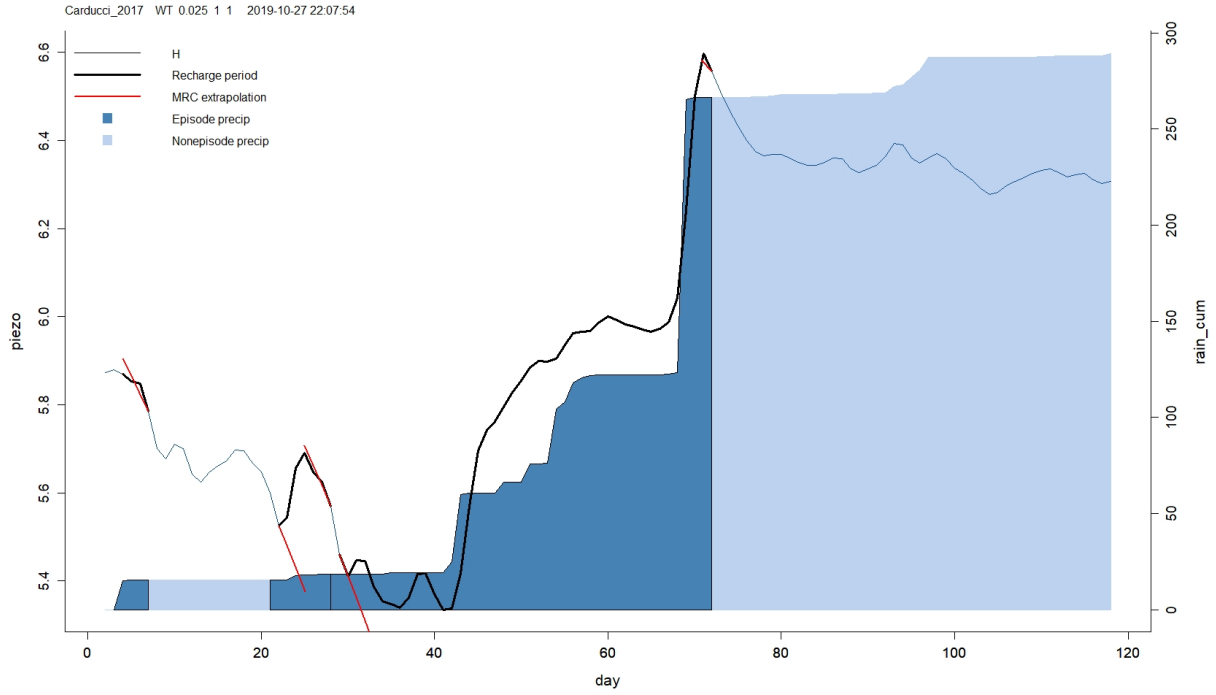

Figure 4.59: *Hydrograph with recharge episodes distinguished for 2015: quantitative identifications are classified in table 4.26.*

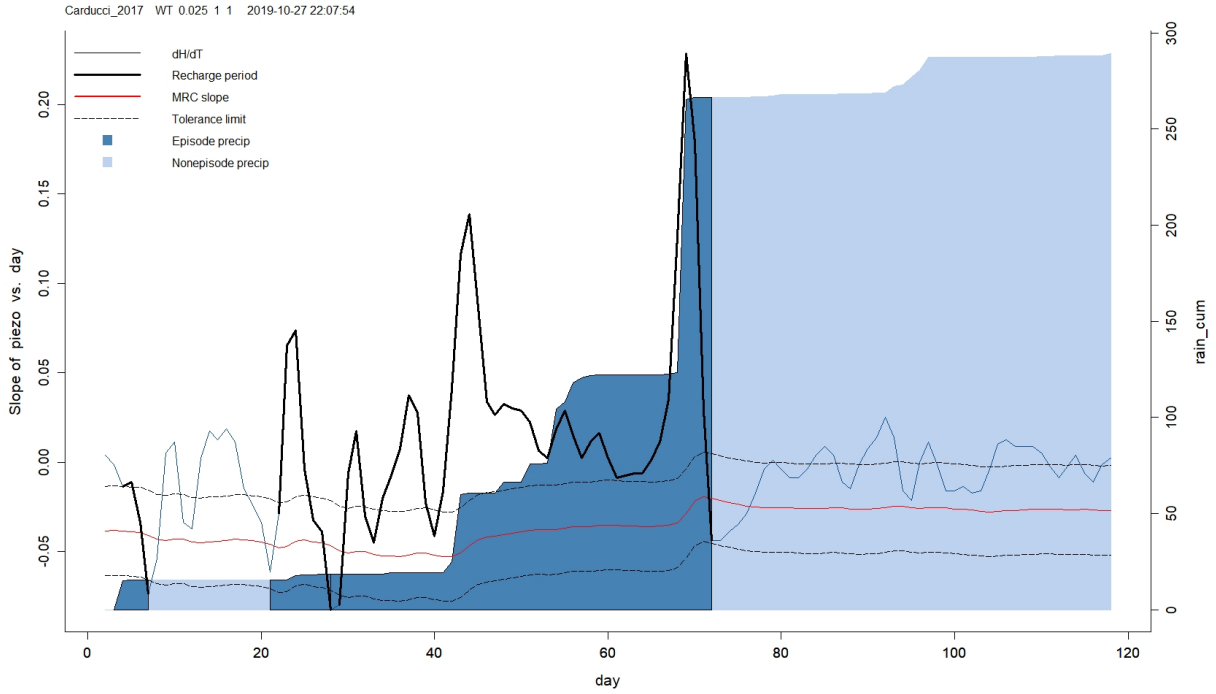

Figure 4.60: *Time derivative hydrograph where instantaneous slope are represented for 2015 from Summer to Autumn.*

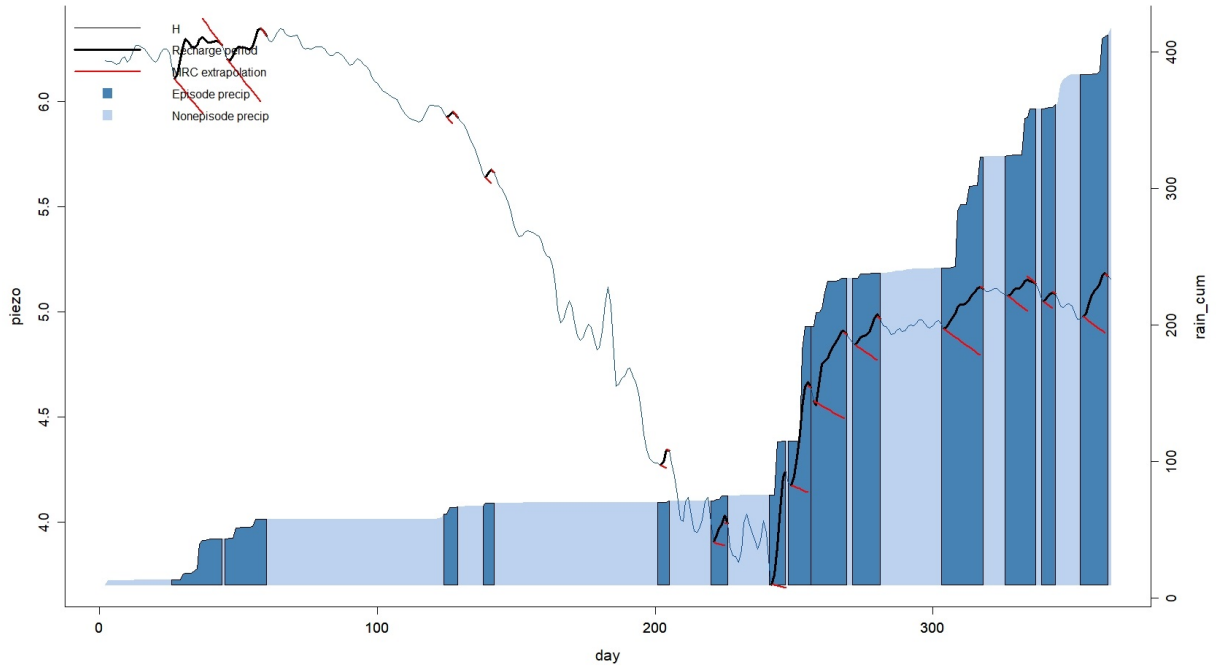

Figure 4.61: *Hydrograph with recharge episodes distinguished for 2017: quantitative identifications are classified in table 4.28.*

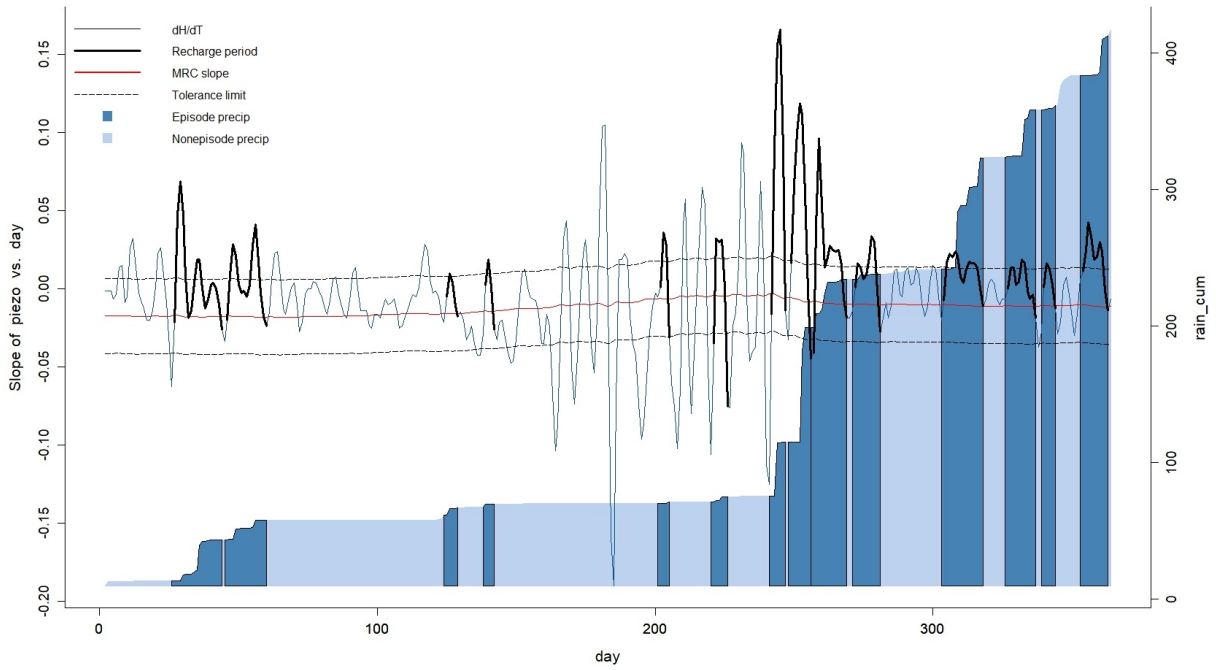

Figure 4.62: *Time derivative hydrograph where instantaneous slope are represented for 2017.*

Table 4.27: *EMR parameters values for 2017.*

Parameter	**value**
capacity	0.12 m
lagtime	1 d
fluctol	0.024 m/d
minprecip	1 mm
ependpar	1 d

Table 4.28: *EMR results for 2017.*

Episode	Duration (d)	Water Input (m)	Episode δH (m)	Episode Recharge (m)	RPR (m)
1	5	0.005	0.26	0.03	6.490
2	10	0.025	0.19	0.02	0.920
3	13	0.015	0.34	0.04	2.767
4	3	0.002	0.06	0.008	3.892
5	3	0.001	0.09	0.01	10.663
6	5	0.004	0.11	0.01	3.603
7	5	0.040	0.55	0.07	1.671
8	7	0.084	0.51	0.06	0.721
9	12	0.035	0.41	0.05	1.412
10	13	0.082	0.31	0.04	0.455
11	9	0.029	0.28	0.03	1.174

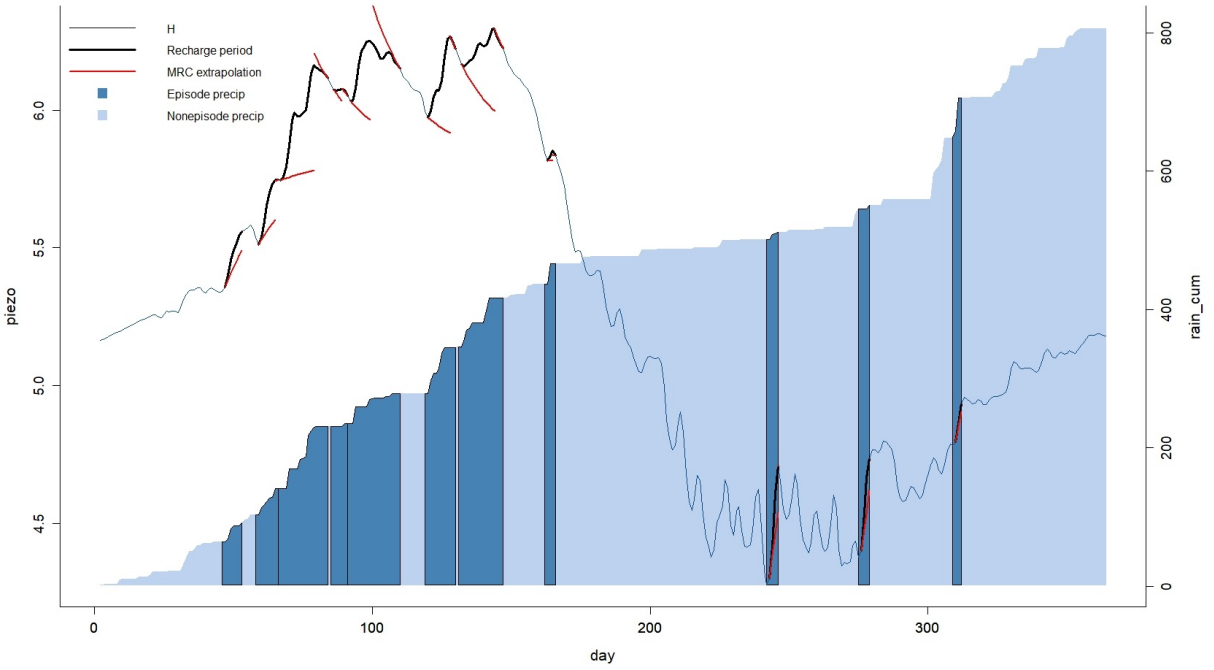

Figure 4.63: *Hydrograph with recharge episodes distinguished for 2018: quantitative identifications are classified in table 4.30.*

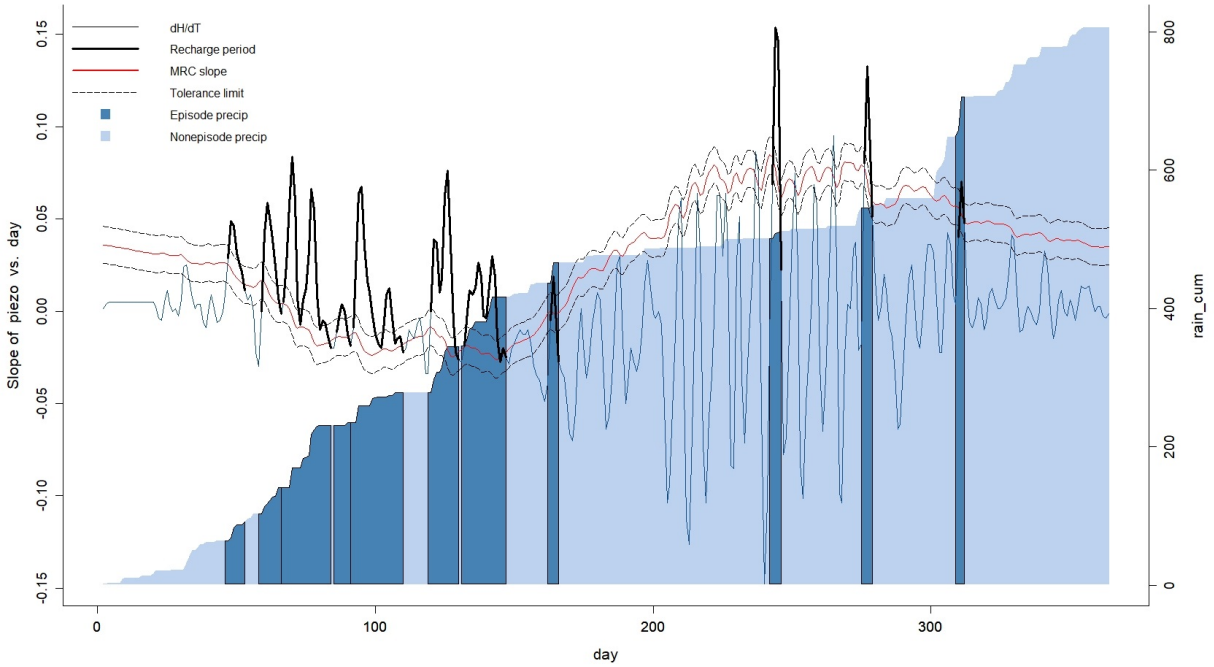

Figure 4.64: *Time derivative hydrograph where instantaneous slope are represented for 2018.*

Table 4.29: *EMR parameters values for 2018.*

Parameter	**value**
capacity	0.12 m
lagtime	1 d
fluctol	0.01 m/d
minprecip	1 mm
ependpar	1 d

Table 4.30: *EMR results for 2018.*

Episode	Duration (d)	Water Input (m)	Episode δH (m)	Episode Recharge (m)	RPR (m)
1	7	0.032	0.06	0.007	0.212
2	26	0.127	0.47	0.06	0.447
3	25	0.048	0.45	0.05	1.126
4	11	0.067	0.34	0.04	0.618
5	16	0.072	0.28	0.03	0.477
6	4	0.030	-0.02	-0.002	-0.081
7	4	0.011	0.05	0.006	0.552
8	4	0.006	0.08	0.01	1.664
9	3	0.057	0.003	0.0003	0.005

Table 4.31: *EMR parameters values for 2019.*

Parameter	**value**
capacity	0.12 m
lagtime	1 d
fluctol	0.024 m/d
minprecip	1 mm
ependpar	1 d

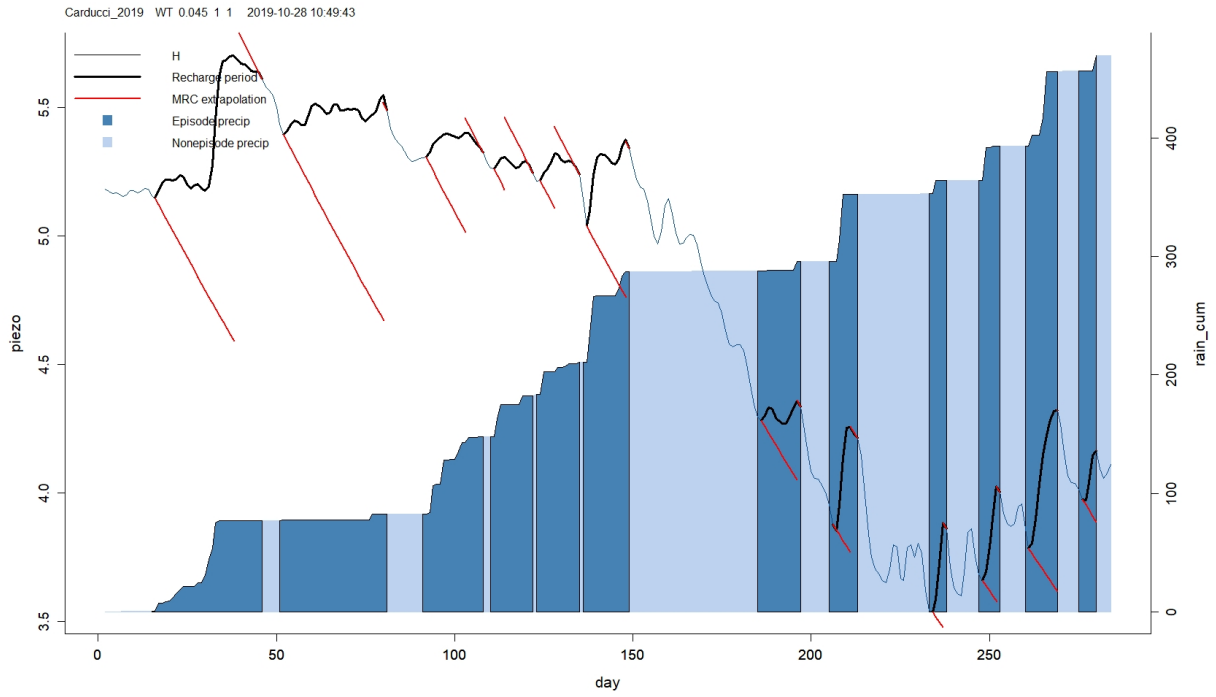

Figure 4.65: *Hydrograph with recharge episodes distinguished for 2019: quantitative identifications are classified in table 4.32.*

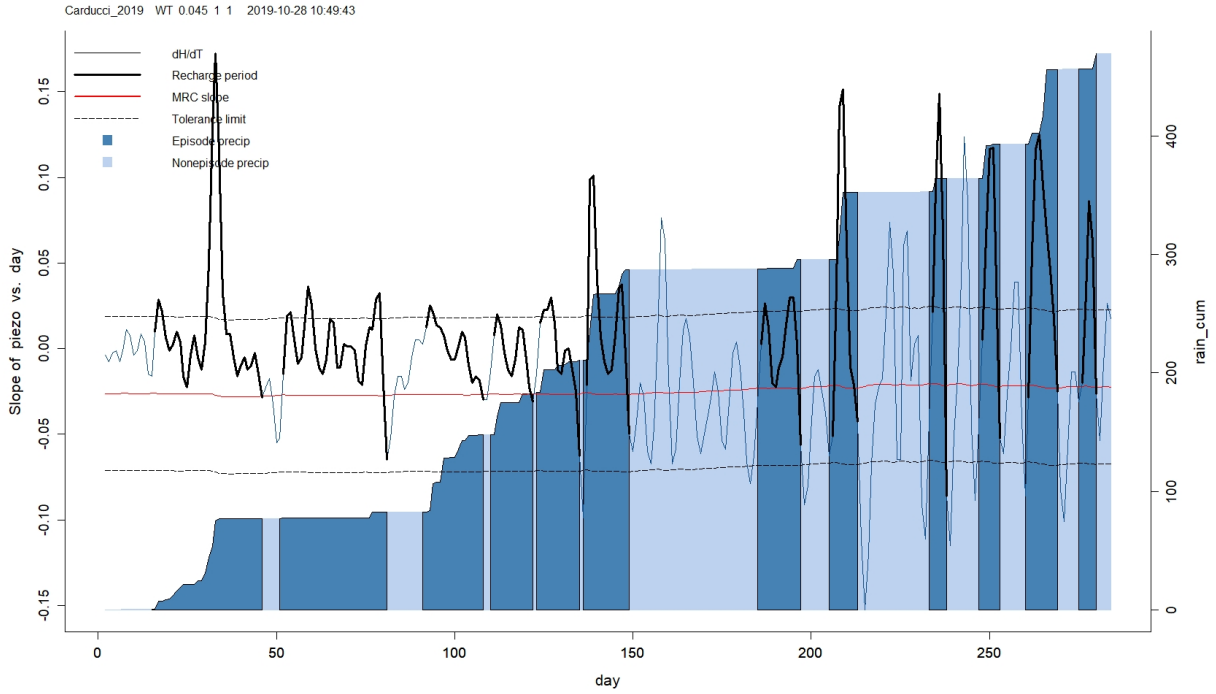

Figure 4.66: *Time derivative hydrograph where instantaneous slope are represented for 2019.*

Table 4.32: *EMR results for 2019.*

Episode	Duration (d)	Water Input (m)	Episode δH (m)	Episode Recharge (m)	RPR (m)
1	30	0.078	1.24	0.15	1.941
2	29	0.005	0.84	0.1	18.704
3	16	0.065	0.44	0.05	0.814
4	11	0.035	0.28	0.03	0.957
5	11	0.027	0.31	0.04	1.389
6	12	0.077	0.6	0.07	0.948
7	11	0.008	0.3	0.04	4.692
8	7	0.057	0.49	0.06	1.027
9	4	0.011	0.4	0.05	4.417
10	5	0.029	0.45	0.05	1.838
11	8	0.063	0.7	0.08	1.334
12	4	0.013	0.28	0.03	2.483

4.4 Hydroclimatic reconstruction for climate change analysis

Based on the gaps present in Carducci1 station, data interpolation was carried out for different time periods, as shown in table 4.33. In order to do this, two or more stations in addition to Carducci1, were selected. These additional stations had to have a statistical significant correlation between them as well with Carducci1 and they could not have gaps in the same days that were to be interpolated to complete Carducci1 station's records. In table 4.33, the correlation between Carducci1-Sassetta2 stations was kept, even though not statistically significant, since Sassetta2 was the only station within the study area that had record for 5 days in 2012, that were not present in any of the other stations referenced in table 3.6.

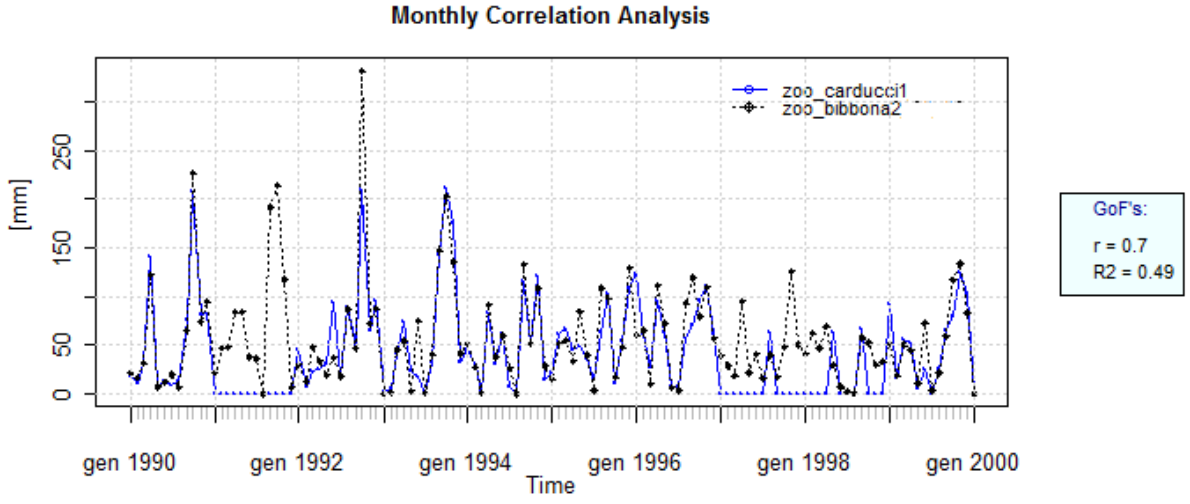

Figure 4.67: *A graphical representation of correlation between two rainfall time series belonging to two different rain gauges. The reference station for time series reconstruction was the historical station of Castagneto Carducci (in table 3.6 named Carducci1, that was different from station used for the recharge calculation, as shown in figure 3.7). The time series of this station starts from 1951 until 2011 and several gaps displayed in table 4.33 have been filled.*

Table 4.33: *Correlations results between rain gauges stations for selected gaps time periods.*

Weather station	**'51-'55**	**'69-'71**	**'72-'74**	**'90-'99**	**'02-'18**
Carducci1-Bibbona1	r = 0.52	r = 0.56	r = 0.51		
Carducci1-Bibbona2				r = 0.70	
Carducci1-Donoratico2				r= 0.69	r = 0.7
Carducci1-Bolgheri	r = 0.59				
Carducci1-Castelluccio		r = 0.65			
Carducci1-Sassetta1			r = 0.72		
Carducci1-Sassetta2					r= 0.23*
Bibbona1-Bolgheri	r = 0.9				
Bibbona1-Castelluccio		r = 0.79			
Bibbona1-Sassetta1			r = 0.76		
Bibbona2-Donoratico2				r = 0.93	
Carducci1-San Vincenzo2					r = 0.55
SanVincenzo2-Donoratico2					r = 0.76
San Vincenzo2-Sassetta2					r = 0.60
Donoratico2-Sassetta2					r = 0.77

For the precipitation reconstruction variable we used the *fillGap* function of the R software [134]. Through the application of this method a complete time series of daily precipitation was obtained for the Castagneto Carducci station from 1951 to 2018. A time series was reconstructed that was at least 50 years long that, according to the guidelines proposed by ISPRA [133], represents the minimum *timeframe* for studying climate change. The reconstructed series is represented in figure 4.68. The present work was carried out on a local scale. Statistical and scientific evidence of climate change has been ascertained, in most cases, only with large-scale studies [47]. To assess whether the changes described are ongoing at local scale (area of study), the statistical approach described in chapter 2 are conducted. The Mann-Kendall calculated on annual cumulative precipitation data, returned a *p-value*= 7.3425e-06, statistically confirming the presence of a trend (in order to assess the existence of positive or negative trends, the Tau index was used, which for the analyzed data is equal to -0.372,2, indicating a minimum negative slope). The Sen's slope test was used to estimate actual slope of the data. The value obtained is equal to -6.6 (dimensionless), indicating the presence of a negative trend (figure 4.69). As you can see from the graph, a local regression line (*lowess*) has been inserted to highlight this trend (figures 3.6, 4.70 and 4.71).

The change points analysis conducted for daily precipitation data is shown in figure 4.68. As you can see, there is a first point of discontinuity starting around 1988. This generates a time series that stops up to the second break point identified at the end of 2017. The points of discontinuity identified, seem to be in agreement with the transition phase identified in the graph 4.69.

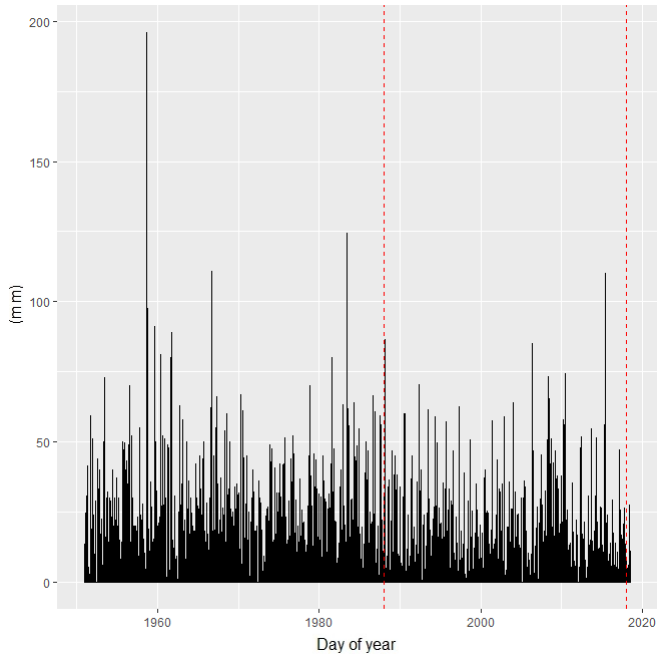

Figure 4.68: *Time series reconstruction and change point precipitation analysis from 1951 to 2019. The red dotted lines represent the points of time in which a significant change in the mean and variance values occurred in the distribution of values.*

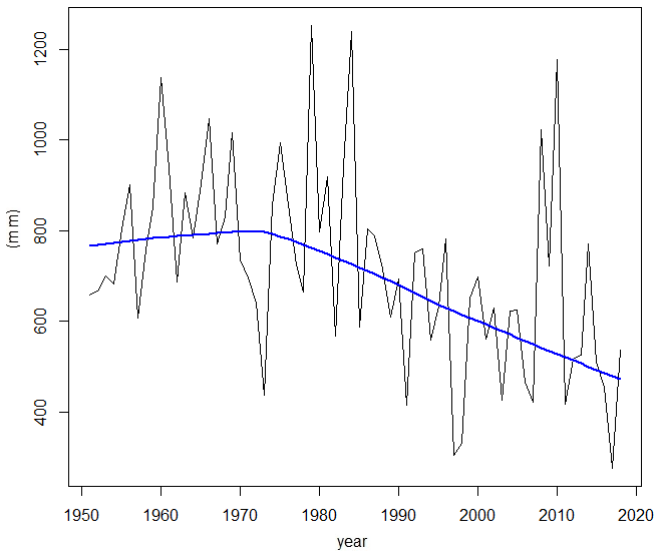

Figure 4.69: *Annual precipitation from 1951 to 2019. The blue line represents local regression (lowess) applied to the annual time series.*

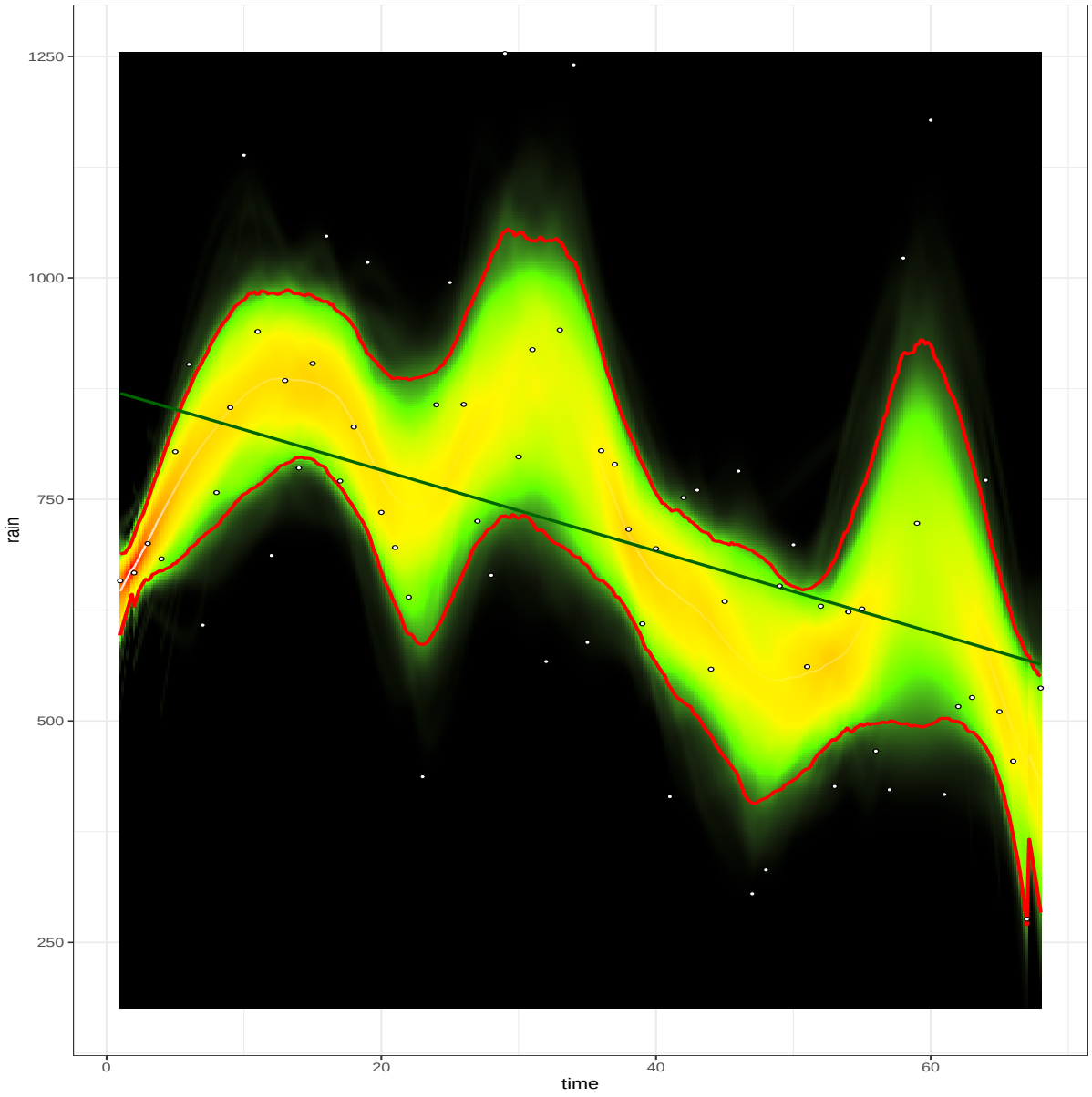

Figure 4.70: *The red lines indicate 95% confidence intervals, while yellow, green and red colors represent the degrees of standard deviation of distribution, from highest to lowest.*

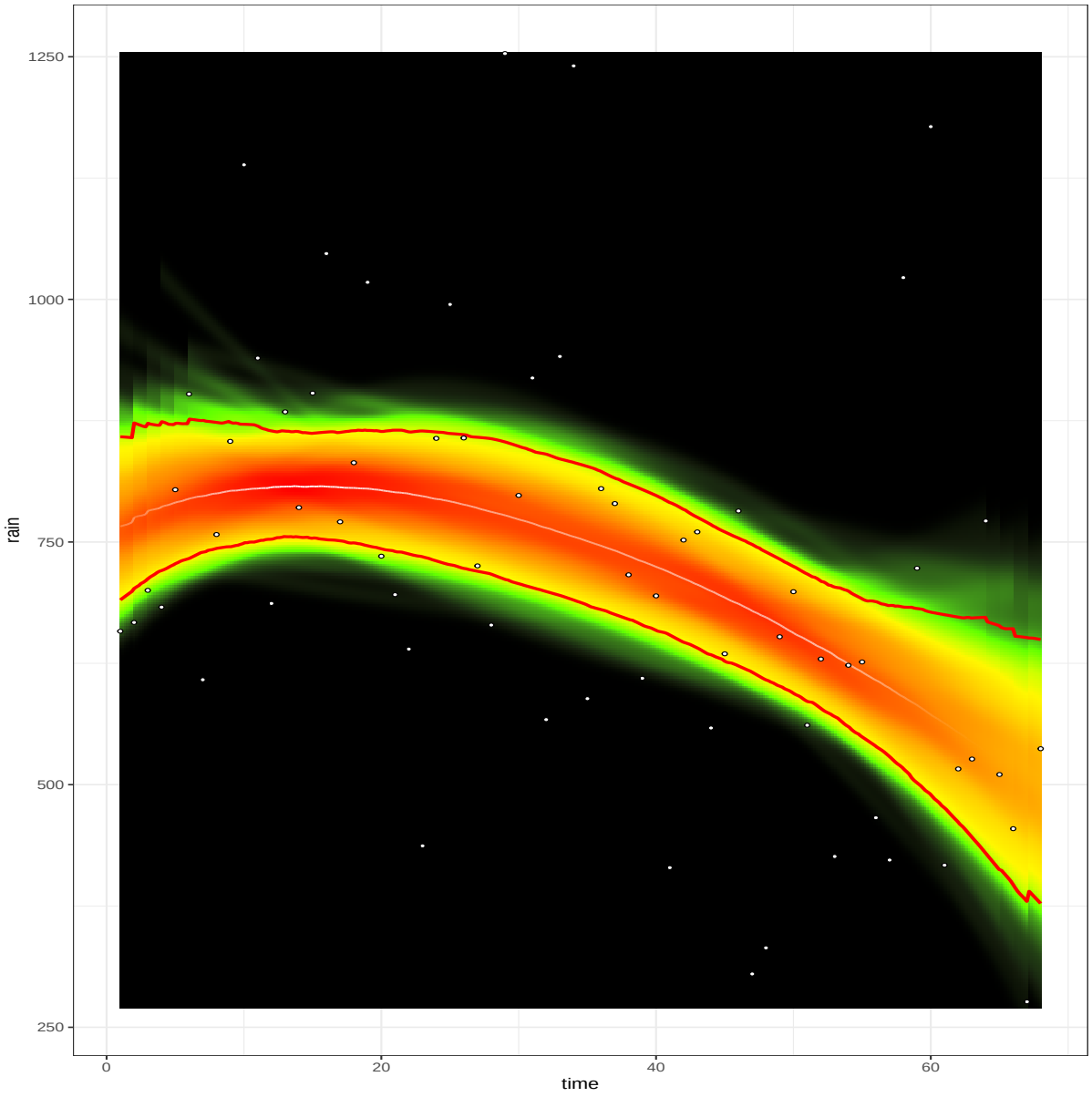

Figure 4.71: *The red lines indicate 95% confidence intervals, while yellow, green and red colors represent the degrees of standard deviation of distribution, from highest to lowest.*

Chapter 5

Discussion

"First they ignore you,
then they laugh at you,
then they fight you.
Then you win"
Mahatma Gandhi

5.1 Recharge characterization in shallow unconfined aquifer

Assessment of the physically meaningful MRC and EMR parameters, used in this study, was conducted on the 2018 time series which contains no gap.

Regards to definition of the MRC, *Mindrytime* parameter (minimum duration of the interval between significant precipitation and the beginning of the recession) was set, for all the time series, equal to 2 or 3 days since a lower setting would have led to start the modeled recession at the rising moment of the curve, while a higher setting would have started too late the recession.

The *Tslenght* parameter (number of days defining the significant recession segment) was also set at 2 or 3 days. In fact, this period of time is better suited to different types of curve decline. Too high number produces fewer number of recession start point and remaining recession points are likely to wrongly "fall" to the next recession curve. While appearing short, on the base of the expected hydraulic properties of the studied aquifer, the setting of 2-3 days has been precautionary chosen to avoid overlaps of the modeled recession period without drawbacks in the model parameters setting, since even a small portion of recession over time [2] is enough to define a recession segment.

The value that allows to decrease variable white noise (*Maxtick*) has been left to default of 0.1 m, having already applied the moving average on distribution of the variable.

The *Binsize* parameter, useful for averaging the values of the MRC points for improvement of the MRC fitting has not been used, obtaining a fitting only from the pure calculated values.

The *Maxslope* parameter (maximum slope angle for the recession element studied) was set with a value equal to 0.01 as found in many cases of literature [2]. A higher value of the parameter would have excluded many points identified by reducing the goodness of the fitting.

The *Throughorigin* parameter (which considers the value of the origin equal to zero in the fitting) was set "False" because physically meaningless for piezometric time series.

In many case studies, the *Maxdelprec* parameter (amount of precipitation that can be considered zero during the recession period) assumes different values depending on lithology and site climate conditions. In the case study called "Shale Hills", described by Nimmo 2018 [2], presents soils composed of silt loam in the first meters of depth and a humid temperate climate (annual rainfall between 700 and 1500 mm [142]). In that case, with soils composition similar to the one of this study, the value attributed to the *Maxdelprec* parameter was 0.4 mm. Considering the variation in precipitation studied in 67 years and the transition from a humid climate to a semi-arid climate, this quantity was considered equal to 1 mm for all the years studied.

To evaluate the EMR, the *Fluctol* parameter (range of the maximum rate of change within which the fluctuation is believed to be white noise or normal oscillation of the aquifer) was studied on significant fluctuations in the change of piezometric levels during storm events (analysis of the cross correlation between rainy event and change of rate of groundwater levels; figure 4.5). In addition, for the different years studied, this parameter has been adjusted with repeated tests in order to represent the hydrographer behavior as realistic as possible.

In several case studies [2, 139], calculation of *Minprecip* parameter (minimum amount of precipitation that will cause a real response) is not explained. Nimmo 2018 [2] attributes a low value to recognize as many recharge episodes as possible. After that, it was adjusted in order to represent the best hydrograph's behavior. From visual analysis of rainfall against water table (4.4), maybe this value could be close to 10 mm, considering minimum groundwater level compared to first amount of rain that occurs in a storm event. However, this value attributed to the parameter excluded evident increases in groundwater levels. So through a trial-and-error process, this parameter has been assigned a value of 1 mm in order to recognize as many recharge episodes as possible.

The *Ependpar* (time for the hydrograph to resume pre-event behavior, although not necessarily the same level, after the input event) parameter was set for different years with values ranging from 1 to 4 days. These results have been achieved through repeated tests in order to represent the best hydrograph's behavior (in the literature examples it is not explained how it was obtained; [2, 139]).

As described in section 4.2, site specific yield average value was calculated through the use of equation 4.14, returning a uniform average value of 0.12. This value is similar to the average specific yield value calculated with different methodologies for similar lithologies. For example, Fettel [143] reports laboratory results in which Sy range ranging from 0.12 to 0.03 corresponds to sandy clay lithology. Pool [144] through temporal gravity survey obtained a value of 0.15 on gravelly sand and reddish clay. Kotchoni [145] obtained a Sy value of 0.16 thanks to magnetotelluric method on Quaternary sands. Varni [50] calculated a value of 0.15 on gravelly sand and reddish clay. Kotchoni [145] estimated a Sy value of 0.16 thanks to magnetotelluric method on Quaternary sands. Varni [50] obtained a Sy value equal to 0.09 on silty sediments using graphical correlation analysis. Tziro [118] achieved a range of Sy 0.09 / 0.18 for silty sediments, while a Sy value of 0.20 for sandy sediments. Chang [146] obtained a range of Sy values between 0.12 and 0.22 for mixed lithologies of sands and gravel through pumping tests. Regard to the study area, analysis conducted by Regional Environmental Protection Agency suggest a Sy range values between 0.10 [147] and 0.15 [148] (obtained from pumping tests carried out around Cecina River, norther part of the study area) while other authors [56, 149] suggest a value of 0.15 for innermost parts of the Val di Cecina (along the river and far from the coastal line). The investigation method

used is non-invasive and allows application in more positions than monitoring point considered. Unlike other methods such as pumping tests, the geoelectric application does not generate waste and or disposal material, ensuring short acquisition times. The data acquiring is less constrained by the presence of other energy sources present in the territory, such as for example electrical and phone cables (as opposed to magnetotelluric methods) and in general the execution costs are lower compared to pumping tests, magnetotelluric and gravimetric methods. The disadvantages include permission location acquisition lines, sometimes located on inaccessible private land. In table 5.1 some indication about prices of considered method to calculate *Sy* parameter.

Table 5.1: *Economic evaluation of Sy method calculation [150, 151]. The range of prices in Euro are only for instruments use and not consider all other costs.*

Geoelectric line (200 m)	**Magnetotelluric (per station)**	**Pumping test**
500 euro	200 - 300 euro	2000 - 3000 euro

The recharge quantity (mm) is indicated as "EMR water input" and expresses total precipitation given by sum of each recharge episodes identified with EMR input parameters values over time (tables 5.2, 5.3). In order to obtain the best characterization of calculated recharge quantities, various changes have been made in calculated quantities. Furthermore, considering total annual precipitation, the percentages that are theoretically used to derive recharge quantity have been included in the absence of other calculation tools or bibliographic information. In table 5.2 are expressed total precipitation amounts for respective years compared to the amount of recharge in input calculated. For complete information, they have also been classified the quantities for the years 2014, 2015 and 2019 although they are incomplete (2016 was not considered because wide gaps in the time series).

Table 5.2: *The results of 2014*, 2015* and 2019* are partial, compared to the total precipitation during the year.*

Year	EMR Water Input recharge (mm)	Total rainfall (mm)	Percentage of recharge (30%)	Percentage of recharge (20%)
2011	359.8	572	171.6	114,4
2012	547.6	742.8	222.84	148.56
2013	683.4	856	256.8	171.2
2014*	333	1323.2	396.96*	264.64
2015*	551.8	799.6	239.88*	159.92
2017	320.2	417.4	125.22	83.48
2018	449.2	806.4	241.92	161.28
2019*	467.6	470.2	141.06*	94.04

Some of the results obtained were modified because RPR rate presented unreasonably negative values. For this reason, values present in 2011 tables (episode 5 and 6, in figure 4.16) and 2018 (episode 6, in figure 4.30) were excluded. Some of calculated recharge quantities were vitiated by linear interpolations that not reflect the response to precipitation events. Despite this, they were necessary to make complete time series and usable by EMR program. In some cases (figure 4.53), linear interpolation line correspond to many precipitation events. This "flat" effect fails to distinguish recharge events from the recession. For these reasons it was eliminate from recharge amount calculated. In 2011 for example, the second recharge episode calculated at 120.8 mm was eliminated and for 2013 the first, tenth and twelfth episode, respectively equal to 290.6 mm, 201.6

mm and 49.2 mm were subtracted. No further changes have been made to eliminate this effect in the remaining years. Setting of parameters relating to recharge episodes calculation has been kept almost constant over the years. The *ependpar* parameter has been assigned values ranging from 1 to 4 based on the diversity of the signal behavior (piezometric level) found year by year. This choice was also facilitated by the use of *fluctol* parameter which had different values for time series studied. The hydrograph analysis developed for complete time series (2011, 2012, 2013, 2017, 2018 and 2019) shows sharp moments of recession for periods, with a range that stars from a few days to several months. In particular, a strong seasonal component is evident. In all cases analyzed, there is a long recession that generally starts from spring until the beginning of autumn, with small and rare cases of recharge events in the summer. Regard to the year 2011, identified recharge episodes (with parameters and applied corrections) appear to be correctly identified, even if some moments are not properly modeled (for example some peaks in main spring-summer recession period). Final part of the year (late autumn), rainy events did not create significant increases (*fluctol* equal to 0.06 m/d). The year 2012 represents one of the best representations for calculation of recharge episodes through the use of the EMR algorithm. Although there are obvious interpolations (2 in the first 100 days of the year), the values attributed to the parameters seem to represent recharge events correctly. The central recession period, around 200 days, is without rain, despite the presence of obvious fluctuations in the water table. Based on these fluctuations, the *fluctol* parameter was set to 0.04 m/d, which is consistent with the rest of the piezometric levels. The year 2013 was characterized by difficulties in parameters values evaluation. Presence of significant interpolations, in piezometric time series variable, does not allow to define the recharge events throughout the year. Consequently, as already reiterated above, these hydrologically incorrect recharge events were excluded from next assessments. Also in this case, the *fluctol* was set based on groundwater fluctuations in the summer spring recession period (0.03 m/d), in which there are no significant rain events. The year 2014 saw only month analysis of January and mid-February. Despite this, the analysis was useful not only to assess the amount of recharge calculated for that period (333 mm), but also to further demonstrate the interaction between precipitation and groundwater levels. In this case the *fluctol* value was kept equal to the year 2013. The analysis carried out on 2015 is divided into two periods. Also in this case there were a partial availability of the data. In particular, recharge episodes have been calculated for spring-winter and autumn-summer periods. The values of *fluctol* attributed to time series (respectively 0.03 and 0.025 m/d) seem to capture well the recharge events, with the exception of two fluctuations between day 30 and day 40 in summer-autumn representation. The year 2017 was characterized by periods of severe drought. The calculated recharge episodes turn out to be hydrologically consistent. The *fluctol* value of 0.024 m/d was established on the basis of the first long dry period in which groundwater fluctuations were not affected by anomaly peaks. The year 2018 shows a signal trend (piezometric levels) very different from the one of 2017. In this case, even if the *fluctol* value is very low (<0.01 m/d), the same number of recharge events were detected. Finally, year 2019 appears to be characterized by consistent recharge episodes. Also in this case the parameter *fluctol* (0.024 m/d) was set on the basis of groundwater level fluctuations in drier period between 150 and 180 days. Table 5.3 summarizes calculated recharge quantities after the above mentioned corrections and it characterizes natural phenomenon of recharge of the aquifer considered starting from 2011 until 2019.

Table 5.3: *The results of 2014*, 2015* and 2019* are partial, compared to the total precipitation during the year.*

Year	EMR Water Input recharge (mm)	Total rainfall (mm)	Percentage of recharge (30%)	Percentage of recharge (20%)
2011	110	572	171.6	114,4
2012	547.6	742.8	222.84	148.56
2013	142	856	256.8	171.2
2014*	333	1323.2	396.96*	264.64
2015*	551.8	799.6	239.88*	159.92
2017	320.2	417.4	125.22	83.48
2018	419.6	806.4	241.92	161.28
2019*	467.6	470.2	141.06*	94.04

5.2 Comprehensive hydrological processes and climate change

Table 5.4 shows the annual cumulative precipitation values. According to FAO climatic zone subdivision www.fao.org, the study area was initially characterized by a sub-humid climate, with cumulative annual rainfall between 700 mm and 1200 mm, from 1951 until 1990. If we divide annual rainfall data considering discontinuity point identified by change point analysis, we get two blocks: first between 1951 and 1989 and second one from 1990 to 2018. From this subdivision, the cases within semi-arid climate area (according to FAO climatic zone subdivision, an area with annual rainfall ranging between 400 and 600 mm) 3 in the first block and 12 in the second block identified by the change point analysis (table 5.4).

Considering a significant change in rainfall time series was identified at the end of the 1980s, the increase of semi-arid climate cases on first block and the presence of an new number of arid climate cases in the 1997-1998-2017 years, it is possible to assume a climate variation in progress for the study area.

Specifically, the investigated area shift in the last 50 years from a sub-humid to a semi-arid climate condition, according to the analysis of historical precipitation. To verify the correspondence between historical trend and rainfall time series considered for recharge estimation, a correlation test was performed. It was based on the years used for recharge calculation (from 2011 to 2018; 2019 excluded because not considered in the historical calculation), which returned a value of 0.98. This result seems to reinforce the concept that precipitation is not only indicative of ongoing climate change, but also that the precipitation used to derive recharge episodes is part of variation rainfall process shown in figure 4.69.

Local regressions of annual rainfall are shown in figures 4.70 and 4.71. The two graphs were constructed considering maximum and minimum value attributable to the "span" parameter. Figure 4.70 was obtained with a minimum span degree. Its setting allows to identify typical cyclical behavior of precipitation, while different position of upper and lower confidence intervals (an interval of plausible values for precipitation values) from 1951 until 2018, suggests a change in their values over time. In particular, cumulative annual rainfall of the last years (2018-2016-2015-2013-2012-2011 years, values attributable to a semi-arid climate, as shown in table 5.4) fall within a range of a distribution of plausible values for that parameter with a confidence level of 95%. Therefore, these values would have been considered anomalous since the 80s (time = 35) until 1951, or years in which the cumulative precipitation values fell within a sub-humid climate

regime. Figure 4.71 instead shows the local regression in which the adapted curve is more uniform over time (developed with the maximum number of spans). Also in this case a change in the confidence levels of the distribution is visible, even if this interval is wider than in the previous representation.

In the correlation matrix (figure 5.1), the recharge events corrected results are compared (total EMR outputs results for 2011, 2012, 2013, 2017, 2018, and 2019 years). As noted, recharge episodes are more influenced by their duration (length of recharge episode) as well as by the amount of precipitation in input, with highly significant correlation indexes of 0.74 and 0.63 respectively. On the other hand, RPR rate is negatively correlated with the amount of precipitation at the input, confirming the fact that the increase in rainfall intensity leads to a decrease in the recharge rate. The RPR rate can systematically vary with intensity of the precipitation. A significant alteration of rainfall quantity, given for example by climate change, can therefore have an impact on the aquifers recharge. A climatic variation connected to a greater storms intensity can make a recharge increase up to certain point, after which input water quantities are lost due several physical processes (e.g. runoff). The value obtained by cross correlation between quantity of water in input and RPR rate of -0.43, could partially represent this phenomenon. Unfortunately, it was not possible to strengthen evaluation of this behavior because was not possible to establish the intensity of rainfall (available data were daily).

Table 5.4: *Total yearly rainfall (mm) for the hydroclimatic reconstruction.*

Before first Change Point	**Total Rainfall (mm)**	**After first Change Point**	**Total Rainfall (mm)**
1951	658.08	1989	609.60
1952	667.10	1990	694.50
1953	700.20	1991	414.48
1954	682.90	1992	752.00
1955	803.90	1993	760.40
1956	902.50	1994	558.40
1957	608.10	1995	634.80
1958	757.70	1996	782.00
1959	853.70	1997	304.95
1960	1138.70	1998	331.85
1961	939.50	1999	652.36
1962	686.70	2000	698.80
1963	884.10	2001	561.20.
1964	785.50	2002	629.44
1965	903.40	2003	426.00
1966	1047.20	2004	622.99
1967	770.80	2005	626.41
1968	831.70	2006	465.90
1969	1017.60	2007	422.32
1970	735.39	2008	1022.41
1971	695.75	2009	723.00
1972	639.70	2010	1178.00
1973	436.94	2011	417.00
1974	856.80	2012	516.19
1975	994.80	2013	526.38
1976	857.20	2014	771.69
1977	725.40	2015	510.44
1978	664.40	2016	454.62
1979	1253.30	2017	276.29
1980	798.00	2018	537.02
1981	919.00	-	-
1982	567.00	-	-
1983	941.20	-	-
1984	1240.60	-	-
1985	588.60	-	-
1986	805.00	-	-
1987	789.60	-	-
1988	716.20	-	-

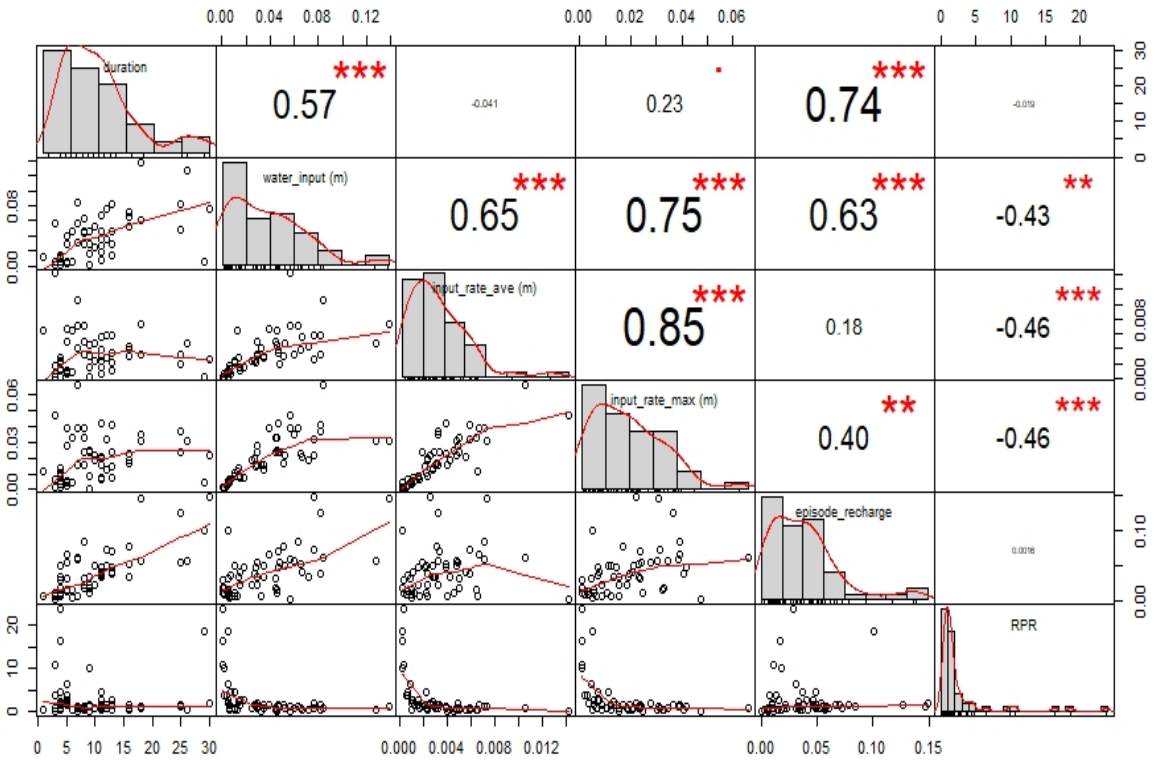

Figure 5.1: *The graphs show the correlation results, considering the most important outputs returned by the recharge calculation, added for all years. This dimensionless correlation coefficient expresses a relationship of linearity (bond) between two statistical variables measured on the same samples, i.e. how they tend to vary simultaneously. It can vary between -1.00 and +1.00, where the extremes represent perfect associative bonds. In case that the coefficient is zero, there is a proof of the absence of a linear relationship between the two variables. In addition, for each coefficients is also reported the significance level, where: "***" corresponds to a p-value of 0.001, "**" corresponds to a p-value of 0.01, "*" corresponds to a p-value of 0.05, and "." corresponds to a p-value of 0.1. In the diagonal of the correlation matrix is reported the frequency distributions of each variable considered and the relative density curve. In the lower triangular portion is reported the bivariate dispersion diagrams for each pair of variables and the relative trend line.*

Conclusions

"Rev.CJ: Do you see the light?
JB: The Band"
Reverend Cleophus James & Jake Blues in The Blues Brothers

The proposed workflow was performed to meet specific research needs and it was performed in an area of Tuscany that currently face water supply challenges, accentuated by the increase over time of dry periods. Considering the objectives pursued, the study area was therefore suitable, even if a good amount of starting data were not available. For example, only one monitoring well time series was present. The research was useful for estimating the amount of recharge of the aquifer in an area where this parameter is unknown. To do this I applied the EMR method, which was found to be the most suitable method that can be implemented, considering the starting dataset and the execution costs for parameters estimation. From the initial explorative data analysis (i.e. cross correlation) between rainfall and daily groundwater levels for the year 2018, a correlation value of 0.15 is obtained. This value suggest a very low correlation between rainfall and groundwater, indicating a non-existent reaction or connection, in contradiction to the other hydrogeological and hydrogeochemical indication. However, this initial information is refuted by repeating the cross correlation analysis using as new variables the rate of change of groundwater levels against precipitation events considered "Storm". In fact, correlation values between the latter variables are significantly high for a one delay lag time. This behavior indicates that the groundwater levels react only after with a certain delay and amount of precipitation. This quantity was set equal to 1 mm in the modeling of the recession curve, even if cross correlation analysis suggests a higher number. A suitable methodology to calculate this quantity could be considered as future development. So, study of stormy events associated with the application of the EMR method confirms that precipitation is still the first source of water supply for groundwater resource in the study area, even if, in some cases, there is a presence of abnormal groundwater level fluctuations in absence of rainfall. A critical element for the studied aquifer and calculation method is the groundwater levels deepening in time, which correspond to a decreasing in sensitivity of the rainfall signal on the water table. The time series studied show a constant decrease over time, passing from a maximum groundwater level of 8.03 meters amsl (2011) to 6.32 meters amsl (2018). The same thing occurs for minimum levels. Consequently the method cannot be used if the depths will continue to increase. The amounts of yearly recharge input calculated were: 110, 547.6, 142, 333, 551.8,320.2, 419.6 and 467.6 mm respectively for the years 2011, 2012, 2013, 2014, 2015, 2017, 2018 and 2019 (considering hydrological corrections and incomplete years). Finally, the recharge quantities calculated in 2017 and 2018 (time series without gaps) were used for a numerical model of groundwater flow, required by Tuscany Public Water Management Authority.

The calculation of the Specific yield with the geoelectric method, allowed me to estimate the

most important/sensitive parameter to be used for aquifer recharge calculation through EMR method. The choice of geoelectric technique was based on cost analysis against other methods for the evaluation and calculation of this parameter.

The statistical trend analysis conducted on the rainfall of the study area provided important information about climate condition. These was useful to better understand implications that rainfall variations have on the hydrological cycle. Compared to rainfall, a statistically significant negative trend has been observed over time. This change was evident above all for the cumulative annual values. Trends, change point and local regression analysis show that, from 1951 to 1989, annual cumulated rainfalls correspond to a sub-humid climate system; while from 1990 to 2018 there was a variation in quantities that leaded to a semi-arid climate system. Despite these indications, the calculation of the recharge quantities was insufficient to establish how these quantities are connected to the climatic variations of the study area. This fact is attributable to the few measures of groundwater levels available and to the many gaps in the time series, which are not allowed to apply the complete calculation for the few years available. Finally, in order to respond to research objectives, the proposed workflow used open source software and low-cost field tools, making it easy to replicate.

Future developments

Evaluation of the recharge, by analyzing its effect on the water table, is an indirect estimation based on site specific data with low-cost acquisition methods. Therefore, a wider use of the proposed method can be suggested to water utilities to help the management of their resources, where the right condition are applied. In particular, given the large number of regional hydroclimatic monitoring stations, one could suggest a study of the hydroclimatic time series aimed at evaluating the main groundwater recharge areas in the Tuscany region. The study would be useful not only for the evaluation of the aforementioned areas, but also to evaluate the geographical location of new well fields for public water supply and water utilities. Considering the recent decline in groundwater levels in study area, understand maximum depth of groundwater levels to applied this method remains a challenge. Also the minimum amount of precipitation that will cause a real response in groundwater levels remains a difficult quantity to estimate, depending not only on the precipitation and the soil properties, but also on the soil moisture dry-wet cycles. On the other hand, during this work emerged the potential interest in apply the study of water table level fluctuation to investigate, by reverse modeling, the lithologies in which the water table fluctuates.

While being an indirect measure, the geoelectrical survey could be in future used to provide a highly discrete (horizontal and vertical) distribution of the Sy, useful to compute a distributed and detailed evaluation of the groundwater recharge provided by the WTF method.

In the end, the possibility to directly link the groundwater recharge, computed on a local scale by means of the WTF method, with a site specific analysis of the climatic condition and evolution, could provide and easy and cost-effective tool, usable by all the stakeholders of the groundwater framework, to gain a more comprehensive understanding of the renewable groundwater resource and forecast future management strategies.

Acknowledgements

First of all, I would like to take this opportunity to express my gratitude to my family (including my dog Archimede) for the great support they gave me every day in these three difficult, but unbelievable, years.

I am grateful to my coadvisor Enrico Guastaldi for the opportunity and the precious suggestions that he gave me to develop my PhD on aquifer recharge, thanks to which I improved a lot my skills in hydrology and hydrogeology fields.

This work would not have been the same without the great contribution of my friend and colleague Alessio Barbagli. I am also grateful to my friend and colleague Stefano Bernardinetti for his fruitful suggestions about Specific yield data elaboration. To others all lab colleagues who collaborated with me and gave me suggestions during the PhD project, I tell you thanks. In particular to my collegues and friends Stefano Maraio for Cross Correlation discussion, Chiara Lanciano and Mariantonietta Brancale for great moral support and working data management.

I am also grateful to University of Cagliari for the opportunity to spend my research period abroad in Oman, Malta and Kenya.

Finally, I also would like to thanks Daniele Pedretti and Chaoshui Xu for their time spent refereeing my PhD thesis and for their precious suggestions.

Cagliari, 2020

Andrea Zirulia

Africa, Kenya, Nakuru.

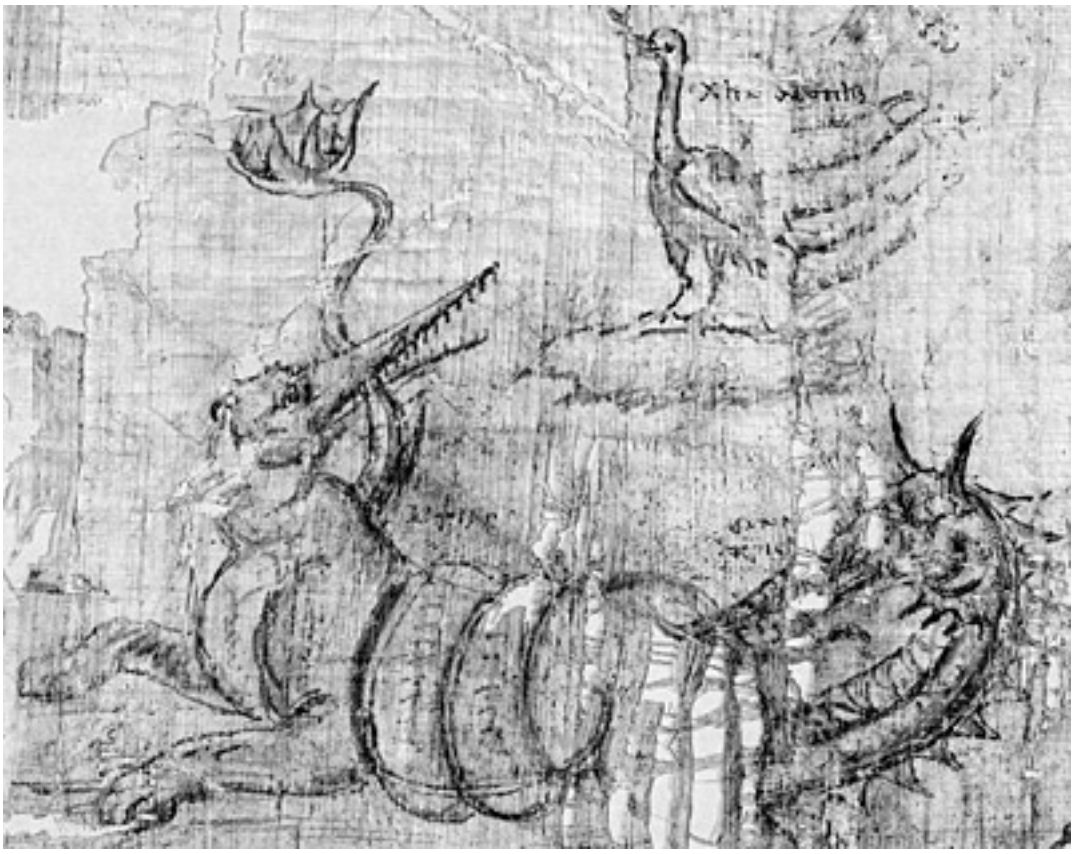

Artemidorus, 2^{nd} century BC.
Pre trama: magari terza, ebeti in volgo.

Bibliography

[1] "Decreto Legislativo, Norme in materia ambientale n. 152," G.U. n. 88, Apr. 2006.

[2] J. Nimmo and K. Perkins, "Episodic Master Recession Evaluation of Groundwater and Streamflow Hydrographs for Water-Resource Estimation," *Vadose Zone Journal*, vol. 17, 12 2018.

[3] Rubin and Hubbard, *Hydrogeophysics*. Springer Science and Business Media, 2005.

[4] A. Samouëlian, I. Cousin, A. Tabbagh, A. Bruand, and G. Richard, "Electrical resistivity survey in soil science: a review," *Soil and Tillage Research*, vol. 83, no. 2, pp. 173–193, 2005. [Online]. Available: http://www.sciencedirect.com/science/article/pii/S0167198704002326

[5] F. Landerer, "GRACE-FO," last login: 28/06/2019. [Online]. Available: https://gracefo.jpl.nasa.gov/science/water-storage/

[6] J. Grönwall and S. Oduro-Kwarteng, "Groundwater as a strategic resource for improved resilience: a case study from peri-urban Accra," *Environmental earth sciences*, vol. 77, no. 1, p. 6, 2018.

[7] G. S. A. Salem, S. Kazama, S. Shahid, and N. C. Dey, "Impacts of climate change on groundwater level and irrigation cost in a groundwater dependent irrigated region," *Agricultural Water Management*, vol. 208, pp. 33–42, 2018.

[8] S. Khalid, M. Shahid, C. Dumat, N. K. Niazi, I. Bibi, H. F. S. G. Bakhat, G. Abbas, B. Murtaza, and H. M. R. Javeed, "Influence of groundwater and wastewater irrigation on lead accumulation in soil and vegetables: implications for health risk assessment and phytoremediation," *International Journal of Phytoremediation*, vol. 19, no. 11, pp. 1037–1046, 2017, pMID: 28463566. [Online]. Available: https://doi.org/10.1080/15226514.2017.1319330

[9] G. S. A. Salem, S. Kazama, S. Shahid, and N. C. Dey, "Groundwater-dependent irrigation costs and benefits for adaptation to global change," *Mitigation and Adaptation Strategies for Global Change*, vol. 23, pp. 953–979, 2018.

[10] W. M. Alley, B. R. Clark, D. M. Ely, and C. C. Faunt, "Groundwater development stress: global-scale indices compared to regional modeling," *Groundwater*, vol. 56, pp. 266–275, 2018.

[11] Z. H. Lauffenburger, J. J. Gurdak, C. Hobza, D. Woodward, and C. Wolf, "Irrigated agriculture and future climate change effects on groundwater recharge, northern High Plains aquifer, USA," *Agricultural Water Management*, vol. 204, pp. 69–80, 2018.

[12] Z. Wang, S. F. D. Marco, and S. A. Socolofsky, "Turbulence measurements in the northern gulf of Mexico: application to the aeepwater aorizon oil spill on droplet dynamics," *Deep Sea Research Part I: Oceanographic Research Papers*, vol. 109, pp. 40–50, 2016.

[13] Herrera-Pantoja, M, and K. Hiscock, "The effects of climate change on potential groundwater recharge in great Britain," *Hydrological Processes*, vol. 22, pp. 73–86, 01 2008.

[14] S. Mustafa, K. Abdollahi, B. Verbeiren, and M. Huysmans, "Identification of the influencing factors on groundwater drought and depletion in north-western Bangladesh," *Hydrogeology Journal*, vol. 25, pp. 1357–1375, 02 2017.

[15] Vetter, Sapkota, Hillier, Stirling, Macdiarmid, Aleksandrowicz, Green, Joy, Dangour, and Smith, "Greenhouse gas emissions from agricultural food production to supply indian diets: implications for climate change mitigation," *Agriculture, ecosystems & environment*, vol. 237, pp. 234–241, 2017. [Online]. Available: http://researchonline.lshtm.ac.uk/3449688/

[16] L. L. Lisa Pfeiffer, "Groundwater pumping and spatial externalities in agriculture," *Journal of Environmental Economics and Management*, vol. 64, no. 1, pp. 16–30, 7 2012.

[17] B. Luinstra, "Groundwater insight: a critical resource," Feb. 2018, last login: 28/06/2019. [Online]. Available: https://www.ausimmbulletin.com/feature/groundwater-insight-critical-resource/

[18] S. Moon, N. Woo, and K. Lee, "Statistical analysis of hydrographs and water-table fluctuation to estimate groundwater recharge," *Journal of Hydrology*, vol. 292, no. 1-4, pp. 198–209, 6 2004.

[19] A. Gemitzi and V. Lakshmi, "Evaluating renewable groundwater stress with GRACE data in Greece," *Groundwater*, vol. 56, no. 3, pp. 501–514, 2018. [Online]. Available: https://ngwa.onlinelibrary.wiley.com/doi/abs/10.1111/gwat.12591

[20] S. Rathay, D. Allen, and D. Kirste, "Response of a fractured bedrock aquifer to recharge from heavy rainfall events," *Journal of Hydrology*, vol. 561, pp. 1048–1062, 2018. [Online]. Available: http://www.sciencedirect.com/science/article/pii/S0022169417305061

[21] Ali, Mubarak, M. Islam, and P. Biswas, "Comparative evaluation of various empirical methods for estimating groundwater recharge," *Archives of Current Research International*, vol. 11, pp. 1–10, 01 2017.

[22] R. Crosbie, J. Mccallum, G. Walker, and F. H. S. Chiew, "Modelling climate-change impacts on groundwater recharge in the Murray-Darling Basin, Australia," *Hydrogeol J*, vol. 18, pp. 1639–1656, 11 2010.

[23] R. W. Healy and B. R. Scanlon, *Estimating groundwater recharge*. Cambridge University Press, 2010.

[24] T. Green, M. Taniguchi, H. Kooi, J. Gurdak, D. Allen, K. Hiscock, H. Treidel, and A. Aureli, "Beneath the surface of global change: impacts of climate change on groundwater," *Journal of Hydrology - J HYDROL*, vol. 405, pp. 532–560, 08 2011.

[25] T. Cui, M. Raiber, D. Pagendam, M. Gilfedder, and D. Rassam, "Response of groundwater level and surface-water/groundwater interaction to climate variability: Clarence-Moreton Basin, Australia," *Hydrogeology Journal*, vol. 26, no. 2, pp. 593–614, Mar 2018. [Online]. Available: https://doi.org/10.1007/s10040-017-1653-6

[26] D. Vries and Simmers, "Groundwater recharge: an overview of processes and challenges," *Hydrogeology Journal*, 2002.

[27] D. Machiwal, M. K. Jha, and B. C. Mal, "Assessment of groundwater potential in a Semi-Arid Region of India Using Remote Sensing, GIS and MCDM Techniques," *Water Resources Management*, vol. 25, no. 5, pp. 1359–1386, Mar 2011. [Online]. Available: https://doi.org/10.1007/s11269-010-9749-y

[28] R. W. Healy and P. G. Cook, "Using groundwater levels to estimate recharge," *Hydrogeology Journal*, vol. 10, no. 1, pp. 91–109, Feb 2002. [Online]. Available: https://doi.org/10.1007/s10040-001-0178-0

[29] Fouépé, Alain, N. Ngoupayou, Jules, Riotte, Jean, Takem, Gloria, Mafany, G. M. chal, Jean-Christophe, and E. Ekodeck, "Estimation of groundwater recharge of shallow aquifer on humid environment in Yaounde (Cameroon), using hybrid water-fluctuation and hydrochemistry methods," *Environmental Earth Sciences*, vol. 64, pp. 107–118, 09 2011.

[30] G. Singh and R. K. Kamal, "Heavy metal contamination and its indexing approach for groundwater of Goa mining region, India," *Applied Water Science*, vol. 7, no. 3, pp. 1479–1485, Jun 2017. [Online]. Available: https://doi.org/10.1007/s13201-016-0430-3

[31] Dragoni and Sukhija, "Climate change and groundwater : a short review," *Geological Society, London, Special Publications.*, vol. 288, pp. 1–12, 02 2008.

[32] H. Delottier, A. Pryet, J.-M. Lemieux, and A. Dupuy, "Estimating groundwater recharge uncertainty from joint application of an aquifer test and the water-table fluctuation method," *Hydrogeology Journal*, 05 2018.

[33] R. Doble and R. Crosbie, "Review: current and emerging methods for catchment-scale modelling of recharge and evapotranspiration from shallow groundwater," *Hydrogeology Journal*, 09 2016.

[34] M. J. Knowling and A. D. Werner, "Estimability of recharge through groundwater model calibration: Insights from a field-scale steady-state example," *Journal of Hydrology*, vol. 540, pp. 973–987, 2016. [Online]. Available: http://www.sciencedirect.com/science/article/pii/S0022169416304334

[35] N. Quinn, L. Brekke, N. Miller, T. Heinzer, H. Hidalgo, and J. Dracup, "Model integration for assessing future hydroclimate impacts on water resources, agricultural production and environmental quality in the San Joaquin Basin, California," *Environmental Modelling & Software*, vol. 19, no. 3, pp. 305–316, 2004, concepts, Methods and Applications in Environmental Model Integration. [Online]. Available: http://www.sciencedirect.com/science/article/pii/S1364815203001555

[36] M. T. Islam, "Effect of climate change on groundwater quality around limestone enriched area," Ph.D. dissertation, BANGLADESH AGRICULTURAL UNIVERSITY, 12 2013.

[37] J. van Engelenburg, R. Hueting, S. Rijpkema, A. J. Teuling, R. Uijlenhoet, and F. Ludwig, "Impact of changes in groundwater extractions and climate change on groundwater-dependent ecosystems in a complex hydrogeological setting," *Water Resources Management*, vol. 32, no. 1, pp. 259–272, Jan 2018. [Online]. Available: https://doi.org/10.1007/s11269-017-1808-1

[38] Ali and Mubarak, "Approaches and methods of quantifying natural groundwater recharge: a review," *Asian Journal of Environment & Ecology*, vol. 5, pp. 1–27, 01 2017.

[39] J. L. García-Aróstegui, J. Molina, and M. Pulido-Velazquez, "Assessment of future groundwater recharge in semi-arid regions under climate change scenarios (Serral-Salinas aquifer, SE Spain). Could increased rainfall variability increase the recharge rate?" *Hydrological Processes*, vol. 29, no. 6, pp. 828–844, 2015. [Online]. Available: https://onlinelibrary.wiley.com/doi/abs/10.1002/hyp.10191

[40] F. Giorgi, "Climate change Hot-Spots," *Geophys. Res. Let*, vol. 33doi, p. 101029, 04 2006.

[41] F. Giorgi and P. Lionello, "Climate change projections for the mediterranean region," *Global and Planetary Change*, vol. 63, no. 2, pp. 90–104, 2008, mediterranean climate: trends, variability and change. [Online]. Available: http://www.sciencedirect.com/science/article/pii/S0921818107001750

[42] B. Smerdon, "A synopsis of climate change effects on groundwater recharge," *Journal of Hydrology*, vol. 555, 09 2017.

[43] J. J. Gurdak and C. D. Roe, "Review: recharge rates and chemistry beneath playas of the High Plains aquifer, USA," *Hydrogeology Journal*, vol. 18, no. 8, pp. 1747–1772, Dec 2010. [Online]. Available: https://doi.org/10.1007/s10040-010-0672-3

[44] J. Pittock, K. Hussey, and A. Stone, *Groundwater management under global change: sustaining biodiversity, energy and food supplies*. Cham: Springer International Publishing, 2016, pp. 75–96. [Online]. Available: https://doi.org/10.1007/978-3-319-23576-9_4

[45] E. Luker and L. M. Harris, "Developing new urban water supplies: investigating motivations and barriers to groundwater use in Cape Town," *International Journal of Water Resources Development*, vol. 0, no. 0, pp. 1–21, 2018. [Online]. Available: https://doi.org/10.1080/07900627.2018.1509787

[46] C. Moeck, P. Brunner, and D. Hunkeler, "The influence of model structure on groundwater recharge rates in climate-change impact studies," *Hydrogeology Journal*, vol. 24, no. 5, pp. 1171–1184, Aug 2016. [Online]. Available: https://doi.org/10.1007/s10040-016-1367-1

[47] G. Bartolini, D. Grifoni, R. Magno, T. Torrigiani, and B. Gozzini, "Changes in temporal distribution of precipitation in a Mediterranean area (Tuscany, Italy) 1955–2013," *International Journal of Climatology*, vol. 38, no. 3, pp. 1366–1374, 2018. [Online]. Available: https://rmets.onlinelibrary.wiley.com/doi/abs/10.1002/joc.5251

[48] RCore Team, "R: a language and environment for statistical computing." R Foundation for Statistical Computing, Vienna, Austria, 2013. [Online]. Available: URLhttp://www.R-project.org/.

[49] R. K. Frohlich and W. E. Kelly, "Estimates of specific yield with the geoelectric resistivity method in glacial aquifers," *Journal of Hydrology*, vol. 97, no. 1, pp. 33–44, 1988. [Online]. Available: http://www.sciencedirect.com/science/article/pii/0022169488900649

[50] M. Varni, R. Comas, P. Weinzettel, and S. Dietrich, "Application of the water table fluctuation method to characterize groundwater recharge in the Pampa plain, Argentina," *Hydrological Sciences Journal*, vol. 58, no. 7, pp. 1445–1455, 2013.

[51] D. Misstear, Brown, and M. Johnston, "Estimation of groundwater recharge in a major sand and gravel aquifer in Ireland using multiple approaches," *Hydrogeology Journal*, vol. 17, pp. 693–706, 05 2008.

[52] T. Sibanda, J. C. Nonner, and S. Uhlenbrook, "Comparison of groundwater recharge estimation methods for the semi-arid Nyamandhlovu area, Zimbabwe," *Hydrogeology Journal*, vol. 17, pp. 1427–1441, 09 2009.

[53] Core Writing Team and Pachauri and Meyer (eds.), "Climate Change 2014: Synthesis Report," Intergovernmental Panel on Climate Change, IPCC, Geneva, Switzerland, 151 pp., techreport, 2014, contribution of Working Groups I, II and III to the Fifth Assessment Report of the Intergovernmental Panel on Climate Change.

[54] A. Cerrina-Feroni, S. Da Prato, M. Doveri, A. Ellero, M. Lelli, G. Masetti, B. Nisi, and B. Raco, "Caratterizzazione geologica, idrogeologica e idrogeochimica dei corpi idrici sotterranei significativi della regione toscana (CISS): 32Ct010 "Acquifero costiero tra Fiume Cecina e San Vincenzo", 32Ct030 "Acquifero costiero tra Fiume Fine e Fiume Cecina", 32Ct050 "Acquifero del Cecina"," in *Memorie della Carta Geologica Italiana*, Maretti, Ed. Servizio Geologico d'Italia, 2010, ch. 1, pp. 5–80.

[55] U. Pianificazione, "Documento programmatico per l'avvio del procedimento di formazione del piano strutturale," Jul. 2003, comune di Castagneto Carducci.

[56] Pranzini, "Studio Idrogeologico della Pianura Costiera fra Rosignano e San Vincenzo," Relazione inedita per Autorità di Bacino Toscana Costa, 2004.

[57] Angeli and M. Chiesi, Ferrari, "Clima che cambia. Gli impatti sul territorio toscano," Consorzio LAMMA, Tech. Rep., 2010.

[58] Kohonen, "Essentials of the self-organizing map," *Neural Networks*, vol. 37, pp. 52–65, 2013.

[59] Tsai, "A data-mining framework for exploring the multi-relation between fish species and water quality through self-organizing map," *Science of the Total Environment*, vol. 579, pp. 474–483, 2017.

[60] T. Li, Y. Sun, G.and Chupeng, K. Liang, M. Shengzhong, and H. Lei, "Using self-organizing map for coastal water quality classification: Towards a better understanding of patterns and processes," *Science of the Total Environment*, vol. 628-629, pp. 1446–1459, 2018.

[61] Haselbeck, "Self-organizing maps for the identification of groundwater salinity sources based on hydrochemical data," *Journal of Hydrogeology*, vol. 576, pp. 610–619, 2019.

[62] A. M. Piper, "A graphic procedure in the geochemical interpretation of water-analyses," *Transactions, American Geophysical Union*, vol. 25, no. 6, pp. 914–928, Jan 1944.

[63] C.-Y. Xu and D. Chen, "Comparison of seven models for estimation of evapotranspiration and groundwater recharge using lysimeter measurement data in germany," *Hydrological Processes*, vol. 19, pp. 3717–3734, 11 2005.

[64] M. Ali, "Quantifying natural groundwater recharge using tracer and other techniques," *Asian Journal of Environment & Ecology*, vol. 5, pp. 1–12, 01 2017.

[65] B. R. Scanlon, R. W. Healy, and P. G. Cook, "Choosing appropriate techniques for quantifying groundwater recharge," *Hydrogeology Journal*, vol. 10, no. 1, pp. 18–39, Feb 2002. [Online]. Available: https://doi.org/10.1007/s10040-001-0176-2

[66] L. Yin, G. Hu, J. Huang, D. Wen, J. Dong, X. Wang, and H. Li, "Groundwater-recharge estimation in the Ordos Plateau, China: comparison of methods," *Hydrogeology Journal*, vol. 19, pp. 1563–1575, 12 2011.

[67] N. D. Lerner and I. S. A. Issar, *Groundwater recharge : a guide to understanding and estimating natural recharge*. Hannover, West Germany : Verlag Heinz Heise, 1990, at head of title: International Association of Hydrogeologists.

[68] M. L. Sharma, "Measurement and prediction of natural groundwater recharge — an overview," *Journal of Hydrology (New Zealand)*, vol. 25, no. 1, pp. 49–56, 1986. [Online]. Available: http://www.jstor.org/stable/43944572

[69] C. Allison, Barnett, G. Walker, I. Jolly, and Hughes, "Land clearance and river salinisation in the Western Murray basin, Australia," *Journal of Hydrology*, vol. 119, pp. 1–20, 11 1990.

[70] G. Delin, R. Healy, D. L. Lorenz, and J. Nimmo, "Comparison of local to regional scale estimates of ground-water recharge in Minnesota, USA," *Journal of Hydrology*, vol. 334, pp. 231–249, 02 2007.

[71] A. Flint, L. Flint, E. Kwicklis, J. Fabryka-Martin, and G. Bodvarsson, "Estimating recharge at Yucca Mountain, Nevada, USA: comparison of methods," *Hydrogeology Journal*, vol. 10, pp. 180–204, 02 2002.

[72] Fayer, "UNSAT-H version 3.0: unsaturated soil water and heat flow model theory, user manual, and examples," *US Department of Energy (US)*, 6 2000.

[73] W. Sanford, "Recharge and groundwater models: an overview," *Hydrogeology Journal*, vol. 10, no. 1, pp. 110–120, Feb 2002. [Online]. Available: https://doi.org/10.1007/s10040-001-0173-5

[74] N. Krishnamurthi, D. K. Sunada, and R. A. Longenbaugh, "Mathematical modeling of natural groundwater recharge," *Water Resources Research*, vol. 13, no. 4, pp. 720–724, 1977. [Online]. Available: https://agupubs.onlinelibrary.wiley.com/doi/abs/10.1029/WR013i004p00720

[75] B. Wang, M. Jin, J. R. Nimmo, L. Yang, and W. Wang, "Estimating groundwater recharge in Hebei Plain, China under varying land use practices using tritium and bromide tracers," *Journal of Hydrology*, vol. 356, no. 1, pp. 209–222, 2008. [Online]. Available: http://www.sciencedirect.com/science/article/pii/S0022169408001947

[76] H. Chand, M. Prakash, and Singh, "Reliable natural recharge estimates in granitic terrain," *CURRENT SCIENCE*, vol. 88, pp. 821–824, 03 2005.

[77] Sharma and Hughes, "Groundwater recharge estimation using chloride, deuterium and oxygen-18 profiles in the deep coastal sands of Western Australia," *Journal of Hydrology*, vol. 81, no. 1, pp. 93–109, 1985. [Online]. Available: http://www.sciencedirect.com/science/article/pii/0022169485901696

[78] E. Eriksson and V. Khunakasem, "Chloride concentration in groundwater, recharge rate and rate of deposition of chloride in the Israel coastal plain," *Journal of Hydrology*, vol. 7, no. 2, pp. 178–197, 1969. [Online]. Available: http://www.sciencedirect.com/science/article/pii/0022169469900559

[79] Allison and Hughes, "The use of natural tracers as indicators of soil-water movement in a temperate semi-arid region," *Journal of Hydrology*, vol. 60, no. 1, pp. 157–173, 1983. [Online]. Available: http://www.sciencedirect.com/science/article/pii/0022169483900197

[80] C. M. Ordens, A. Werner, V. E. A. Post, J. L. Hutson, C. Simmons, and B. M. Irvine, "Groundwater recharge to a sedimentary aquifer in the topographically closed Uley South Basin, South Australia," *Hydrogeology Journal*, vol. 20, 02 2011.

[81] G. Jacks and M. Traoré, "Mechanisms and rates of groundwater recharge at Timbuktu, Republic of Mali," *Journal of Hydrologic Engineering*, vol. 19, pp. 422–427, 02 2014.

[82] W. Wood, "Use and misuse of the chloride-mass balance method in estimating ground water recharge," *Groundwater*, vol. 37, pp. 2–3, 08 2005.

[83] D. Lin, M. Jin, X. Liang, and Zhan, "Estimating groundwater recharge beneath irrigated farmland using environmental tracers fluoride, chloride and sulfate," *Hydrogeology Journal*, vol. 21, 11 2013.

[84] B. Scanlon, K. Keese, A. Flint, L. Flint, E. Gaye, and Simmers, "Global synthesis of groundwater recharge in semiarid and arid regions," *Hydrological Processes*, vol. 20, pp. 3335–3370, 10 2006.

[85] T. Dinçer and Davis, "Application of environmental isotope tracers to modeling in hydrology," *Journal of Hydrology*, vol. 68, pp. 95–113, 02 1984.

[86] P. Cook and D. Solomon, "Recent advances in dating young groundwater: chlorofluorocarbons, 3h/3he and 85kr," *Journal of Hydrology*, vol. 191, pp. 245–265, 04 1997.

[87] S. Karami, H. Madani, H. Katibeh, and A. Fatehi Marj, "Assessment and modeling of the groundwater hydrogeochemical quality parameters via geostatistical approaches," *Applied Water Science*, vol. 8, no. 1, p. 23, Jan 2018. [Online]. Available: https://doi.org/10.1007/s13201-018-0641-x

[88] J. Mallick, C. K. Singh, H. Al-Wadi, M. Ahmed, A. Rahman, S. Shashtri, and S. Mukherjee, "Geospatial and geostatistical approach for groundwater potential zone delineation," *Hydrological Processes*, vol. 29, no. 3, pp. 395–418, 2015. [Online]. Available: https://onlinelibrary.wiley.com/doi/abs/10.1002/hyp.10153

[89] L. Kaur and M. S. Rishi, "Integrated geospatial, geostatistical, and remote-sensing approach to estimate groundwater level in north-western India," *Environmental Earth Sciences*, vol. 77, no. 23, p. 786, Nov 2018. [Online]. Available: https://doi.org/10.1007/s12665-018-7971-8

[90] A. Carletti, S. Canu, A. Motroni, and G. Ghiglieri, "A combined methodology for estimating the potential natural aquifer recharge in an arid environment," *Hydrological Sciences Journal*, vol. 64, no. 14, pp. 1727–1745, 2019. [Online]. Available: https://doi.org/10.1080/02626667.2019.1662422

[91] J. R. Nimmo, C. Horowitz, and L. Mitchell, "Discrete-storm water-table fluctuation method to estimate episodic recharge," *Groundwater*, vol. 53, no. 2, pp. 282–292, 2015. [Online]. Available: https://ngwa.onlinelibrary.wiley.com/doi/abs/10.1111/gwat.12177

[92] A. M. Tashie, B. B. Mirus, and T. M. Pavelsky, "Identifying long-term empirical relationships between storm characteristics and episodic groundwater recharge," *Water Resources Research*, vol. 52, no. 1, pp. 21–35, 2016. [Online]. Available: https://agupubs.onlinelibrary.wiley.com/doi/abs/10.1002/2015WR017876

[93] S. Carretero and E. Kruse, "Relationship between precipitation and water table fluctuation in a coastal dune aquifer: northeastern coast of the Buenos Aires province, Argentina," *Hydrogeology Journal*, vol. 20, 12 2012.

[94] Tallaksen, "A review of baseflow recession analysis," *Journal of Hydrology*, vol. 165, no. 1, pp. 349–370, 1995. [Online]. Available: http://www.sciencedirect.com/science/article/pii/002216949402540R

[95] B. Smith and S. Schwartz, "Automating recession curve displacement recharge estimation," *Groundwater*, vol. 55, no. 1, pp. 81–87, 2017. [Online]. Available: https://ngwa.onlinelibrary.wiley.com/doi/abs/10.1111/gwat.12439

[96] M. K. Stewart, "Promising new baseflow separation and recession analysis methods applied to streamflow at Glendhu catchment, New Zealand," *Hydrology and Earth System Sciences*, vol. 19, no. 6, pp. 2587–2603, 2015. [Online]. Available: https://www.hydrol-earth-syst-sci.net/19/2587/2015/

[97] Carlotto and Chaffe, "Master recession curve parameterization tool (mrcptool): different approaches to recession curve analysis," *Computers & Geosciences*, vol. 132, pp. 1–8, 2019. [Online]. Available: http://www.sciencedirect.com/science/article/pii/S0098300419301025

[98] R. Crosbie, P. Binning, and J. Kalma, "A time series approach to inferring groundwater recharge using the water table fluctuation method," *Water Resources Research*, vol. 41, p. 01008, 01 2005.

[99] C. Voss, "Editor's message: groundwater modeling fantasies-part 2, down to earth," *Hydrogeology Journal*, vol. 19, 12 2011.

[100] Heppner and Nimmo, "A computer program for predicting recharge with a master recession curve." U.S. Geological Survey Scientific Investigations, techreport 5172, 2005.

[101] S. Dietrich, J. Carrera, P. Weinzettel, and L. Sierra, "Estimation of specific yield and its variability by electrical resistivity tomography," *Water Resources Research*, vol. 54, no. 11, pp. 8653–8673, 2018. [Online]. Available: https://agupubs.onlinelibrary.wiley.com/doi/abs/10.1029/2018WR022938

[102] Boulton, "Analysis of data from non-equilibrium pumping tests allowing for delayed yield from storage," *Proceedings of the Institution of Civil Engineers*, vol. 26, no. 3, pp. 469–482, 1963. [Online]. Available: https://doi.org/10.1680/iicep.1963.10409

[103] S. P. Neuman, "Analysis of pumping test data from anisotropic unconfined aquifers considering delayed gravity response," *Water Resources Research*, vol. 11, no. 2, pp. 329–342, 1975. [Online]. Available: https://agupubs.onlinelibrary.wiley.com/doi/abs/10.1029/WR011i002p00329

[104] G. I. Nwankwor, J. A. Cherry, and R. W. Gillham, "A comparative study of specific yield determinations for a shallow sand aquifer," *Groundwater*, vol. 22, no. 6, pp. 764–772, 1984. [Online]. Available: https://ngwa.onlinelibrary.wiley.com/doi/abs/10.1111/j.1745-6584.1984.tb01445.x

[105] Remson and Lang, "A pumping-test method for the determination of specific yield," *Eos, Transactions American Geophysical Union*, vol. 36, no. 2, pp. 321–325, 1955. [Online]. Available: https://agupubs.onlinelibrary.wiley.com/doi/abs/10.1029/TR036i002p00321

[106] A. F. Moench, "Analytical and numerical analyses of an unconfined aquifer test considering unsaturated zone characteristics," *Water Resources Research*, vol. 44, no. 6, 2008. [Online]. Available: https://agupubs.onlinelibrary.wiley.com/doi/abs/10.1029/2006WR005736

[107] Neuman, "On methods of determining specific yield." *Groundwater*, vol. 25, no. 6, pp. 679–684, 11 1987.

[108] S. A. Mathias and A. P. Butler, "Linearized Richards' equation approach to pumping test analysis in compressible aquifers," *Water Resources Research*, vol. 42, no. 6, 2006. [Online]. Available: https://agupubs.onlinelibrary.wiley.com/doi/abs/10.1029/2005WR004680

[109] G. Tartakovsky and S. Neuman, "Three-dimensional saturated-unsaturated flow with axial symmetry to a partially penetrating well in a compressible unconfined aquifer," *Water Resources Research - WATER RESOUR RES*, vol. 43, 01 2007.

[110] P. M. Meier, J. Carrera, and X. Sánchez-Vila, "An evaluation of jacob's method for the interpretation of pumping tests in heterogeneous formations," *Water Resources Research*, vol. 34, no. 5, pp. 1011–1025, 1998. [Online]. Available: https://agupubs.onlinelibrary.wiley.com/doi/abs/10.1029/98WR00008

[111] X. Sánchez-Vila, P. M. Meier, and J. Carrera, "Pumping tests in heterogeneous aquifers: an analytical study of what can be obtained from their interpretation using jacob's method," *Water Resources Research*, vol. 35, no. 4, pp. 943–952, 1999. [Online]. Available: https://agupubs.onlinelibrary.wiley.com/doi/abs/10.1029/1999WR900007

[112] R. P. Silberstein, W. R. Dawes, T. P. Bastow, J. Byrne, and N. F. Smart, "Evaluation of changes in post-fire recharge under native woodland using hydrological measurements, modelling and remote sensing," *Journal of Hydrology*, vol. 489, pp. 1–15, 2013. [Online]. Available: http://www.sciencedirect.com/science/article/pii/S0022169413000942

[113] C. L. Gehman, D. L. Harry, W. E. Sanford, J. D. Stednick, and N. A. Beckman, "Estimating specific yield and storage change in an unconfined aquifer using temporal gravity surveys," *Water Resources Research*, vol. 45, no. 4, 2009. [Online]. Available: https://agupubs.onlinelibrary.wiley.com/doi/abs/10.1029/2007WR006096

[114] B. N. Damiata and T.-C. Lee, "Simulated gravitational response to hydraulic testing of unconfined aquifers," *Journal of Hydrology*, vol. 318, no. 1-4, pp. 348–359, 2006.

[115] Vouillamoz, Lawson, Yalo, and Descloitres, "The use of magnetic resonance sounding for quantifying specific yield and transmissivity in hard rock aquifers: the example of Benin," *Journal of Applied Geophysics*, vol. 107, pp. 16–24, 2014. [Online]. Available: http://www.sciencedirect.com/science/article/pii/S0926985114001463

[116] M. Wehrer and L. D. Slater, "Characterization of water content dynamics and tracer breakthrough by 3-D electrical resistivity tomography (ERT) under transient unsaturated conditions," *Water Resources Research*, vol. 51, no. 1, pp. 97–124, 2015. [Online]. Available: https://agupubs.onlinelibrary.wiley.com/doi/abs/10.1002/2014WR016131

[117] S. Niwas, B. Tezkan, and M. Israil, "Aquifer hydraulic conductivity estimation from surface geoelectrical measurements for Krauthausen test site, Germany," *Hydrogeology Journal*, vol. 19, pp. 307–315, 03 2011.

[118] A. T. Tizro, K. Voudouris, and Y. Basami, "Estimation of porosity and specific yield by application of geoelectrical method – A case study in western Iran," *Journal of Hydrology*, vol. 454-455, pp. 160–172, 2012. [Online]. Available: http://www.sciencedirect.com/science/article/pii/S0022169412004921

[119] D. Michot, Y. Benderitter, A. Dorigny, B. Nicoullaud, D. King, and A. Tabbagh, "Spatial and temporal monitoring of soil water content with an irrigated corn crop cover using surface

electrical resistivity tomography," *Water Resources Research*, vol. 39, no. 5, 2003. [Online]. Available: https://agupubs.onlinelibrary.wiley.com/doi/abs/10.1029/2002WR001581

[120] J. Busby and M. B. I. H. Kearey, "An Introduction to Geophysical Exploration," *Geophysical Journal International*, vol. 152, no. 2, pp. 506–506, 02 2003. [Online]. Available: https://doi.org/10.1046/j.1365-246X.2003.01868.x

[121] K. R. Sheets and J. M. H. Hendrickx, "Noninvasive Soil Water Content Measurement Using Electromagnetic Induction," *Water Resources Research*, vol. 31, no. 10, pp. 2401–2409, 1995. [Online]. Available: https://agupubs.onlinelibrary.wiley.com/doi/abs/10.1029/95WR01949

[122] P. D. Jackson, D. T. Smith, and P. N. Stanford, "Resistivity-porosity-particle shape relationships for marine sands," *Geophysics*, vol. 43, no. 6, pp. 1250–1268, 1978. [Online]. Available: https://doi.org/10.1190/1.1440891

[123] McNeill, *Electrical conductivity of soils and rocks.* Mississisauga, Ont. : Geonics, 1980.

[124] R. De Franco, G. Biella, L. Tosi, P. Teatini, A. Lozej, B. Chiozzotto, M. Giada, F. Rizzetto, C. Claude, A. Mayer, V. Bassan, and G. Gasparetto Stori, "Monitoring the saltwater intrusion by time lapse electrical resistivity tomography: The Chioggia test site Venice Lagoon, Italy)," *Journal of Applied Geophysics*, vol. 69, pp. 117–130, 12 2009.

[125] M. Zarroca, J. Bach, R. Linares, and X. Pellicer, "Electrical methods (VES and ERT) for identifying, mapping and monitoring different saline domains in a coastal plain region (Alt Empordà, Northern Spain)," *Journal of Hydrology*, vol. 409, pp. 407–422, 10 2011.

[126] R. Kalinski and W. Kelly, "Estimating water content of soils from electrical resistivity," *Geotechnical Testing Journal*, vol. 3, no. 16, pp. 323–329, 1993.

[127] Loke, "Tutorial: 2-D and 3-D electrical imaging surveys," 2004.

[128] S. Bernardinetti, T. Colonna, D. Pieruccioni, M. Abbigliati, M. Trotta, G. Algeri, E. Tufarolo, S. Minucci, E. Mugnaioli, F. M. Talarico, C. Viti, A. Harroud, M. Guernouche, and A. Cinà, "A pilot study to test the reliability of the ERT method in the identification of mixed sulphides bearing dykes: the example of Skoura mine (Morocco)," 2015.

[129] Loke, "RES2DINV, Ver. 3.50, Rapid 2-D Resistivity and IP Inversion Using the Least Square Method," Geotomo Software, 2002. [Online]. Available: http://www.geoelectrical.com/contact.html

[130] L. S. Edwards, "A modified pseudosection for resistivity and IP," *Geophysics*, vol. 42, no. 5, pp. 1020–1036, 08 1977. [Online]. Available: https://doi.org/10.1190/1.1440762

[131] D. Groot-Hedlin and Constable, "OCCAM's inversion to generate smooth, two-dimensional models from magnetotelluric data," *Geophysics*, vol. 55, pp. 1613–1624, 12 1990.

[132] Loke and Barker, "Rapid least-squares inversion of apparent resistivity pseudosections by a quasi-Newton method1," *Geophysical Prospecting*, vol. 44, no. 1, pp. 131–152, 1996. [Online]. Available: https://onlinelibrary.wiley.com/doi/abs/10.1111/j.1365-2478.1996.tb00142.x

[133] G. Braca, *Linee guida per l'analisi e l'elaborazione statistica di base delle serie storiche di dati idrologici*, ISPRA - Dipartimento Tutela delle Acque Interne e Marine – Servizio Monitoraggio e Idrologia delle Acque Interne, Settore Idrologia, 2013.

[134] Y. Xu, *Hyfo: hydrology and climate forecasting*, 2018, r package version 1.4.0. [Online]. Available: https://CRAN.R-project.org/package=hyfo

[135] R. Killick, K. Haynes, and I. A. Eckley, *changepoint: an R package for changepoint analysis*, 2016, r package version 2.2.2. [Online]. Available: https://CRAN.R-project.org/package=changepoint

[136] McLeod, *Kendall: kendall rank correlation and Mann-Kendall trend test*, 2011, r package version 2.2. [Online]. Available: https://CRAN.R-project.org/package=Kendall

[137] C. J. Stone, "Consistent nonparametric regression," *Ann. Statist.*, vol. 5, no. 4, pp. 595–620, 07 1977. [Online]. Available: https://doi.org/10.1214/aos/1176343886

[138] W. Cleveland and S. Devlin, "Locally weighted regression: an approach to regression analysis by local fitting," *Journal of the American Statistical Association*, vol. 83, pp. 569–610, 09 1988.

[139] Allocca, D. Vita, Manna, and Nimmo, "Groundwater recharge assessment at local and episodic scale in a soil mantled perched karst aquifer in southern Italy," *Journal of Hydrology*, vol. 529, pp. 843–853, 2015. [Online]. Available: http://www.sciencedirect.com/science/article/pii/S0022169415006046

[140] A. Knapp, D. Hoover, K. Wilcox, M. Avolio, S. Koerner, K. La Pierre, M. Loik, Y. Luo, O. Sala, and M. Smith, "Characterizing differences in precipitation regimes of extreme wet and dry years: implications for climate change experiments," *Global Change Biology*, vol. 21, 02 2015.

[141] A. Maydeu-Olivares and C. Forero, *Goodness-of-Fit Testing*, 12 2010, vol. 7, pp. 190–196.

[142] S. Lupia Palmieri Parotto, Saraceni, *Scienze naturali.* Zanichelli editore S.p.A., 2011.

[143] Fetter, *Applied Hydrogeology: Fourth Edition.* Waveland Press, 2018. [Online]. Available: https://books.google.it/books?id=BYZXDwAAQBAJ

[144] D. R. Pool and J. H. Eychaner, "Measurements of aquifer-storage change and specific yield using gravity surveys," *Groundwater*, vol. 33, no. 3, pp. 425–432, 1995. [Online]. Available: https://ngwa.onlinelibrary.wiley.com/doi/abs/10.1111/j.1745-6584.1995.tb00299.x

[145] D. Kotchoni, J.-M. Vouillamoz, F. M. Lawson, P. Adjomayi, M. Boukari, and R. Taylor, "Relationships between rainfall and groundwater recharge in seasonally humid Benin: a comparative analysis of long-term hydrographs in sedimentary and crystalline aquifers," *Hydrogeology Journal*, 06 2018.

[146] P.-Y. Chang, L.-C. Chang, S.-Y. Hsu, J.-P. Tsai, and W.-F. Chen, "Estimating the hydrogeological parameters of an unconfined aquifer with the time-lapse resistivity-imaging method

during pumping tests: Case studies at the Pengtsuo and Dajou sites, Taiwan," *Journal of Applied Geophysics*, vol. 144, pp. 134–143, Sep 2017.

[147] ARPAT, "Groundwater numerical flow and transport model of the Montescudaio (PI) and Cecina (LI) area," Agenzia Regionale protezione Ambientale Toscana, Technical Report, Tuscan Environmental Authority, 2013, accordo di Programma per l'attuazione degli interventi urgenti per la bonifica della falda acquifera a seguito inquinamento da organoalogenati, comuni di Montescudaio (PI) e Cecina (LI), Modello di Flusso e Trasporto.

[148] ——, "Groundwater numerical modeling for the water resource management," Agenzia Regionale protezione Ambientale Toscana, Technical Report, Tuscan Environmental Authority, 2018, modellistica idrogeologica per la gestione della disponibilità delle risorse idriche.

[149] S. P. Greco, Lorenzini S, "Groundwater numerical model of the Cecina River alluvional aquifer between Ponte di Ferro and Ponte di Monterufoli," techreport, 2002, modello Matematico di Flusso dell'Acquifero Alluvionale del Fiume Cecina tra Ponte di Ferro e Ponte di Monterufoli.

[150] I. H. Association, "Price list ANIPA," Feb. 2020, last login: 06/02/2020. [Online]. Available: http://www.anipapozzi.com/?q=content/nuovo-preziario

[151] I. G. Association, "Price list," Feb. 2020, last login: 06/02/2020. [Online]. Available: http://www.associazionegeofisica.org/wordpress/?page_id=299